Reprint of Structures and Materials Research Bulletin
Series 100, Issue 3

BEHAVIOR OF PRESTRESSED CONCRETE BEAMS AT TRANSFER

A Report of an Investigation by

A. C. SCORDELIS
Associate Professor of Civil Engineering

T. Y. LIN
Professor of Civil Engineering

H. R. MAY
Graduate Research Engineer

of the

INSTITUTE OF ENGINEERING RESEARCH
UNIVERSITY OF CALIFORNIA
Berkeley, California

October, 1957

to the

DIVISION OF ARCHITECTURE
DEPARTMENT OF PUBLIC WORKS
STATE OF CALIFORNIA

FOREWORD

The Research Program of the Division of Architecture, of which this project is a part, is intended to develop information in those fields of materials, designs and construction which would be in the best interest of the State of California in connection with the economy and safety of design and construction of public school buildings and which is of such general nature as to be overlooked by industry research and other research organizations.

It should be recognized that the information presented in this report is not regulatory but may aid in the development of new standards or the modification of existing standards, all leading towards more economical, safe school building construction. The findings of this project should contribute to economy and safety not only in public schools but in the building industry in general.

ANSON BOYD
State Architect

May 8, 1958

Structures and Materials Research
Division on Civil Engineering

BEHAVIOR OF PRESTRESSED CONCRETE BEAMS AT TRANSFER

A Report of an Investigation

by

A. C. Scordelis
Associate Professor of Civil Engineering

T. Y. Lin
Professor of Civil Engineering

H. R. May
Graduate Research Engineer

to the

DIVISION OF ARCHITECTURE
DEPARTMENT OF PUBLIC WORKS
STATE OF CALIFORNIA

Institute of Engineering Research
University of California
Berkeley 4, California
October 1957

TABLE OF CONTENTS

		Page
I.	INTRODUCTION	1
	1. Object	1
	2. Scope	1
	3. Acknowledgments	2
	4. Notation	2
II.	DESCRIPTION OF TEST BEAMS, FABRICATION, AND MATERIALS	4
	1. Test Beams	4
	2. Fabrication	5
	3. Materials	5
III.	METHOD OF LOADING AND INSTRUMENTATION	7
	1. Method of Loading	7
	2. Instrumentation	8
IV.	THEORETICAL STUDIES	9
	1. Basic Assumptions and Behavior	9
	2. Expressions for Cracking Strengths of Beams with or Without Mild Steel	13
	a. Cross-sections, Forces, and Stresses	
	(1) Rectangular Section	
	(2) Tee Section	
	(3) Inverted Tee Section	
	(4) I Sections	
	b. Section Properties	
	c. Cracking Strength by the Elastic Theory	

TABLE OF CONTENTS (CONT'D)

		Page
3.	Expressions for Ultimate Strength of Beams Without Mild Steel	15
	a. $0 \leq a \leq \phi h$	
	b. $\phi h \leq a \leq h$ and $\beta a \leq \phi h$	
	c. $\phi h \leq a \leq h$ and $\beta a \geq \phi h$	
	d. $a \geq h$ and $\beta a \leq \phi h$	
	e. $a \geq h$ and $\phi h \leq \beta a \leq h$	
4.	Expressions for Ultimate Strength of Beams with Mild Steel	23
	a. $0 \leq a \leq \phi h$	
	(1) Balanced Failure (2) Tension Failure (3) Compression Failure	
	b. $\phi h \leq a \leq \frac{d'}{h}$ and $\beta a \leq \phi h$	
	c. $\phi h \leq a \leq \frac{d'}{h}$ and $\beta a \geq h$	
V.	TEST RESULTS	29
1.	General Behavior	29
2.	Photographs of Beams After Failure	30
3.	Load-Deflection Curves	30
4.	Load-Strain Curves	31
5.	Stress in Top Concrete Fiber at Cracking	31
6.	Strain in Bottom Concrete Fiber at Ultimate	32
7.	F/Af'c and e/h at Cracking and Ultimate	32
VI.	DISCUSSION AND CONCLUSIONS	33

LIST OF TABLES

TABLE	TITLE	PAGE
I	Sieve Analysis of Aggregates	37
II	Properties of Concrete Mixes	38
III	Properties of 1/4 In. Diameter Steel Prestressing Wire	39
IV	Properties of 1/2 In. Diameter Intermediate Grade Steel ASTM A-305 Bars	40
V	Test Results	41

LIST OF FIGURES

FIGURE	TITLE	PAGE
1	Section Properties at Midspan of Test Specimens	42
2A	Elevation of Cable Layout for all Beams	43
2B	Plan View of B1A, B1B, B1C, B2A, B2B, and B2C	43
2C	Plan View of B3A, B3B, B3C, and B4A	43
2D	Plan View of B5A, B5B, B5C, and B6A	43
3	Typical Stress-Strain Curve for Concrete 6 x 12 In. Cylinder at Age of 14 Days	44
4	Details of 12 Wire Prestressing Cable	45
5	Typical Stress-Strain Curve for 1/4 In. Dia., Prestressing Wire	46
6	Typical Stress-Strain Curve for 1/2 In. Dia., Intermediate Grade, Steel Bar	47
7	First Loading Arrangement	48
8	Second Loading Arrangement	49
9	Location of SR-4 Gages at Midspan	50
10	Assumed Compressive Stress-Strain Curve by Jensen	51
11	Strain Distribution Under Increasing Prestress Force or External Moment (Beam Without Mild Steel in Top)	52
12	Stress Distribution Under Increasing Prestress Force or External Moment (Beam Without Mild Steel in Top)	52
13	Strain Distribution Under Increasing Prestress Force or External Moment (Beam With Mild Steel in Top)	53
14	Stress Distribution Under Increasing Prestress Force or External Moment (Beam With Mild Steel in Top)	53
15	Theoretical Cracking and Ultimate Strength Curves for a Rectangular Section	54
16	Theoretical Cracking and Ultimate Strength Curves for a Tee Section	55
17	Theoretical Cracking and Ultimate Strength Curves for a Tee Section	56

LIST OF FIGURES (CONT'D)

FIGURE	TITLE	PAGE
18	Theoretical Cracking and Ultimate Strength Curves for an Inverted Tee Section	57
19	Theoretical Cracking and Ultimate Strength Curves for an I Section	58
20	Rectangular Beam Specimens After Failure	59
21	Thin Flange Tee Beam Specimens After Failure	60
22	Thick Flange Tee Beam Specimens After Failure	61
23	Beam B-1A, Prestress Force and Moment vs. Center Deflection	62
24	Beam B-1B, Prestress Force and Moment vs. Center Deflection	63
25	Beam B-1C, Prestress Force and Moment vs. Center Deflection	64
26	Beam B-2A, Prestress Force and Moment vs. Center Deflection	65
27	Beam B-2B, Prestress Force and Moment vs. Center Deflection	66
28	Beam B-2C, Prestress Force and Moment vs. Center Deflection	67
29	Beam B-3A, Prestress Force and Moment vs. Center Deflection	68
30	Beam B-3B, Prestress Force and Moment vs. Center Deflection	69
31	Beam B-3C, Prestress Force and Moment vs. Center Deflection	70
32	Beam B-4A, Prestress Force and Moment vs. Center Deflection	71
33	Beam B-5A, Prestress Force and Moment vs. Center Deflection	72
34	Beam B-5B, Prestress Force and Moment vs. Center Deflection	73
35	Beam B-5C, Prestress Force and Moment vs. Center Deflection	74

LIST OF FIGURES (CONT'D)

FIGURE	TITLE	PAGE
36	Beam B-6A, Prestress Force and Moment vs. Center Deflection	75
37	Beam B-1A, Prestress Force and Moment vs. Unit Strain	76
38	Beam B-1B, Prestress Force and Moment vs. Unit Strain	77
39	Beam B-1C, Prestress Force and Moment vs. Unit Strain	78
40	Beam B-2A, Prestress Force and Moment vs. Unit Strain	79
41	Beam B-2B, Prestress Force and Moment vs. Unit Strain	80
42	Beam B-2C, Prestress Force and Moment vs. Unit Strain	81
43	Beam B-3A, Prestress Force and Moment vs. Unit Strain	82
44	Beam B-3B, Prestress Force and Moment vs. Unit Strain	83
45	Beam B-3C, Prestress Force and Moment vs. Unit Strain	84
46	Beam B-4A, Prestress Force and Moment vs. Unit Strain	85
47	Beam B-5A, Prestress Force and Moment vs. Unit Strain	86
48	Beam B-5B, Prestress Force and Moment vs. Unit Strain	87
49	Beam B-5C, Prestress Force and Moment vs. Unit Strain	88
50	Beam B-6A, Prestress Force and Moment vs. Unit Strain	89
51	Cracking and Ultimate Strength Curves for a Rectangular Section	90
52	Cracking and Ultimate Strength Curves for a Tee Section	91

LIST OF FIGURES (CONT'D)

FIGURE	TITLE	PAGE
53	Cracking and Ultimate Strength Curves for a Tee Section	92
54	Ratio of Ultimate $(\frac{F}{Af'_c})$ to Cracking $(\frac{F}{Af'_c})$ for Various Eccentricity Ratios (Beams Without Mild Steel)	93
55	Ratio of Ultimate $(\frac{e}{h})$ to Cracking $(\frac{e}{h})$ for Various Prestress Ratios (Beams Without Mild Steel)	94

I. INTRODUCTION

1. Object

The object of this research project was to determine the behavior and ultimate strength of concrete beams under the action of excessive eccentric prestressing. Present practice bases the design at transfer of prestress on an allowable amount of tensile stress or in some cases no tensile stress at all. It is felt that such arbitrary rules yield varying factors of safety. This project was designed to develop a rational theoretical approach to the study of the strength of prestressed beams at transfer and to support this theory by sufficient tests on full scale beams.

2. Scope

The effects of the following variables on the strength of beams at transfer were studied:

(a) The shape of the cross section.

(b) The amount and location of prestress force.

(c) The amount of external moment, acting to increase the eccentricity of prestress.

(d) The amount of mild steel on the tensile side of the beam.

The analytical studies consisted of the development of rational formulas for the prediction of cracking and ultimate strengths of prestressed beams under excessive eccentric prestress. The development of these formulas was based on the elastic and plastic theories as applied to concrete beams.

The experimental program investigated the effect of these variables by testing fourteen beams. Three different shapes were used, one rectangular, and two tee-shapes, to investigate the effect of variable (a). Each specimen was subjected to a different combination of prestress and external moment to note the effect of variables (b) and (c). Approximately two thirds of the

beams were tested without mild steel and one third with mild steel to note the effect of variable (d). All beams were tested to ultimate failure.

3. Acknowledgments

The program reported herein was conducted in the Structural Engineering Laboratory, Division of Civil Engineering, University of California, Berkeley. The program was sponsored by the Division of Architecture, Department of Public Works, State of California, through a research grant administered by the Institute of Engineering Research, University of California. The program was carried on between May 1, 1956 and June 30, 1957.

The Division of Architecture is under the direction of Anson Boyd, State Architect. Special appreciation for their help and suggestions is due to C. M. Herd, Chief Construction Engineer, Charles Peterson, M. W. Sahlberg, Principal Structural Engineers, and A. H. Brownfield, Supervising Structural Engineer, all of the Division of Architecture.

Much credit for the successful conduct of the program should go to S. A. Ravid and S. Y. Chang, Graduate Research Assistants, who participated extensively in the theoretical studies, the conduct of the tests, and the reduction and interpretation of the data.

4. Notation

The letter symbols used in this report are generally defined when they are introduced. The most frequently used symbols are listed below for convenient reference:

A	=	gross area of section
A_s	=	area of mild steel reinforcement in top of section
a	=	depth of trapezoidal stress block in the concrete
b	=	width of section, flange or web depending on type of section
b'	=	web thickness
C	=	total internal compressive force on section

C_1, C_2, C_3 = portions of C

c_b = distance from c.g.c. to bottom fiber of member

c_t = distance from c.g.c. to top fiber of member

c.g.c. = centroid of gross area of section

c.g.s. = centroid of prestressing steel

d = distance from extreme top fiber to c.g.s.

d' = distance from extreme bottom fiber to centroid of top mild steel reinforcement

E_c = modulus of elasticity of concrete

E_s = modulus of elasticity of steel

e = distance from c.g.c. to resultant force on section; i.e., $e = d - c_t + \frac{M}{F}$

F = total effective prestress force at a section

f_b = bottom fiber stress in concrete

f'_c = compressive strength of 6 by 12 in. concrete cylinders

f'_t = modulus of rupture of concrete

f_s = stress in mild steel reinforcement

f_y = yield point of mild steel reinforcement

g = a/h, ratio of depth of concrete stress block to total depth of section

g_o = ratio of depth of concrete stress block to total depth of section for balanced failure

h = total depth of section

I = gross moment of inertia of section

k_1 = $\frac{1+\beta}{2}$, coefficient denoting magnitude of a trapezoidal stress block over a uniform width

k_2 = $\frac{1+\beta+\beta^2}{3(1+\beta)}$, coefficient denoting the position of the center of volume of a trapezoidal stress block over a uniform width

M = total external bending moment acting at a section

m = $\frac{f_s}{f'_c}$, ratio of stress in top mild steel reinforcement to concrete compressive strength

p or p_g = $\frac{A_s}{A}$, ratio of area of top mild steel reinforcement to gross area of section

t = flange thickness

T = total internal tensile force on section

β = Jensen's plasticity ratio

γ = A/bh

δ = c_t/h

ε_c = bottom fiber strain in concrete

ε_u = ultimate concrete strain in flexure

ε_s = strain in top mild steel reinforcement

ε_y = yield point strain of top mild steel reinforcement

η = ratio of widths, generally ratio of bottom width to top width of section

θ = I/bh^3

ϕ = ratio of depth of bottom rectangular portion of section to total depth of section

II. DESCRIPTION OF TEST BEAMS, FABRICATION, AND MATERIALS

1. Test Beams

The beams were so designed that the critical cross section was at mid-span. Cross-sectional properties for each of the fourteen beams are given in Figure 1. Three shapes were used: (1) a rectangular 6 x 20 in. cross section; (2) a tee section 20 in. deep, with a flange 17.5 in. wide and 4 in. thick, and a stem 3.5 in. wide; (3) a tee section 20 in. deep, with a flange 17.5 in. wide and 8 in. thick, and a stem 3.5 in. wide. All beams were 20 ft. long.

Each beam contained one prestressing cable consisting of 12-$\frac{1}{4}$ in. diameter wires. The cable profile was parabolic in the center 4 ft. portion of the beam and thence straight to each end of the beam. At each end of the beam, the c.g.s. of the cable was positioned at the c.g.c. of the section; the c.g.s. was dropped to 2 in. above the bottom at the midspan section. (see Figure 2a) The rectangular sections were prismatic throughout their entire length, but the tee sections were provided with thickened stems at support points and ends. These dimensions are shown in Figures 2b, 2c, and 2d.

2. Fabrication

The beams were cast in wooden forms coated with a bond breaker material. The forms were so designed that they could be disassembled at the time of stripping and reused for the next beam. Five-sixteenths in. diameter steel rods placed horizontally through the side forms held the cable in its correct profile during casting. These rods were removed about 4 hours after casting. The holes left by the rods were not grouted. Wire ties were used to hold the cable in its correct horizontal alignment. The concrete was mixed in a 2.5 cubic foot mixer, eight and one half batches being required to cast each beam and corresponding control specimens.

The forms were stripped 3 to 7 days after casting. All specimens were cured moist for 7 days using damp burlap and then left air dry until testing at the age of 14 days.

3. Materials

Concrete mixes were designed by the trial batch method. Type I, Santa Cruz Cement and locally available Elliot sand and gravel were used in all mixes. Sieve analyses for the aggregate are given in Table I.

Mix No. 1 used in the first three beams tested, B1A, B1B, B1C, had a cement factor of 7 sacks/cu. yd. The water-cement ratio was 0.44 by weight

or 5 gallons per sack. Mix proportions were 1 : 1.78 : 2.93 by weight. All aggregate weights were based on a saturated surface dry condition. Kelly ball penetrations varied between 2.3 in. and 2.7 in. which are equivalent to slumps of $4\frac{1}{2}$ and $5\frac{1}{2}$ inches.

Mix No. 2 used on the remaining eleven beams tested had a cement factor of 6.3 sks. per cu. yd. The water-cement ratio was 0.49 by weight or $5\frac{1}{2}$ gallons per sack. Mix proportions were 1 : 2.17 : 3.20 by weight. Kelly ball penetrations varied between 2.1 in. and 2.5 in. Mix data are tabulated in Table II.

Control specimens consisted of a minimum of three 6 x 12 in. cylinders and three 6 x 6 x 20 in. beams for each test specimen. All control specimens were cured in the same manner as the test beams and tested at 14 days. Compressive strength, f'_c, and secant modulus of elasticity at 1000 psi, E_c, were obtained for each cylinder. Modulus of rupture, f'_t, was obtained for each 6 x 6 x 20 in. beam by loading at the third points of an 18 in. span. Average values for these quantities for each specimen are tabulated in Table II. A typical stress strain diagram for a 6 x 12 in. cylinder is shown in Figure 3.

The prestressing cables each contained 12-$\frac{1}{4}$ in. diameter, cold-drawn steel wires. The wires were greased and wrapped with paper and remained unbonded throughout each test. Over-all diameter of the cable was approximately 1 in. Details of the cable assembly and end anchorages are given in Figure 4. The cables were supplied by Western Concrete Structures and the Prescon Corporation.

Seven 24 in. long samples of the prestressing wires were tested on a 10 in. gage length to determine the proportional limit, f_{pl}; yield point, f_y, as measured by the 0.2 per cent offset method; ultimate strength, f_u; modulus of elasticity, E_s; and per cent elongation in a 10 in. gage length.

The results of these tests are shown in Table III. It can be noted that the samples exhibited relatively uniform properties. A typical stress-strain curve for the prestressing wire is shown in Figure 5.

One-half in. diameter mild steel bars were used on tension side of some of the beams. These bars conformed to ASTM A-305 specifications and were of intermediate grade. Ten 24 in. long samples of these bars were tested on an 8 in. gage length to determine properties similar to those found for the prestressing steel. These results are tabulated in Table IV and a typical stress-strain diagram is shown in Figure 6.

III. METHOD OF LOADING AND INSTRUMENTATION

1. Method of Loading

It was desired to have a method of loading which could apply to the critical midspan section of the beam varying amounts of prestress force, F, and external moment, M.

Two loading arrangements were devised to accomplish this purpose. The first, shown in Figure 7, was used where the amount of negative external moment required for ultimate failure at midspan was relatively small and could be obtained by adding a dead weight, W, to the end of the steel loading beams shown. The supports could be positioned so that the dead load moment at midspan was zero. This arrangement was used on all specimens which had no mild steel on the tensile side since it was felt that this arrangement of loading would permit sudden failures to take place and thus simulate actual conditions in the field.

The second loading arrangement, shown in Figure 8, was used in the cases where large external moments were needed and a sudden failure was not possible because of the mild steel reinforcement on the tension side of the beam. Large moments could be produced by exerting forces on the beam by means of

the jacks at A and B. Both jacks were connected to the same hydraulic line so that the force exerted at each point on the beam was the same. Again the supports could be positioned so that the dead load moment at midspan was zero. This arrangement was not used where it was desired to permit a sudden failure since the hydraulic jacks would not keep the load constant with rapid deflections of the test beam. In the first loading arrangement described this does not happen; the load remains nearly constant throughout a sudden failure.

The amount of prestressing force was controlled by a hydraulic jack at one end. The twelve wire cable in each beam was tensioned as a single unit. The value of the force was determined from a pressure gage, connected to the jack, which had been previously calibrated. From earlier pilot tests in the laboratory, the friction loss in the cable to the center of the beam was known to be approximately 5% and this factor was used to determine the prestress force existing at the center cross-section.

2. Instrumentation

Instrumentation was designed to measure strain distributions at the center cross-section and deflections at the center and two ends of the beam.

Strains in the concrete were measured by means of SR-4, type A9, strain gages which have a gage length of 6 in. Standard procedures were used in bonding these gages to the beams. Strains in the mild steel reinforcement were measured by means of SR-4, type A5, strain gages which have a gage length of $\frac{1}{2}$ in. In order to place these gages on the bar, the bar deformations were first ground off of half the circumference of the bar over a length of about 1 in. The gage was then bonded to the bar and allowed to dry. It was then waterproofed with Epoxylite 222, a waterproofing compound, prior to the casting of the beam. In order to insure yielding of the mild steel bars at the gage location, an artificial crack was cast at the center cross-section into all beams with mild steel by means of a thin sheet of

metal. This crack had a depth of approximately 2 in.

The location of the strain gages for the various test specimens is given in Figure 9.

Gages placed symmetrically about the axis of symmetry of the cross-section were wired in parallel so that an average value for strain at these levels was recorded. A four channel Sanborn Recorder was used to give a continuous record on paper of the strain at four levels as the test progressed. The remainder of the gages were read independently by means of a standard SR-4 strain indicator box. This was done by taking readings after each load increment had been applied. Strains obtained by means of the Sanborn Recorder had a maximum probable error of 5 per cent. Strains measured with the SR-4 strain indicator had an accuracy of 5 micro inches.

Deflections at the center and at each end of the beam were measured by simple dial gages bearing on top of the beams. The dials had a least count of 0.001 inches.

Each of the beams was coated with whitewash over the center portion of the span to aid in the visual inspection for cracks.

IV. THEORETICAL STUDIES

1. Basic Assumptions and Behavior

A theory is developed below to predict the cracking strength and the ultimate strength of a beam section subjected to eccentric prestress and external moment, both of which tend to produce tensile stresses in the top fibers of a section, which under normal working load conditions would have compression in the top fibers. The above condition could develop at transfer of prestress or during the erection of members, when erection procedures might, either by chance or by design, subject the beam to external moments which produce tensile stresses in the top fibers. This condition could also

occur in continuous beams under certain circumstances.

This situation may prove serious since a sudden failure immediately following the formation of a crack in the top fibers is possible in certain cases. In other cases the situation is not serious since a crack may form, progress a short distance, and then stop. Upon application of the normal working load, the crack will close and the beam will perform satisfactorily. The type of action which will occur as well as the strength of a section, is dependent on the variables which this program has investigated.

The theoretical studies are based on the following assumptions:

(a) Plane sections remain plane after bending occurs.

(b) The actual stress-strain curve for the concrete is replaced by the curve shown in Figure 10. This curve is based on the well known Jensen theory for ultimate strength.[1]

(c) The plasticity of the concrete in compression may be defined by Jensen's plasticity ratio, β .

$$\beta = \frac{1}{1 + \left[\frac{f'_c}{4000} \right]^2}$$

(d) The concrete has a specified tensile strength up to and through the cracking range, but its contribution to the ultimate strength is neglected because it is small.

(e) The cracking strengths of beams of the same cross sectional dimensions with or without mild steel in the top are equal.

The general behavior of a beam subjected to eccentric prestress force and external negative moment may be described by considering a simple rectangular cross section first without and then with mild steel in the top.

---

1. V. P. Jensen: "The Plasticity Ratio of Concrete and Its Effect on the Ultimate Strength of Beams", Journal of ACI, Vol. 39, June 1943, pp. 565 - 584.

Figures 11 and 12 depict the strains and stresses under increasing values of F or M for a section without mild steel in the top. (a) The top fiber strain and stress increase until finally the tensile strength of the concrete, f'_t, is reached and an initial crack forms at the top; (b) and (c) the crack progresses downward, with a corresponding downward movement of the neutral axis, until finally the bottom fiber stress reaches f'_c and plasticity starts; (d) the plasticity of the concrete is exhausted and the concrete crushes resulting in ultimate failure.

For beams without mild steel it should be noted that in certain cases, depending on the shape of cross section and the combination of F and M, the theoretical ultimate strength is less than the cracking strength. In these cases once the beam has cracked at the top a sudden failure will ensue.

Figures 13 and 14 depict the strains and stresses under increasing values of F or M for a section with mild steel in the top assuming a tension failure in the mild steel. (a) The top fiber strain and stress increase until finally the tensile strength of the concrete, f'_t, is reached, a crack is formed, but stops a short distance down because of the mild steel; (b) the tensile strength of the concrete is now neglected, increasing values of F do not cause the neutral axis to shift down, but simply increase the magnitudes of the stresses in the steel and concrete, increasing values of M would cause the neutral axis to move down slowly; (c) the steel reaches its yield point; (d) the neutral axis shifts down, the concrete reaches f'_c, plasticity takes place, the concrete crushes, resulting in ultimate failure.

If at the stage shown in Figure 14 (d) the steel had not reached its yield point, and the concrete crushed at the bottom, the failure could be termed a compression failure.

A sudden failure following intial cracking of the top fibers is not possible for beams with nominal amounts of mild steel in the top.

In the next three sections of the report formulae for the cracking and ultimate strength of rectangular, tee, inverted tee, and I sections will be developed. While the formulae developed for these sections may appear complex, they are only algebraically so. The formulae for ultimate strength of sections without mild steel in the top are in all cases developed from the assumed Jensen stress block and two equations of statics, namely $\Sigma H = 0$ and $\Sigma M = 0$. The cracking strengths of beams of the same cross section with and without mild steel in the top are assumed to be equal. For beams with mild steel in the top, the formulae for ultimate strength are developed from the assumed Jensen stress block, the two equations of statics, plus an equation representing the geometry of strains.

The formulae developed in the next three sections of the report have been plotted in Figures 15 through 19. These figures give cracking and ultimate strength curves for sections with and without mild steel. Shown are plots of prestress ratio, F/Af'_c versus eccentricity ratio, e/h. F is the prestress force and A is the gross concrete cross-sectional area. F/A represents the stress existing at the c.g.c. of the section. The eccentricity, e, is the distance from the c.g.c. to the c.g.s. if no external moment is acting. If an external moment also exists at the section, the eccentricity increases by an amount equal to the moment divided by the prestress force.

2. Expressions for Cracking Strengths of Beams With or Without Mild Steel

As mentioned earlier it is assumed that the cracking strengths of beams of the same cross section with or without mild steel are equal.

a. Cross-sections, Forces, and Stresses.

1) Rectangular Section

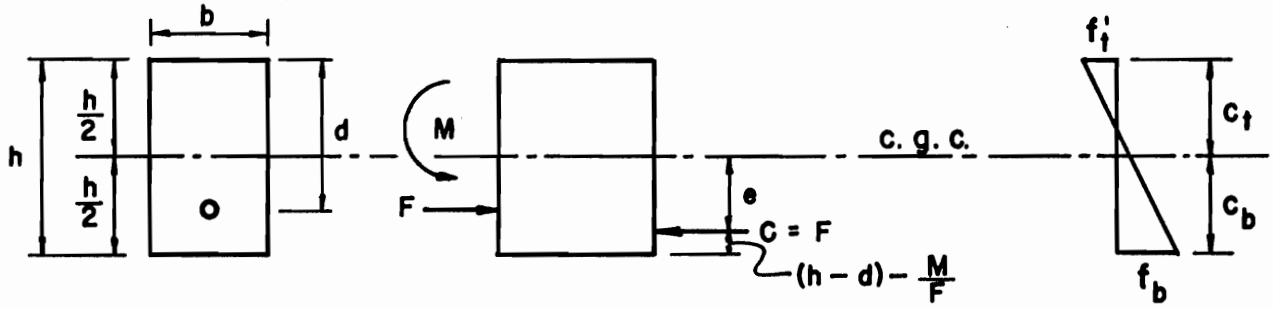

2) Tee Section

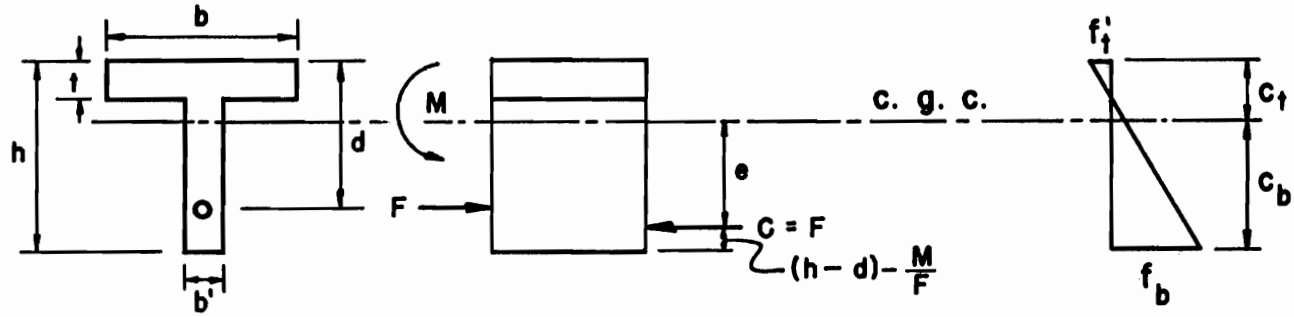

3) Inverted Tee Section

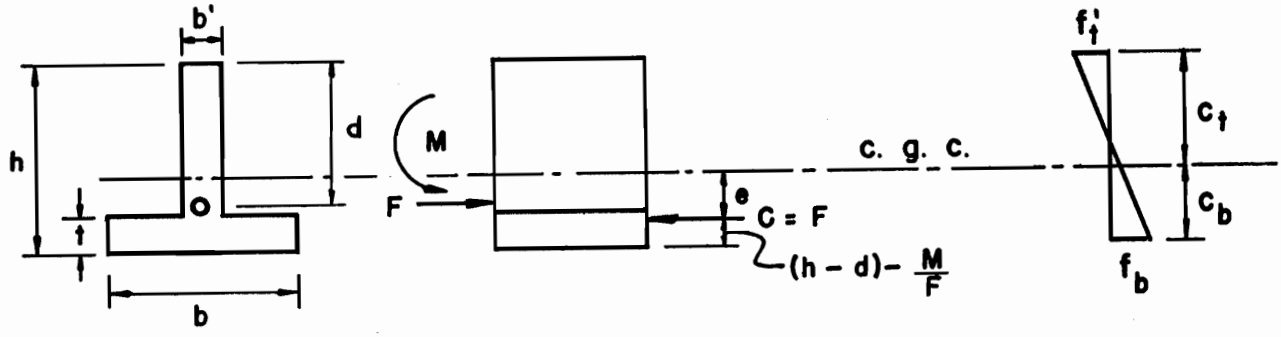

4) I Section

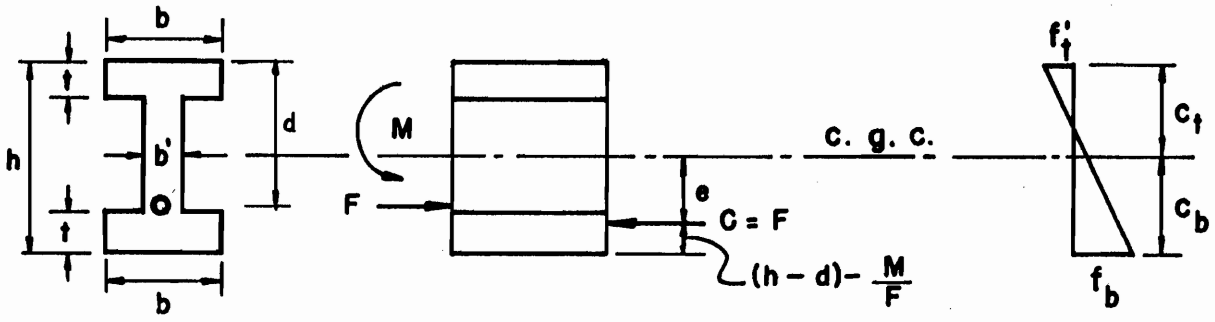

b. Section Properties:

$A = \gamma bh$ $\qquad c_b = (1 - \delta)h$

$I = \theta\, bh^3$ $\qquad c_t = \delta h$

c. Cracking Strength by the Elastic Theory:

$$f'_t = -\frac{F}{A} + \frac{Fec_t}{I}$$

Rearranging terms and substituting, the cracking strength is:

$$\frac{F}{Af'_c} = \frac{f'_t/f'_c}{\left[\frac{\gamma\delta}{\theta}\frac{e}{h} - 1\right]} \qquad (1)$$

For rectangular sections:

$$\gamma = 1, \quad \theta = \frac{1}{12}, \quad \delta = \frac{1}{2}$$

Therefore, the cracking strength for rectangular sections is:

$$\frac{F}{Af'_c} = \frac{f'_t/f'_c}{\frac{6e}{h} - 1} \qquad (2)$$

For tee, inverted tee, and I sections, values of γ, θ, and δ have been tabulated by Lin and Scordelis[2] for various ratios of b'/b and t/h.

Cracking strength curves for various cross sections are shown in Figures 15 through 19.

3. Expressions for Ultimate Strength of Beams Without Mild Steel

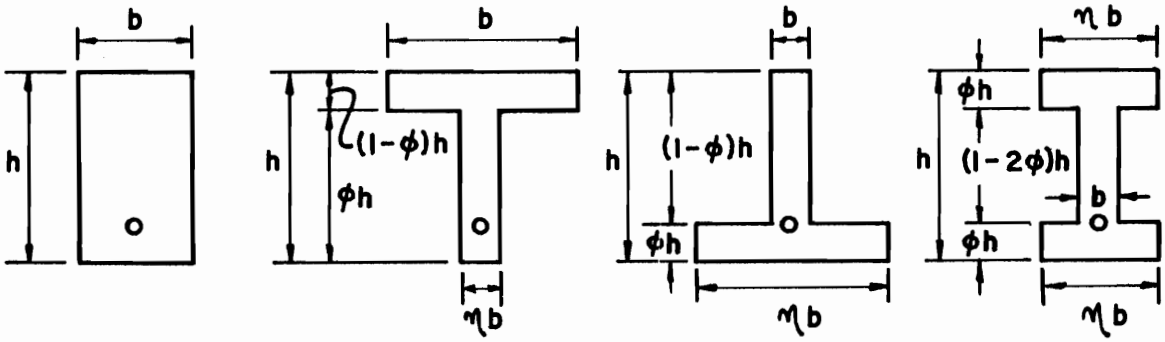

1) Rectangular 2) Tee 3) Inverted Tee 4) I

Note that the rectangular, tee, and inverted tee differ only in the values of η and ϕ. That is, for the rectangular section, $\eta = 1$ and $\phi = 1$. The inverted tee differs from the tee only in the relative magnitudes of η and ϕ.

The I section differs from the inverted tee section only by the presence of the top flange. If the neutral axis is below the bottom of the top flange, it is identical with the inverted tee section. The expressions for the ultimate strength of I sections when the neutral axis is above the bottom of the top flange will be different than for the other sections. However, this case is of little practical importance and will not be considered.

---

2. T. Y. Lin and A. C. Scordelis, "Selection and Design of Prestressed Concrete Beam Sections", Journal of the ACI, Vol. 25, November 1953, pp. 209-224.

Because of the similarity of the sections, the following derivations apply to all sections.

a. $0 \leq a \leq \phi h$

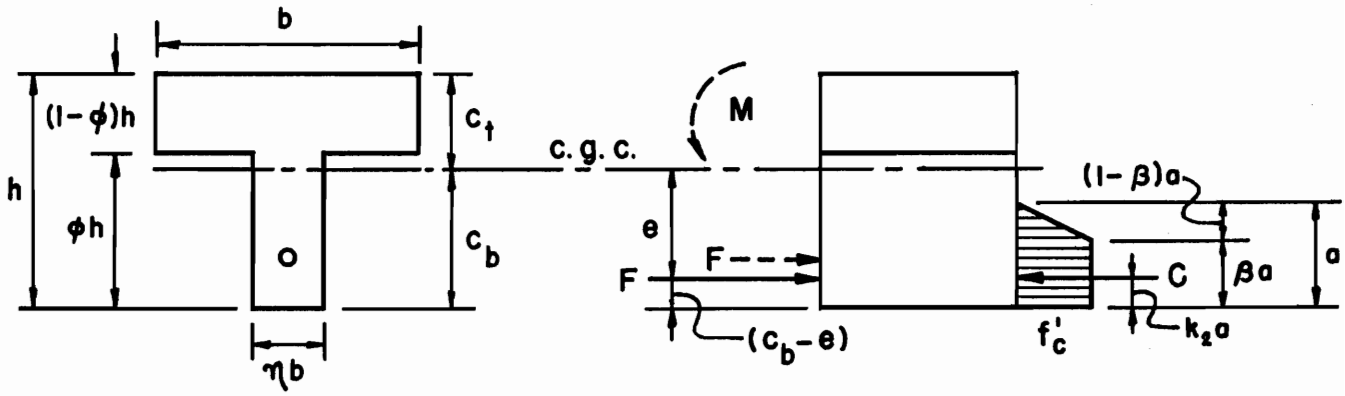

From Jensen's Theory:

$$\beta = \frac{1}{1 + \left[\frac{f'_c}{4000}\right]^2}$$

$$\sum H = 0 \qquad F = C = k_1 a \eta b f'_c$$

where $k_1 = \frac{1 + \beta}{2}$

$$\sum M = 0 \quad c_b - e = k_2 a; \qquad a = \frac{1}{k_2}(c_b - e)$$

where $k_2 = \frac{1 + \beta + \beta^2}{3(1 + \beta)}$

Defining the total cross-sectional area as $A = \gamma bh$ and then substituting, simplifying and rearranging, the ultimate strength is:

$$\frac{F}{Af'_c} = \frac{\eta}{\gamma} \frac{k_1}{k_2}\left[\frac{c_b}{h} - \frac{e}{h}\right] \qquad (3)$$

For rectangular sections:

$$\eta = 1, \quad \gamma = 1, \quad \frac{c_b}{h} = \frac{1}{2}$$

Therefore,

$$\frac{F}{Af'_c} = \frac{k_1}{k_2}\left[\frac{1}{2} - \frac{e}{h}\right] \tag{3a}$$

The limiting case for Equations (3) and (3a) is when $a = \phi h$, from which:

$$\frac{e}{h} = \frac{c_b}{h} - \phi k_2 \tag{4}$$

Then, for $a = \phi h$;

$$\frac{F}{Af'_c} = \frac{\phi \eta}{\gamma} k_1 \tag{5}$$

For the rectangular section, for $a = \phi h = h$:

$$\phi = 1, \quad \eta = 1, \quad \gamma = 1$$

Therefore,

$$\frac{e}{h} = \frac{1}{2} - k_2 \tag{4a}$$

$$\frac{F}{Af'_c} = k_1 \tag{5a}$$

The eccentricity as given by Equation (4a) locates a point which is equivalent to the kern point by the elastic theory. Since k_2 is equal to

0.452 to 0.358 for f'_c equal to 2000 psi to 6000 psi respectively, e/h from Equation (4a) equals 0.048 to 0.142 by ultimate theory, while the kern point by the elastic theory is located at e/h equal to 0.167.

Note that for a given cross section and strength of concrete, Af'_c, $\frac{c_b}{h}$, ϕ, η, γ, k_1, k_2 and β are constants. The ultimate strength curves for this case are shown in Figures 15 through 19.

b. $\phi h \leq a \leq h$ and $\beta a \leq \phi h$

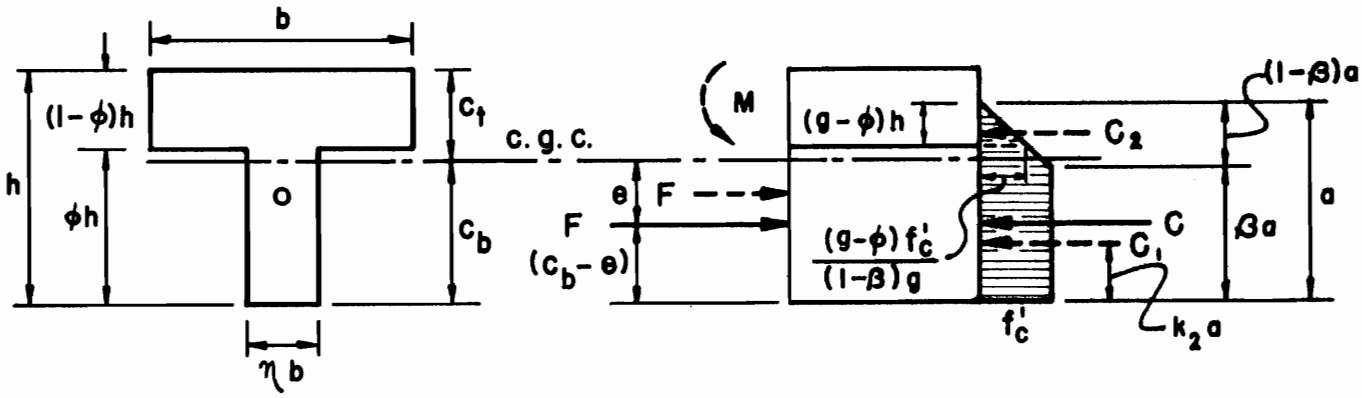

Let $a = gh$ and $A = \gamma bh$

$$C_1 = k_1 a(\eta b) f'_c = k_1 gh\, \eta b f'_c$$

$$C_2 = \frac{1}{2}[(g - \phi)h]\left[\frac{(g - \phi) f'_c}{g(1 - \beta)}\right][b(1 - \eta)] = \frac{(g - \phi)^2}{2g(1 - \beta)}(1 - \eta)\, bhf'_c$$

$$\sum H = 0; \quad F = C = C_1 + C_2$$

Substituting, simplifying, and rearranging, the ultimate strength is:

$$\frac{F}{Af'_c} = \frac{\eta}{\gamma} k_1 g + \left|\frac{1 - \eta}{\gamma}\right| \frac{(g - \phi)^2}{2g(1 - \beta)} \qquad (6)$$

$$\sum M = 0 \qquad F(c_b - e) = C_1 k_2 a + C_2\left(\phi h + \frac{(g - \phi)h}{3}\right)$$

Substituting, simplifying, and rearranging:

$$\frac{e}{h} = \frac{c_b}{h} - \left\{ \frac{\frac{\eta}{\gamma} k_1 k_2 g^2 + \left[\frac{1-\eta}{2\gamma(1-\beta)}\right]\left[\frac{(g-\phi)^2}{g}\right]\left[\frac{g+2\phi}{3}\right]}{\frac{\eta}{\gamma} k_1 g + \left[\frac{1-\eta}{2\gamma(1-\beta)}\right]\left[\frac{(g-\phi)^2}{g}\right]} \right\} \tag{7}$$

k_1 and k_2 are the same as given in paragraph 3 a). For rectangular sections Equations (6) and (7) reduce to Equation (3a). For I sections Equations (6) and (7) are valid for $\phi h \leq a \leq (1-\phi)h$ and $\beta a \leq \phi h$.

Note that for a given cross section and strength of concrete, Af'_c, c_b/h, ϕ, η, γ, k_1, k_2, and β are constants. Therefore for assumed values of g and f'_c, Equation (6) vs. Equation (7) may be plotted and a curve of ultimate F/Af'_c vs. e/h obtained. These curves are shown in Figures 15 through 19.

c. $\phi h \leq a \leq h$ and $\beta a \geq \phi h$

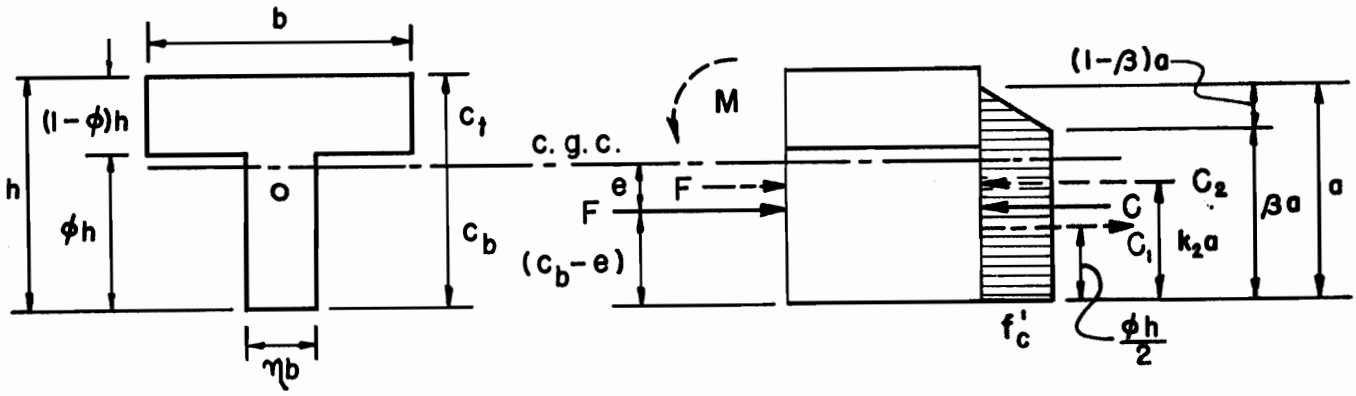

Let a = gh and A, k_1, and k_2 be defined as in paragraphs 3 (a) and c).

$$C_1 = \phi h\, b\, (1 - \eta)\, f'_c \quad ; \qquad \frac{C_1}{A\, f'_c} = \frac{\phi}{\gamma}\,(1 - \eta)$$

$$C_2 = k_1 a b f'_c \quad ; \qquad \frac{C_2}{A\, f'_c} = \frac{1}{\gamma}\, k_1 g$$

$$\Sigma H = 0 : \qquad F = C = C_2 - C_1$$

Substituting, simplifying, and rearranging, the ultimate strength is:

$$\frac{F}{Af'_c} = \frac{1}{\gamma}\, k_1 g - \frac{\phi}{\gamma}\,(1 - \eta) \tag{8}$$

$$\Sigma M = 0 : \qquad F\,(c_b - e) = C_2 k_2 a - C_1 \frac{\phi h}{2}$$

Substituting, simplifying, and rearranging:

$$\frac{e}{h} = \frac{c_b}{h} - \left\{ \frac{1/\gamma\; k_1 k_2 g^2 - \frac{\phi^2}{2\gamma}\,(1 - \eta)}{1/\gamma\; k_1 g - \frac{\phi}{\gamma}\,(1 - \eta)} \right\} \tag{9}$$

For rectangular sections Equations (8) and (9) reduce to Equation (3a). For I sections Equations (8) and (9) are valid for $\phi h \leq a \leq (1 - \phi)h$ and $\beta a \geq \phi h$.

Again Equations (8) and (9) can be plotted for assumed values of g and f'_c and a curve of ultimate F/Af'_c vs. e/h obtained. These curves are shown for the tee, inverted tee, and I sections in Figures 16 through 19.

d. Entire Section in Compression. $a \geq h$ and $\beta a \leq \phi h$.

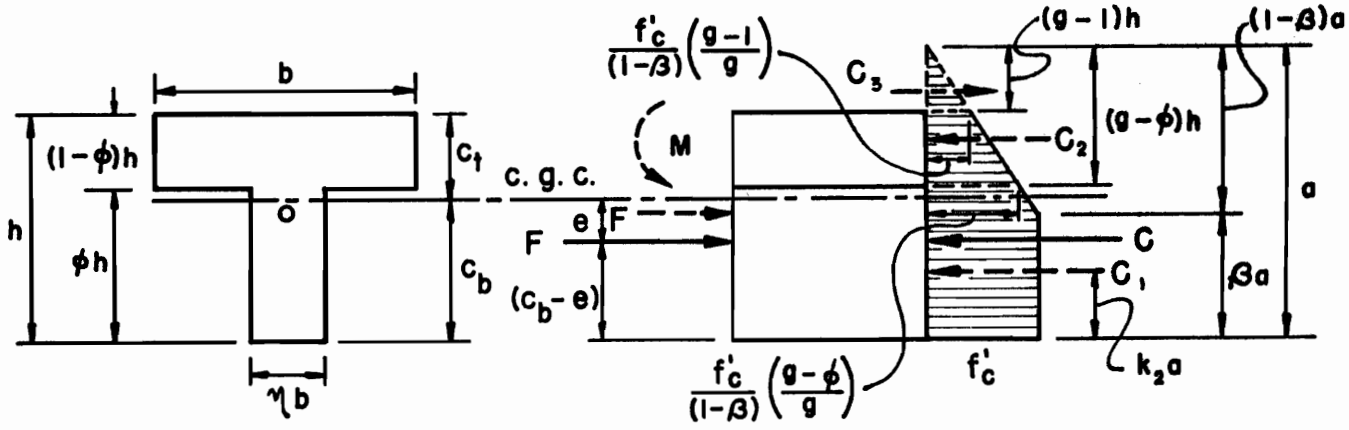

Let $a = gh$ and A, k_1, k_2 be defined as in paragraph 3 a) and b).

$$C_1 = k_1 a \eta b f'_c \; ; \qquad \frac{C_1}{Af'_c} = \frac{\eta}{\gamma} k_1 g$$

$$C_2 = \frac{1}{2}(g - \phi)h\left[\frac{f'_c}{1-\beta}\left(\frac{g-\phi}{g}\right)\right] b(1-\eta) \; ; \; \frac{C_2}{Af'_c} = \left[\frac{1-\eta}{\gamma}\right]\left[\frac{(g-\phi)^2}{2g(1-\beta)}\right]$$

$$C_3 = \frac{1}{2}(g-1)h\left[\frac{f'_c}{1-\beta}\left(\frac{g-1}{g}\right)\right] b \; ; \; \frac{C_3}{Af'_c} = \frac{1}{\gamma}\left[\frac{(g-1)^2}{2g(1-\beta)}\right]$$

$$\Sigma H = 0 : \qquad F = C = C_1 + C_2 - C_3$$

Substituting, simplifying, and rearranging, the ultimate strength is:

$$\frac{F}{Af'_c} = \frac{\eta}{\gamma} k_1 g + \left[\frac{1-\eta}{\gamma}\right]\left[\frac{(g-\phi)^2}{2g(1-\beta)}\right] - \left[\frac{1}{\gamma}\right]\left[\frac{(g-1)^2}{2g(1-\beta)}\right] \tag{10}$$

$$\Sigma M = 0 \qquad F(c_b - e) = C_1 k_2 a + C_2\left(\phi h + \frac{(g-\phi)h}{3}\right) - C_3\left(h + \frac{(g-1)h}{3}\right)$$

Substituting, simplifying, and rearranging:

$$\frac{e}{h} = \frac{c_b}{h} - \left\{ \frac{\frac{\eta}{\gamma} k_1 k_2 g^2 + \left[\frac{1-\eta}{2\gamma(1-\beta)}\right]\left[\frac{(g-\phi)^2}{g}\right]\left[\frac{g+2\phi}{3}\right] - \left[\frac{1}{2\gamma(1-\beta)}\right]\left[\frac{(g-1)^2}{g}\right]\left[\frac{g+2}{3}\right]}{\frac{\eta}{\gamma} k_1 g + \left[\frac{1-\eta}{2\gamma(1-\beta)}\right]\left[\frac{(g-\phi)^2}{g}\right] - \left[\frac{1}{2\gamma(1-\beta)}\right]\left[\frac{(g-1)^2}{g}\right]} \right\} \tag{11}$$

For rectangular sections, Equations (10) and (11) reduce to:

$$\frac{F}{Af'_c} = k_1 g - \frac{(g-1)^2}{2g(1-\beta)} \tag{10a}$$

$$\frac{e}{h} = \frac{1}{2} - \left\{ \frac{k_1 k_2 g^2 - \left[\frac{(g-1)^2}{2g(1-\beta)}\right]\left[\frac{g+2}{3}\right]}{k_1 g - \left[\frac{(g-1)^2}{2g(1-\beta)}\right]} \right\} \qquad (11a)$$

Equations (10) and (11) do not apply to I sections. Expressions for I sections in full compression will not be derived since they are of little practical importance. For inverted tee sections this case will occur only when e/h is small and ϕ is large.

Again Equations (10) and (11) can be plotted for assumed values of g and f'_c and a curve of ultimate F/Af'_c vs. e/h obtained. These curves are shown for the rectangular and tee sections in Figures 15 through 17.

e. Entire Section in Compression $a \geq h$, $\phi h \leq \beta a \leq h$

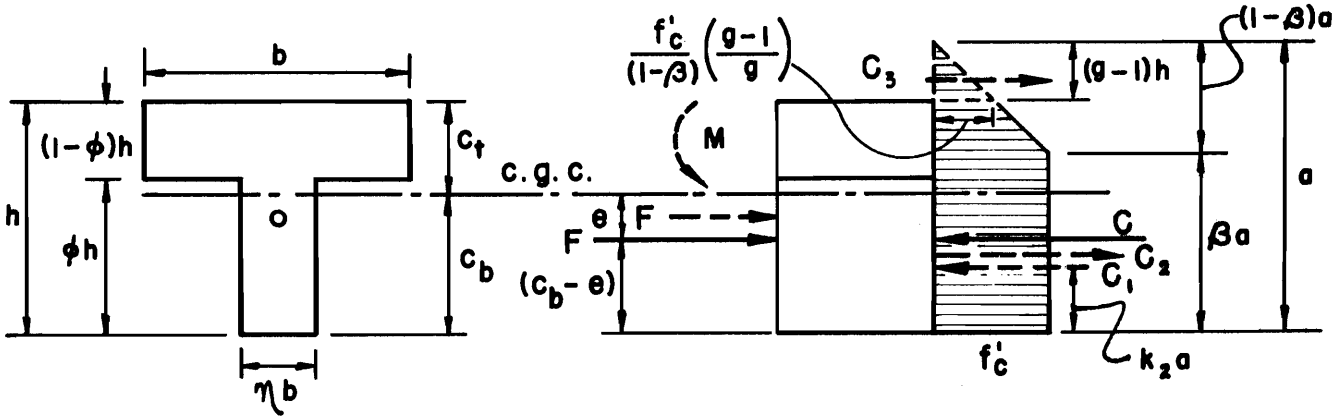

Let $a = gh$ and A, k_1, k_2 be defined as in paragraphs 3a) and b).

$$C_1 = k_1 abf'_c \quad ; \quad \frac{C_1}{Af'_c} = \frac{1}{\gamma} k_1 g$$

$$C_2 = \phi h(1-\eta)bf'_c \quad ; \quad \frac{C_2}{Af'_c} = \frac{\phi}{\gamma}(1-\eta)$$

$$C_3 = \frac{1}{2}(g-1)h\frac{f'_c}{1-\beta}\left(\frac{g-1}{g}\right)b \quad ; \quad \frac{C_3}{Af'_c} = \frac{1}{\gamma}\left[\frac{(g-1)^2}{2g(1-\beta)}\right]$$

$$\Sigma H = 0: \qquad F = C = C_1 - C_2 - C_3$$

Substituting, simplifying, and rearranging, the ultimate strength is:

$$\frac{F}{Af'_c} = \frac{1}{\gamma} k_1 g - \frac{\phi}{\gamma}(1 - \eta) - \frac{1}{\gamma}\left[\frac{(g-1)^2}{2g(1-\beta)}\right] \qquad (12)$$

$$\sum M = 0: \quad F(c_b - e) = C_1 k_2 a - C_2 \frac{\phi h}{2} - C_3\left[h + \frac{(g-1)h}{3}\right]$$

Substituting, simplifying, and rearranging:

$$\frac{e}{h} = \frac{c_b}{h} - \left\{ \frac{\frac{1}{\gamma} k_1 k_2 g^2 - \frac{\phi^2}{2\gamma}(1-\eta) - \left[\frac{1}{2\gamma(1-\beta)}\right]\left[\frac{(g-1)^2}{g}\right]\left[\frac{g+2}{3}\right]}{\frac{1}{\gamma} k_1 g - \frac{\phi}{\gamma}(1-\eta) - \frac{1}{\gamma}\left[\frac{(g-1)^2}{2g(1-\beta)}\right]} \right\} \qquad (13)$$

For rectangular sections, Equations (12) and (13) reduce to Equations (10a) and (11a). Equations (12) and (13) do not apply to I sections.

Equations (12) and (13) can be plotted for assumed values of g and f'_c and a curve of ultimate F/Af'_c vs. e/h obtained. This case, however, is of little practical importance.

4. Expressions for Ultimate Strength of Beams With Mild Steel

It is assumed in this case that the ultimate stress, f'_c, and the ultimate compressive strain, ε_u, of the concrete together with the yield stress, f_y, and yield strain, ε_y, of the steel are known properties of the materials used.

Two types of a failure may be defined. A tension failure occurs when the strain in the steel reaches ε_y before the extreme fiber strain in the concrete reaches ε_u. Once the steel yields the strain and stress in the concrete increases rapidly until finally the concrete exhausts its plasticity and crushes in failure. A compression failure occurs when the extreme fiber strain in the concrete reaches ε_u before the strain in the steel reaches ε_y.

The dividing point between tension and compression failures occurs when ε_y and ε_u are reached simultaneously. This might be called a balanced failure.

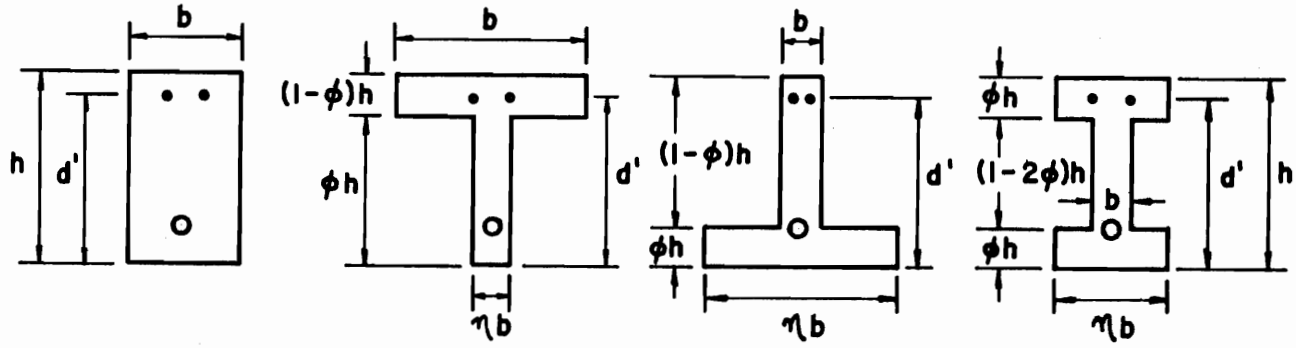

1) Rectangular 2) Tee 3) Inverted Tee 4) I

Cross section properties:

$$A = \gamma bh \; ; \qquad c_t = \delta h$$

$$I = \theta bh^3 \; ; \qquad c_b = (1 - \delta)h$$

Let A_s = Area of mild steel

$$p = \frac{A_s}{A}$$

$$m = \frac{f_s}{f'_c}$$

$$a = gh$$

The following formulae apply to rectangular, tee, inverted tee, and I sections unless otherwise specified.

a. $0 \leq a \leq \phi h$

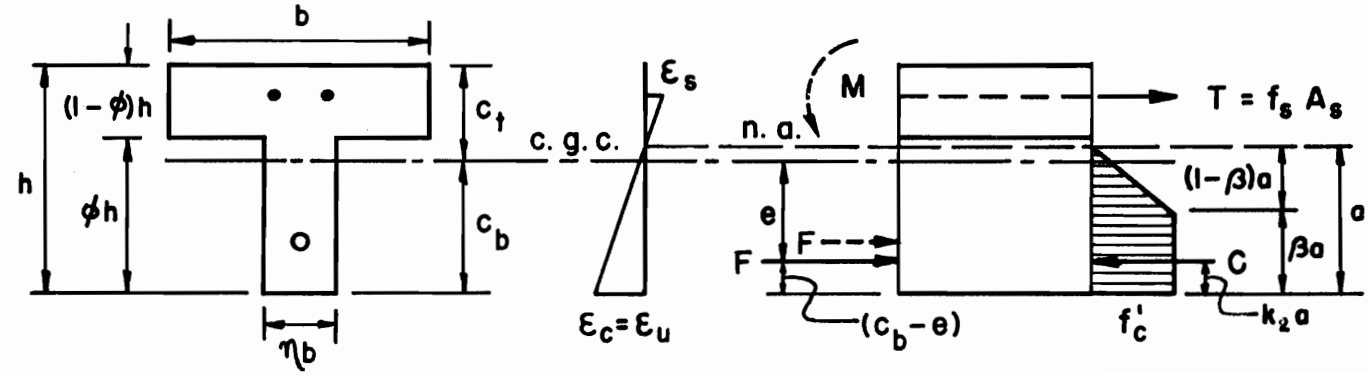

$$C = k_1 a \eta b f'_c \quad ; \quad \frac{C}{Af'_c} = \frac{\eta}{\gamma} k_1 g$$

$$T = A_s f_s = pAmf'_c \quad ; \quad \frac{T}{Af'_c} = pm$$

$$\sum H = 0: \quad F = C - T$$

$$\frac{F}{Af'_c} = \frac{\eta}{\gamma} k_1 g - pm \tag{14}$$

$$\sum M = 0: \quad F(c_b - e) = Ck_2 a - Td'$$

Substituting, simplifying, and rearranging:

$$\frac{e}{h} = \frac{c_b}{h} - \left[\frac{\frac{\eta}{\gamma} k_1 k_2 g^2 - pm \frac{d'}{h}}{\frac{\eta}{\gamma} k_1 g - pm} \right] \tag{15}$$

For rectangular sections:

$$\eta = 1; \quad \gamma = 1; \quad \frac{c_b}{h} = \frac{1}{2}$$

Therefore,

$$\frac{F}{Af'_c} = k_1 g - pm \tag{14a}$$

$$\frac{e}{h} = \frac{1}{2} - \left[\frac{k_1 k_2 g^2 - pm \frac{d'}{h}}{k_1 g - pm} \right] \tag{15a}$$

From the geometry of strains:

$$\frac{d'}{\varepsilon_u + \varepsilon_s} = \frac{gh}{\varepsilon_u}$$

$$g = \left[\frac{\varepsilon_u}{\varepsilon_u + \varepsilon_s} \right] \frac{d'}{h} \tag{16}$$

$$\varepsilon_s = \left[\frac{d'/h - g}{g}\right] \varepsilon_u \qquad (17)$$

Equation 17 is valid for $\varepsilon_s < \varepsilon_y$.

1. Balanced Failure:

$$\varepsilon_s = \varepsilon_y \; ; \quad \varepsilon_c = \varepsilon_u \; ; \quad f_s = f_y \; ; \quad g = g_o$$

$$g_o = \left[\frac{\varepsilon_u}{\varepsilon_u + \varepsilon_y}\right] \frac{d'}{h} \qquad (16a)$$

Using g_o from Equation (16a), $\frac{F}{Af'_c}$ and $\frac{e}{h}$ can be calculated from Equations (14) and (15).

2. Tension Failure:

$g < g_o$; $\varepsilon_s = \varepsilon_y$ reached first; then $\varepsilon_c = \varepsilon_u$ reached;

$f_s = f_y$

For any assumed value of g and given material properties, F/Af'_c and e/h can be calculated using Equations (14) and (15).

3. Compression Failure:

$$g > g_o \; ; \quad \varepsilon_c = \varepsilon_u \; ; \quad \varepsilon_s < \varepsilon_y \; ; \quad f_s < f_y$$

For any assumed value of g and given material properties, F/Af'_c and e/h can be calculated using Equations (14) and (15).

Using a procedure similar to that outlined above, ultimate strength curves of F/Af'_c vs. e/h may be plotted for any section with mild steel.

Note that Equations (16), (17), and (16a) are valid for any cross section. These equations were obtained from the geometry of strains and are independent of the shape of the cross section.

For each cross section studied and for various locations of the neutral axis, equations analogous to Equations (14) and (15) must be derived. As the shape of the section becomes more complex the equations will also become algebraically more complex. Given below are these equations which apply to rectangular, tee, inverted tee, I and box sections which were derived in a manner similar to the above case.

b. $\phi h \leq a \leq \frac{d'}{h}$ and $\beta a \leq \phi h$

$$\frac{F}{Af'_c} = \frac{\eta}{\gamma} k_1 g + \left[\frac{1-\eta}{\gamma}\right]\left[\frac{(g-\phi)^2}{2g(1-\beta)}\right] - pm \qquad (18)$$

$$\frac{e}{h} = \frac{c_b}{h} - \left\{\frac{\frac{\eta}{\gamma} k_1 k_2 g^2 + \left[\frac{1-\eta}{2\gamma(1-\beta)}\right]\left[\frac{(g-\phi)^2}{g}\right]\left[\frac{(g+2\phi)}{3}\right] - pm\,\frac{d'}{h}}{\frac{\eta}{\gamma} k_1 g + \left[\frac{1-\eta}{2\gamma(1-\beta)}\right]\left[\frac{(g-\phi)^2}{g}\right] - pm}\right\} \qquad (19)$$

For I and box sections Equations (18) and (19) are valid if $\phi h \leq a \leq (1-\phi)h$ and $\beta a \leq \phi h$.

c. $\phi h \leq a \leq \frac{d'}{h}$ and $\beta a \geq \phi h$

$$\frac{F}{Af'_c} = \frac{1}{\gamma} k_1 g - \frac{\phi}{\gamma}(1-\eta) - pm \qquad (20)$$

$$\frac{e}{h} = \frac{c_b}{h} - \left\{\frac{\frac{1}{\gamma} k_1 k_2 g^2 - \frac{\phi^2}{2\gamma}(1-\eta) - pm\,\frac{d'}{h}}{\frac{1}{\gamma} k_1 g - \frac{\phi}{\gamma}(1-\eta) - pm}\right\} \qquad (21)$$

For I and box sections Equations (20) and (21) are valid if $\phi h \leq a \leq (1 - \phi)h$ and $\beta a \geq \phi h$.

For rectangular sections Equations (18) through (21) reduce to Equations (14a) and (15a). Equations (18) through (21) are used with Equations (16), (17), and (16a) in the same manner as Equations (14) and (15) to obtain ultimate strength curves of F/Af'_c vs. e/h.

V. TEST RESULTS

1. General Behavior

The fourteen beams tested behaved essentially as predicted by the theory. The loading sequence for beams B1A, B1B, B3B, B3C, B5B, and B5C, all of which had no mild steel, was selected so that the theoretical ultimate strength would be greater than the cracking strength and therefore no sudden failure should occur at cracking. Even though initial cracking occurred at relatively low loads these beams did not show any major signs of distress until much heavier loads had been introduced. Tensile cracks became larger, with one crack predominating, as the external loads, and therefore the external moments were increased. Final failure occurred when the cracks had propagated down to a level where the remaining concrete section could not sustain the eccentric prestress force in compression and a final crushing of the concrete took place. Just prior to failure, the width of the tensile cracks at the top of the beams measured as much as 1/4 in. across.

The loading sequence for beams B1C, B3A, and B5A, all of which had no mild steel, was selected so that the theoretical ultimate strength was less than the cracking strength, thus yielding a sudden failure. In these tests it was found that once the beam experienced a major tensile crack it failed suddenly and completely.

Beams B2A, B2B, B2C, B4A, and B6A all had mild steel in the top. Each beam had an artificial crack, approximately 2 in. deep, cast in it at midspan. No cracking strengths were therefore obtained. As the external loads were increased fine hairline cracks developed over the middle portion of the beam. No appreciable downward shifting of the neutral axis was indicated by the strain readings until the mild steel reinforcement yielded after which the cracks in the top became larger and larger as the neutral axis moved

downward. Final failure occurred by crushing of the concrete at the bottom. The maximum center deflection obtained for these beams was much greater than for the second group described. This was expected and indicated the high energy absorbing capacity of these beams. This asset could be important under impact loads during erection.

From the experimental data collected during each beam test, the following items were obtained:

(a) Photograph of beam after ultimate failure.

(b) Load (F and M) vs center deflection curve.

(c) Load (F and M) vs strain curves, for each gage level.

(d) Stress in top concrete fiber at cracking.

(e) Strain in bottom concrete fiber at ultimate.

(f) F/Af'_c and e/h at cracking and at ultimate.

Wherever possible, the above experimental results were compared with corresponding theoretical values.

2. Photographs of Beams After Ultimate Failure

Photographs of beams after ultimate failure are shown in Figures 20, 21, and 22. In comparing the crack patterns at failure for the rectangular beams shown in Figure 20, beams without mild steel, (B1A, B1B, and B1C) had one large major crack while for beams with mild steel, (B2A, B2B, and B2C) the cracks were smaller and were spread over a larger portion of the beam.

The typical failure of crushing of the bottom fibers of the beams is evident in all cases.

3. Load-Deflection Curves

Theoretical deflections were computed using the elastic theory based on the uncracked section. Moduli of elasticity shown in Table I together with the gross moments of inertia of the cross-sections were used in these computations.

Theoretical and experimental results for each of the beams are shown in Figures 23 through 36. For beams B1C, B3A, and B5A, which were subjected to a combination of F and M such that the theoretical ultimate strength was less than the cracking strength, it can be seen that the experimental values agree rather closely with the theoretical values and further that the maximum deflection prior to failure is very small. For the other beams the load-deflection curves generally verify theoretical values up to cracking. After cracking the rate of increase of deflection was lower for beams with mild steel than for beams without mild steel. Beams with mild steel, in most cases, were able to develop the largest deflections before ultimate failure.

4. Load-Strain Curves

Experimental load-strain curves were plotted to study the general behavior of each beam. A linear relation between load and strain existed generally for all beams up to cracking after which the indicated strain at the top of the beam either increased or decreased more rapidly with load indicating that a crack had occurred either inside or outside of limits of the gage. The progression of neutral axis downward as the load was increased could be followed from these curves. Some of the gages indicated a change from compression to tension strain as the neutral axis moved down through them.

The assumption that plane sections remain plane up to the ultimate was checked by plotting strain distributions for each beam at various stages of loading. These plots verified the assumption.

Load-strain curves are shown in Figures 37 through 50.

5. Stress in Top Concrete Fiber at Cracking

In Table V values of top fiber stress at cracking are given for each beam. These stresses were computed by the elastic theory using the experimental values obtained for F/Af'_c and e/h at cracking. No stresses at crack-

ing are given for beams with mild steel since as mentioned earlier these beams had an artificial crack cast into them at midspan to insure yielding of the steel at the gage location.

A comparison of the stresses at cracking with the modulus of rupture obtained from control specimens indicates differences up to about 20% for some beams.

6. Strain in Bottom Concrete Fiber at Ultimate

Also shown in Table V are values of the strain in the bottom concrete fiber at ultimate failure for each beam. These values varied from 3250 to 4800 micro inches of strain and averaged 3700 micro inches for the beam tested. This value of 3700 was adopted as the ultimate concrete strain for use in plotting the theoretical curves of F/Af'_c vs e/h.

7. F/Af'_c and e/h at Cracking and Ultimate

These values are also given in Table V. It is noted that f'_c and f'_t varied considerably for the beams. In order to compare these values with the theoretical values given in the curves of Figures 51, 52, and 53, the test values were adjusted to a common value of $f'_c = 4000$ psi, and $f'_t = .12f'_c = 480$ psi. This was accomplished in the following manner; (a) the theoretical values of the cracking and ultimate strengths were calculated for the actual f'_c, and f'_t, and e/h values of the test specimen using the proper equations, (b) the theoretical values of the cracking and ultimate strengths were calculated for $f'_c = 4000$ psi, $f'_t = 480$ psi, and the e/h values obtained from the test, (c) the adjusted test values for cracking and ultimate strength were then obtained by multiplying the actual test values by the ratio of (b) to (a).

The adjusted test values have been plotted on Figures 51, 52, and 53 and may be compared with the theoretical curves. The agreement is generally

good, indicating that for most practical purposes, the theoretical curves can be used to obtain a good estimate of the cracking and ultimate strengths of beams at transfer for various eccentricities of prestress force.

VI. DISCUSSION AND CONCLUSIONS

Both analytical and experimental findings clearly indicated that divergent factors of safety and various modes of failure will be obtained if a fixed value of allowable tensile stress at transfer is used in design as is usually done in present practice. For example with a fixed allowable tensile stress of say $0.05\ f'_c$, the factor of safety on the ultimate failure would range from barely higher than 1.0 to 4.0 or more depending upon (a) the shape and proportions of the section; (b) the eccentricity ratio, e/h; (c) the prestress ratio, F/Af'_c; (d) the amount and location of mild steel.

The effect of shape on the ratio of ultimate to cracking strengths is indicated in Figures 54 and 55, assuming that no mild steel is added to the tensile side. The shapes considered in these figures are those for which Figure 15 through Figure 19 were drawn.

In Figure 54, it is assumed that the prestressing force F is increased while the eccentricity is kept constant. The ratio of the force F producing ultimate failure of the section to that producing cracking is then plotted along the ordinate axis. This is done for various shapes and for various values of eccentricity ratios. Figure 54 is useful for many purposes. For example, it can be seen that the prestress F required for failure of the inverted tee section is about 3.3 times that required for cracking, when the eccentricity ratio e/h is around 0.23. It can also be observed that for the I section, ultimate failure and cracking will occur simultaneously for $e/h = 0.33$ and also for $e/h = 0.45$.

In Figure 55, it is assumed that the prestress F remains constant in magnitude but its eccentricity is varied. The ratio of the eccentricity producing ultimate failure to that producing cracking is then plotted along the ordinate axis. Again, many observations can be made from Figure 55. For example, with a prestress ratio $F/Af'_c = 0.10$, cracking and ultimate failure would occur simultaneously for the thin-flange tee section, but the eccentricity at cracking will have to be increased by about 28% to produce ultimate failure in the thick-flange tee section.

It is evident from Figures 54 and 55 that the margin of safety between cracking and ultimate will differ considerably depending upon the type of section and the magnitude and location of F. The presence of mild steel and its amount will further affect the ultimate strength, although that is not described by Figures 54 and 55.

The desired value of the factor of safety will vary with each situation and will depend on such factors as the possibility of adverse external moments, the seriousness of cracking, the chances of misplacement of the tendons, conditions of continuity, possibility of overtensioning, etc. It is perhaps best not to specify a fixed factor of safety to cover all conditions. The choice of a desirable factor of safety should be left to the judgement of the engineer, who in turn must understand the behavior of beams at transfer.

Analytical studies made on the behavior of I, box sections, and inverted tee sections indicated that for these sections, assuming no mild steel is provided, once cracking has occurred the crack may rapidly progress downward to the bottom of the web. While these sections have high ultimate strengths at transfer because of the large compression areas available in their bottom flanges, the appearance of large cracks would be serious and might result in a shear failure of the beam.

Although only 14 beams were tested, the range of practical values for prestress and eccentricity for rectangular and tee sections were included in the test program. The following conclusions are advanced on the basis of the results of the theoretical and experimental studies:

1. The cracking strength of rectangular and tee shaped concrete sections under excessive eccentric prestress can be evaluated by the elastic theory using the modulus of rupture of concrete, f'_t, as a measure of the starting of cracks. The combinations of prestress ratio, F/Af'_c and eccentricity ratio, e/h, which will produce cracking are not very sensitive to a change in modulus of rupture, f'_t.
2. The ultimate strength of rectangular or tee shaped concrete sections at transfer can be predicted using an ultimate theory based on the "Jensen stress block".
3. The camber of concrete beams at transfer can be computed by the elastic theory provided there has been no cracking. It is difficult to choose a proper value for the modulus of elasticity for long time loading. However, for short duration effects, the use of E_c obtained from a standard test on a 6 x 12 in. cylinder will yield satisfactory results.
4. For sections without mild steel, cracking and ultimate strength curves, such as shown in Figures 15 through 19, will intersect at two locations. The two intersections define what might be called "critical eccentricity ratios" at which the cracking and ultimate strengths are equal.
5. For e/h less than the lower critical ratio the beam will never crack, but will fail under compression. This case is seldom encountered in practice.

6. For e/h greater than the higher critical ratio, an ultimate compression failure will occur immediately following the cracking of the beam. This condition must be avoided and whenever there is a possibility of e/h approaching this value, mild steel must be used on the tension side existing at transfer.

7. For e/h values between the two critical ratios, the beam will crack first, but will not rupture completely until the prestress or the eccentricity or both are further increased. The factor of safety of the beam between cracking and ultimate will vary with the e/h ratio and the F/Af'_c ratio. The factor of safety of beams without mild steel is lowest for e/h values near the critical values. By plotting cracking and ultimate strength curves for any particular section, the factor of safety available for any eccentricity ratio can be readily determined.

8. The addition of a nominal amount of mild steel in the beam, on the tensile side existing at transfer, increases the factor of safety and will prevent a sudden failure from occurring. It will reduce the deflections of the beam after cracking, but will enable it to experience larger deflections (larger energy absorption capacity) before ultimate failure. The desired amount of mild steel will depend upon the given conditions.

9. The conventional practice of specifying a fixed allowable tensile stress at transfer will yield widely divergent factors of safety. Proper design should take into account the behavior and ultimate strength of beams at transfer as presented in this report.

TABLE I

SIEVE ANALYSES OF AGGREGATES

Kind of Aggregate	PERCENTAGE RETAINED ON SIEVE									Fineness Modulus
	3/4 in.	1/2 in.	3/8 in.	No. 4	No. 8	No. 16	No. 30	No. 50	No. 100	
Sand				0	14	45	72	91	98	3.20
Gravel	3	39	60	96						6.59

Average of 8 samples of sand and 8 samples of gravel.

TABLE II

PROPERTIES OF CONCRETE MIXES

Test Specimen	Mix by weight [a] C : S : G	Water/Cement by wt,	gals/sack	Cement Factor Sacks/cu.yd.	Kelly Ball Penetration in.	Comp. Strength f'c psi	Mod. of Rupture f't psi	Mod. of Elast.[b] E_c psi
B1A	1 : 1.78 : 2.93	0.44	4.96	7.0	2.7	4901	530	3.23×10^6
B1B	1 : 1.78 : 2.93	0.44	4.96	7.0	2.4	5492	602	3.29
B1C	1 : 1.78 : 2.93	0.44	4.96	7.0	2.4	4724	488	3.18
B2A	1 : 2.17 : 3.20	0.49	5.52	6.3	2.2	3849	521	2.63
B2B	1 : 2.17 : 3.20	0.49	5.52	6.3	2.5	3478	506	2.61
B2C	1 : 2.17 : 3.20	0.49	5.52	6.3	2.3	3770	472	2.64
B3A	1 : 2.17 : 3.20	0.49	5.52	6.3	2.2	3920	474	3.26
B3B	1 : 2.17 : 3.20	0.49	5.52	6.3	2.4	3826	515	3.19
B3C	1 : 2.17 : 3.20	0.49	5.52	6.3	2.3	3932	475	2.82
B4A	1 : 2.17 : 3.20	0.49	5.52	6.3	2.1	3470	493	3.06
B5A	1 : 2.17 : 3.20	0.49	5.52	6.3	2.3	4007	557	3.25
B5B	1 : 2.17 : 3.20	0.49	5.52	6.3	2.2	4180	594	3.19
B5C	1 : 2.17 : 3.20	0.49	5.52	6.3	2.1	3950	605	3.13
B6C	1 : 2.17 : 3.20	0.49	5.52	6.3	2.3	4956	664	3.17

a. Saturated surface dry. Santa Cruz Type I cement; Elliot S.E. Sand; and Elliot 3/4 in. gravel used in all mixes.

b. Secant modulus of elasticity at 1000 psi, from 6 x 12 in. cylinder tests.

TABLE III

PROPERTIES OF 1/4 IN. DIAMETER STEEL PRESTRESSING WIRE

Sample		Proportion Limit $f_{p.l.}$	Yield Point[a] f_y	Ultimate Strength f_u	Modulus of Elasticity[b] E_s	% Elongation in 10 in.
No.	Lot[c]	ksi	ksi	ksi	psi	%
1		151	227	252	26.8×10^6	4.0
2	I	140	230	252	27.1	2.4
3		145	223	252	26.4	2.0
4		152	207	246	26.1	6.4
5		147	204	243	26.2	5.5
6	II	130	212	246	25.3	5.7
7		157	217	256	26.7	5.0

a. As measured by 0.2% offset.

b. Up to proportional limit.

c. Wire was purchased in two lots, I and II.

TABLE IV

PROPERTIES OF 1/2 IN. DIAMETER INTERMEDIATE GRADE STEEL ASTM A-305 BARS

Beam	Yield Strength f_y ksi	Ultimate Strength f_u ksi	Modulus of Elasticity E_s psi	% Elongation in 8 in. %
B2A	51.0 47.0	78.0 72.4	31.8×10^6 28.6	20.8 21.9
B2B	48.0 45.9	73.6 71.1	28.1 27.2	19.4 19.0
B2C	47.2 48.5	79.9 78.3	30.1 --	22.0 --
B4A	51.2 46.3	78.6 73.1	29.8 27.3	20.0 19.5
B6A	49.1 49.4	81.5 80.7	-- --	17.9 22.5

TABLE V

TEST RESULTS

Beam No.	Gross Concrete Area A in^2	Comp. Strength f'_c psi	Mod. of Rupture f'_t psi	Stress in Top Fiber at Cracking psi	Strain in Bottom Fiber at Ultimate Micro in Per in.	Cracking		Ultimate	
						F/Af'_c	e/h	F/Af'_c	e/h
B1A	120	4901	530	482	4800	0.0660	0.415	0.0686	0.488
B1B	120	5492	602	436	3600	0.0527	0.418	0.1210	0.436
B1C	120	4724	488	503	--[a]	0.0302	0.755	0.0302	0.758
B2A	120	3849	521	--[b]	3300	--	--	0.0875	0.965
B2B	120	3478	506	--[b]	4200	--	--	0.1910	0.600
B2C	120	3770	472	--[b]	3250	--	--	0.2440	0.530
B3A	126	3920	474	427	--[a]	0.0665	0.717	0.0665	0.717
B3B	126	3826	515	499	3400	0.1155	0.578	0.1155	0.602
B3C	126	3932	475	546	3700	0.1265	0.570	0.1400	0.570
B4A	126	3470	493	--[b]	4000	--	--	0.1560	0.779
B5A	182	4007	557	496	--[a]	0.0450	0.731	0.0450	0.731
B5B	182	4180	594	500	3500	0.0601	0.584	0.0601	0.658
B5C	182	3950	605	500	3400	0.0635	0.584	0.0960	0.584
B6A	182	4956	664	--[b]	3800	--	--	0.1000	0.688

a. Sudden failure, cracking strength less than ultimate strength.

b. Beams with mild steel in top had artifical crack cast in top at midspan, therefore no cracking strength was obtained.

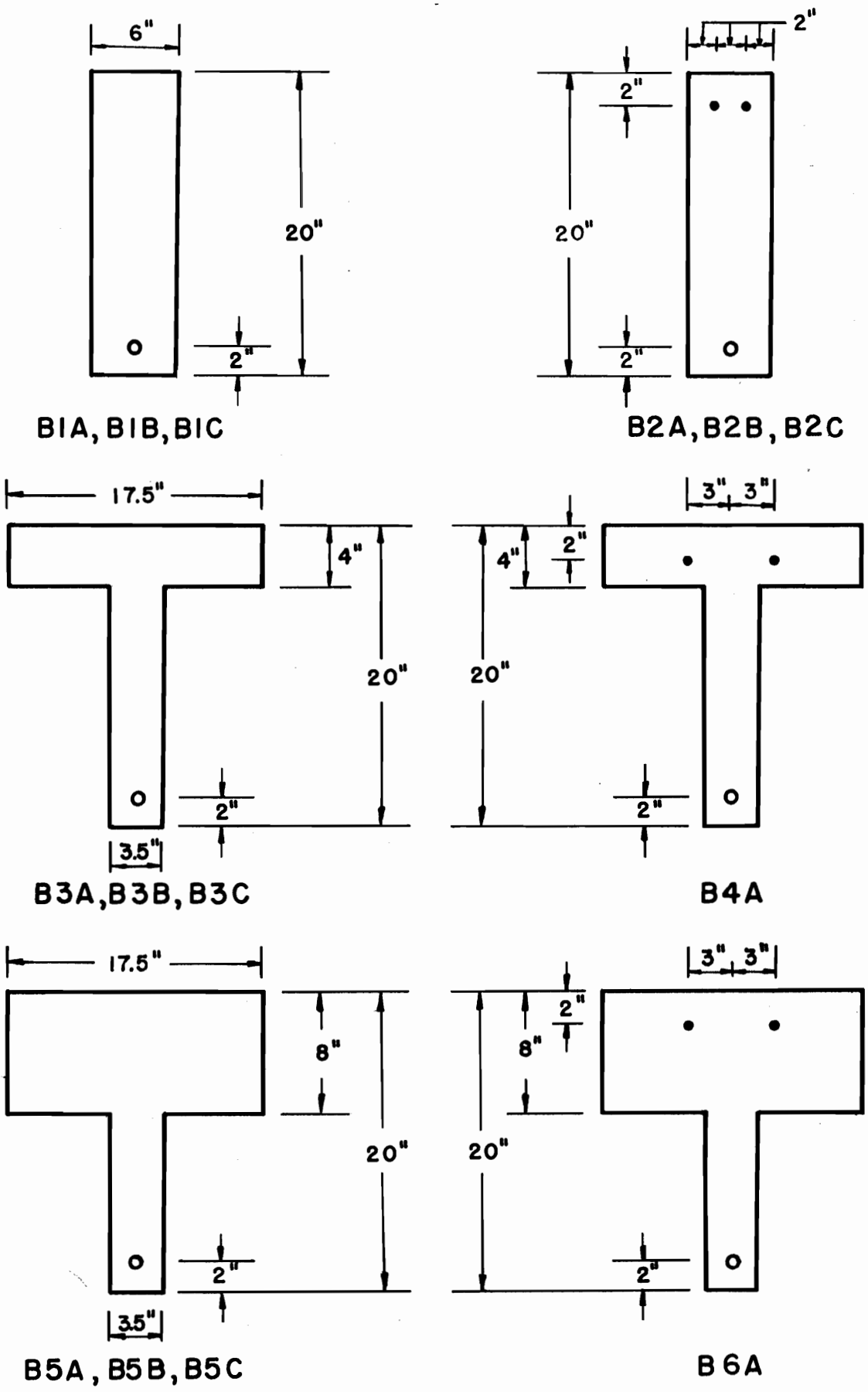

FIG. 1 SECTION PROPERTIES AT MIDSPAN OF TEST SPECIMENS

o — Prestressing Cable; 12—1/4" Dia. Wires For All Cases

• — Mild Steel; No. 4 Deformed Bars In All Cases

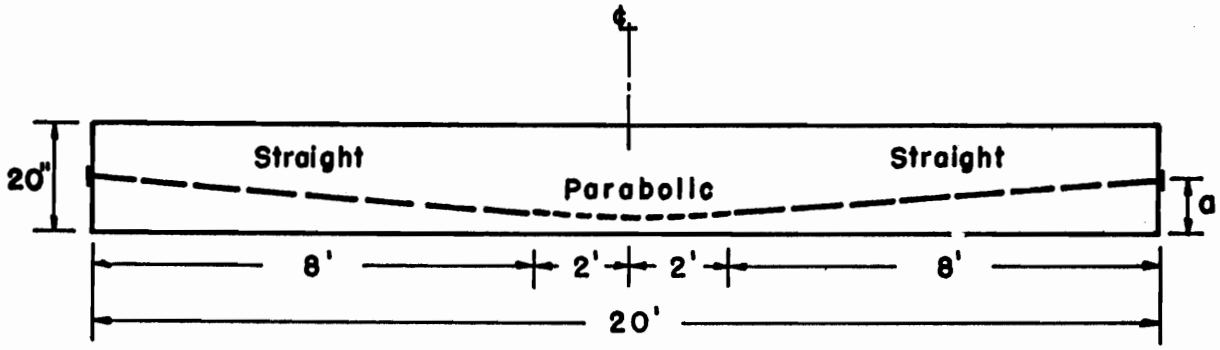

FIG. 2A ELEVATION OF CABLE LAYOUT FOR ALL BEAMS

Dimension "a"	
B-1 & B-2	10.00"
B-3 & B-4	13.56"
B-5 & B-6	13.68"

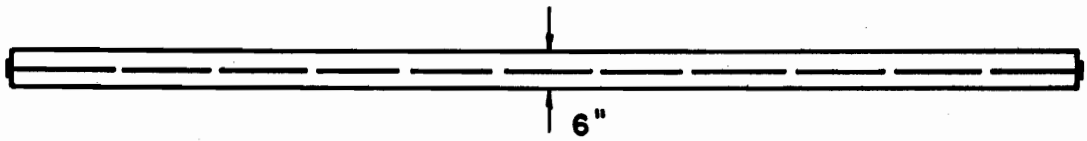

FIG. 2B PLAN VIEW OF B1A, B1B, B1C, B2A, B2B, AND B2C

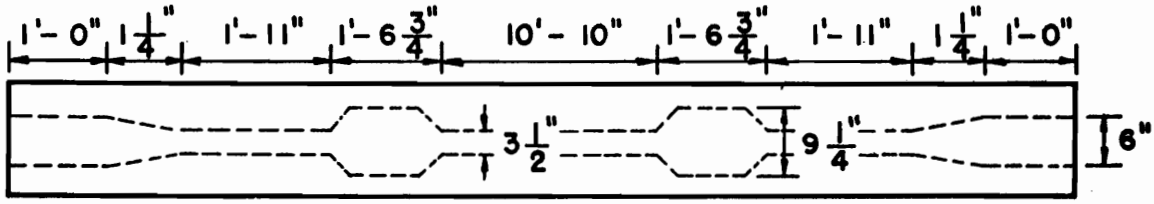

FIG. 2C PLAN VIEW OF B3A, B3B, B3C, AND B4A

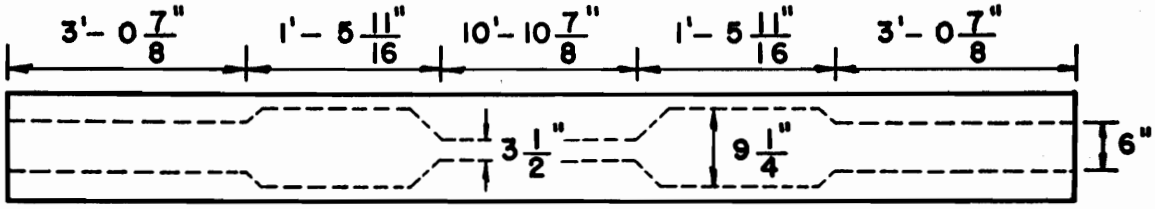

FIG. 2D PLAN VIEW OF B5A, B5B, B5C, AND B6A

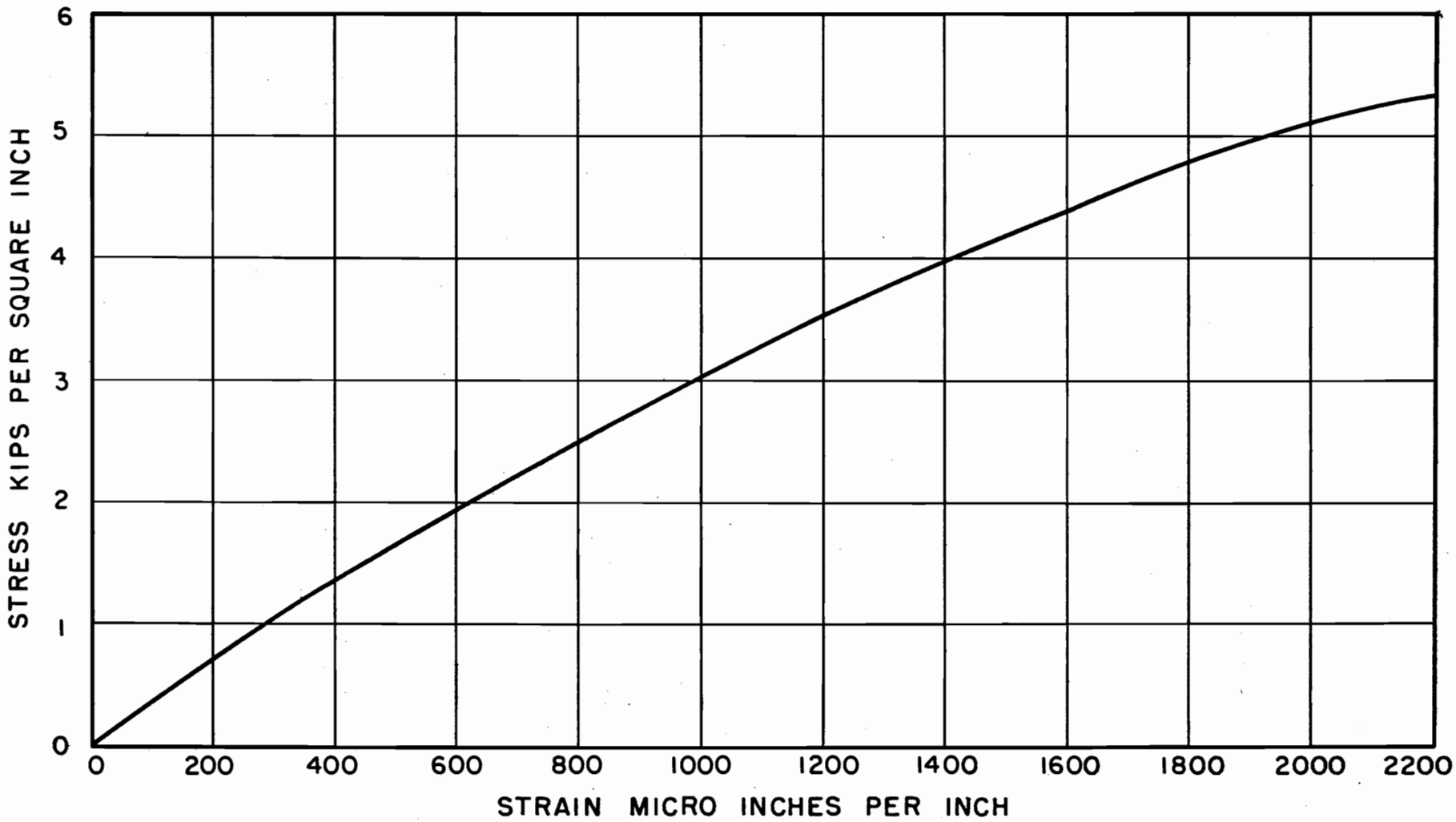

FIG. 3 TYPICAL STRESS STRAIN FOR CONCRETE. 6 x 12 IN. CYLINDER AT AGE OF 14 DAYS

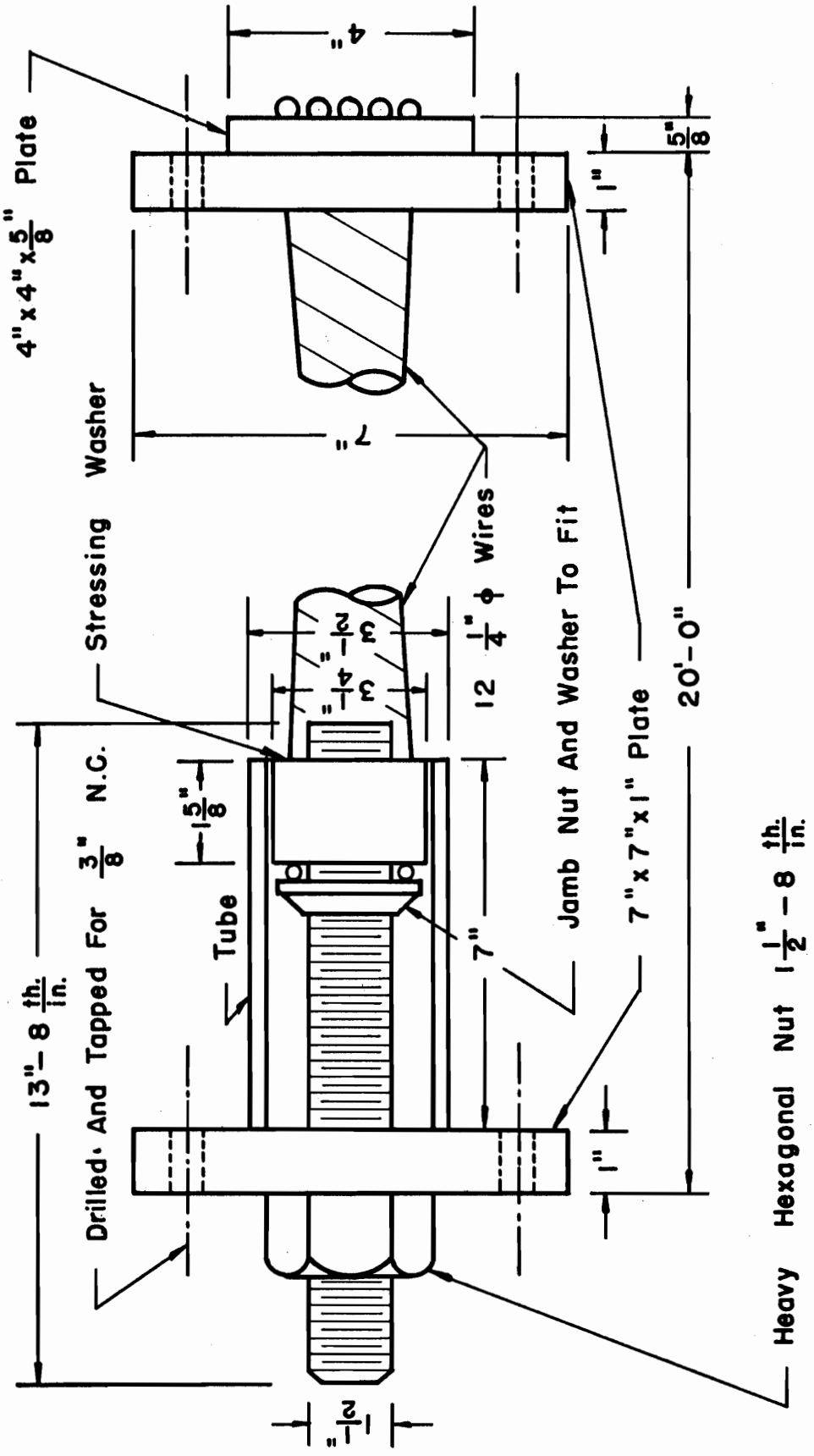

FIG. 4 DETAILS OF 12 WIRE PRESTRESSING CABLE

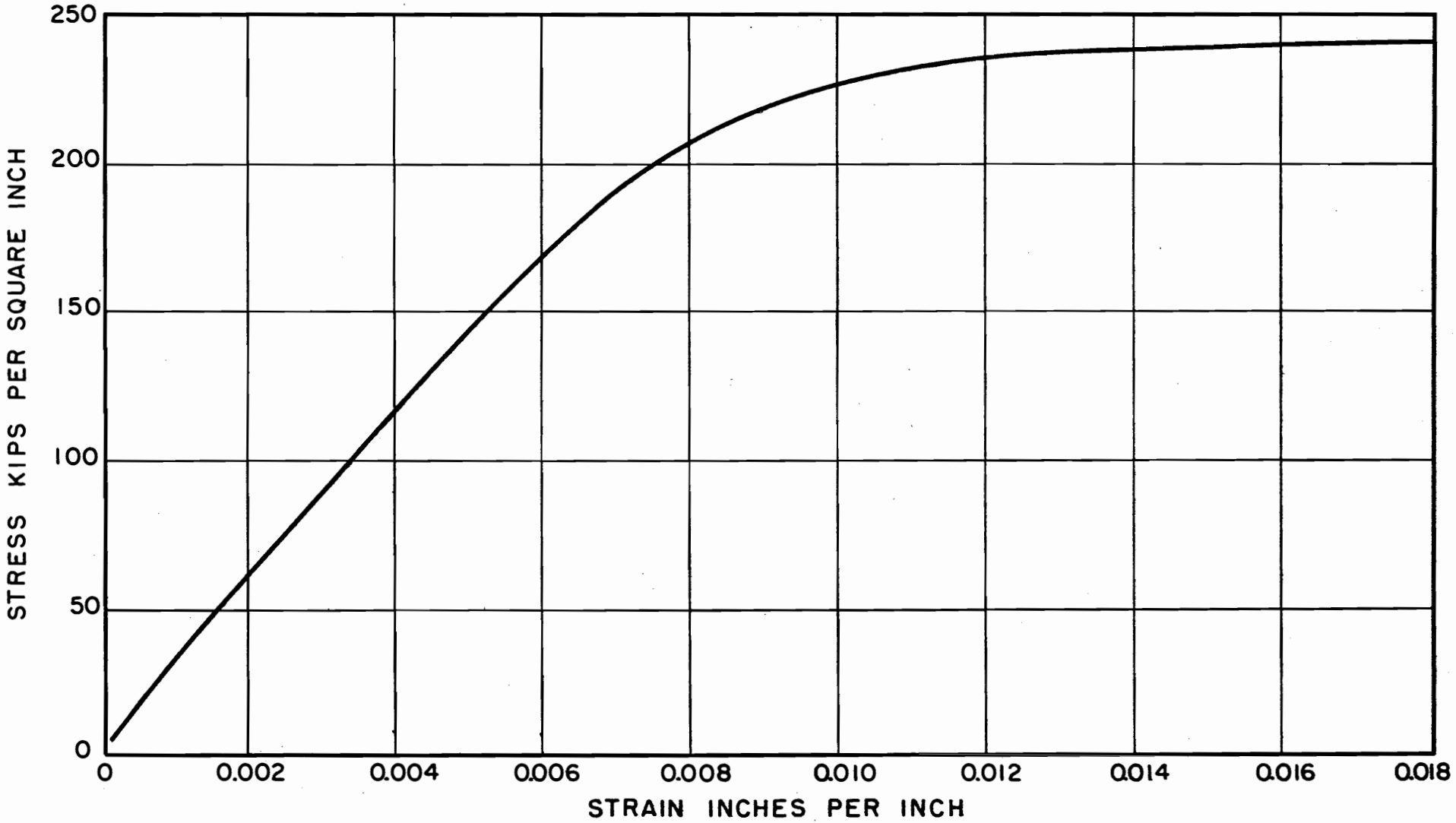

FIG. 5 TYPICAL STRESS STRAIN CURVE FOR 1/4 IN. DIA. PRESTRESSING STEEL WIRE

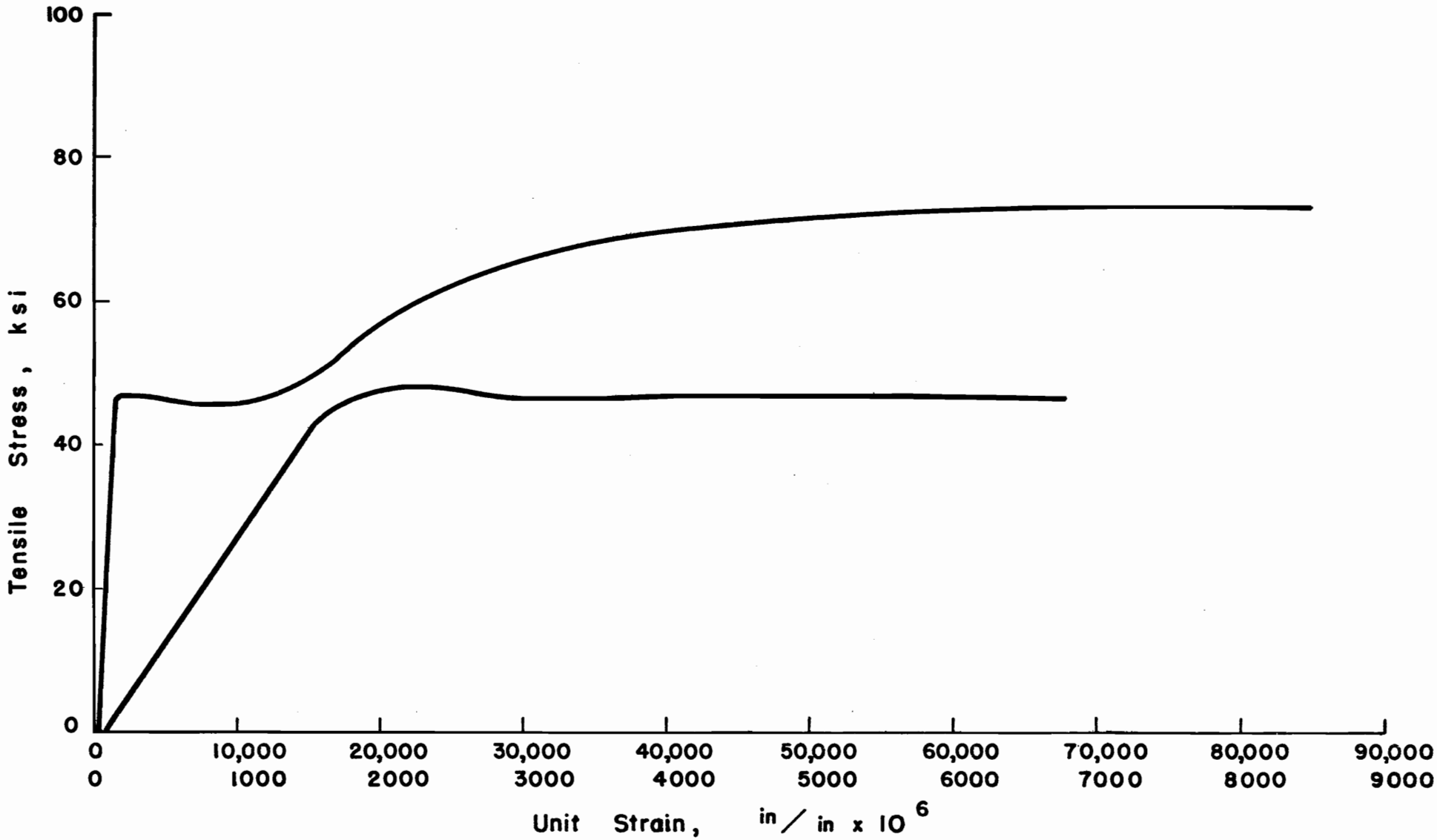

FIG. 6 TYPICAL STRESS-STRAIN CURVE FOR 1/2 in. DIAMETER, INTERMEDIATE GRADE, STEEL BAR

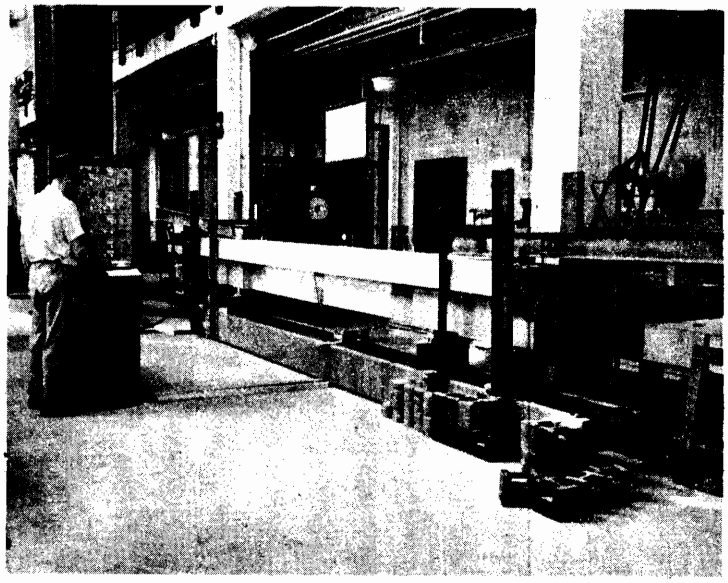

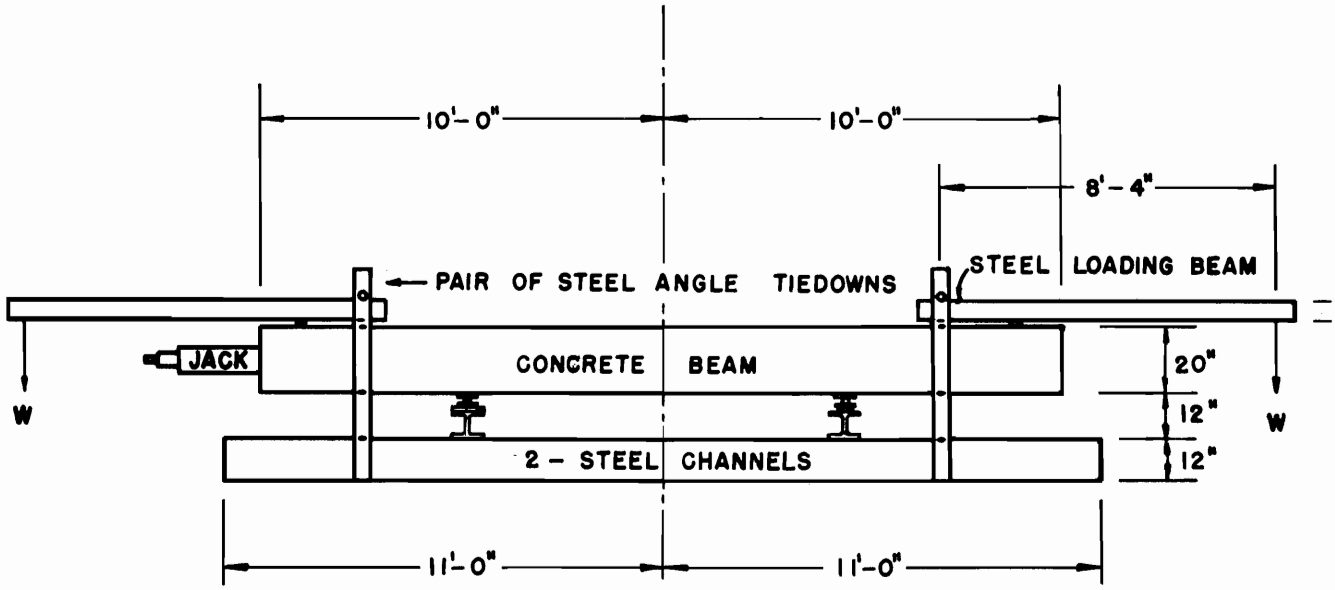

FIG. 7 FIRST LOADING ARRANGEMENT

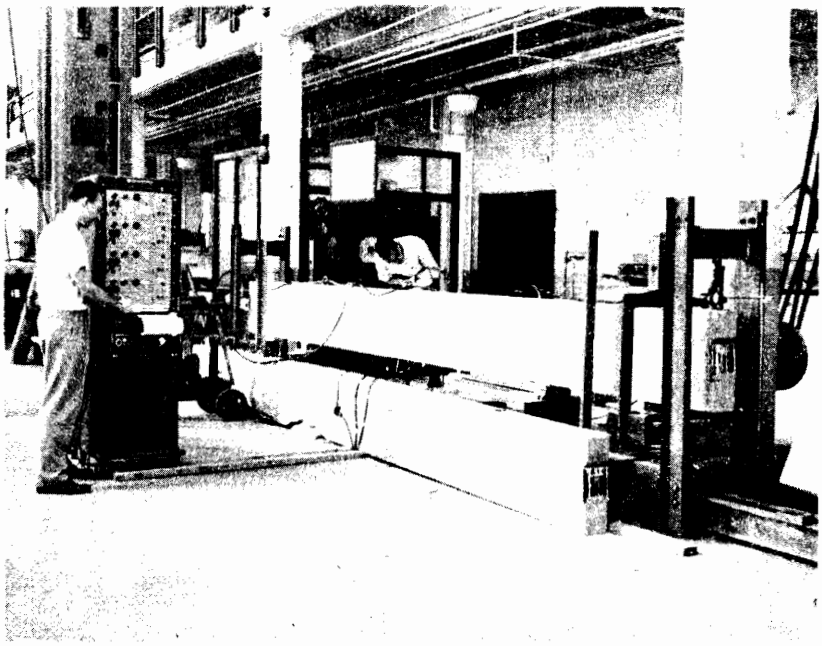

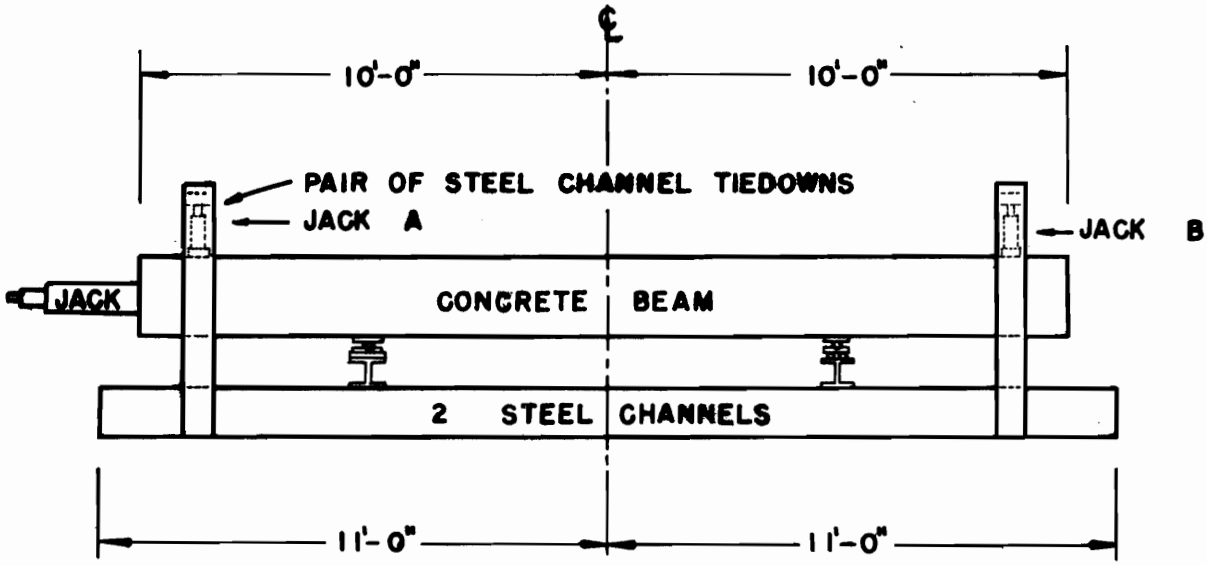

FIG. 8 SECOND LOADING ARRANGEMENT

Note: Jacks A And B Connected To Same Hydraulic Line

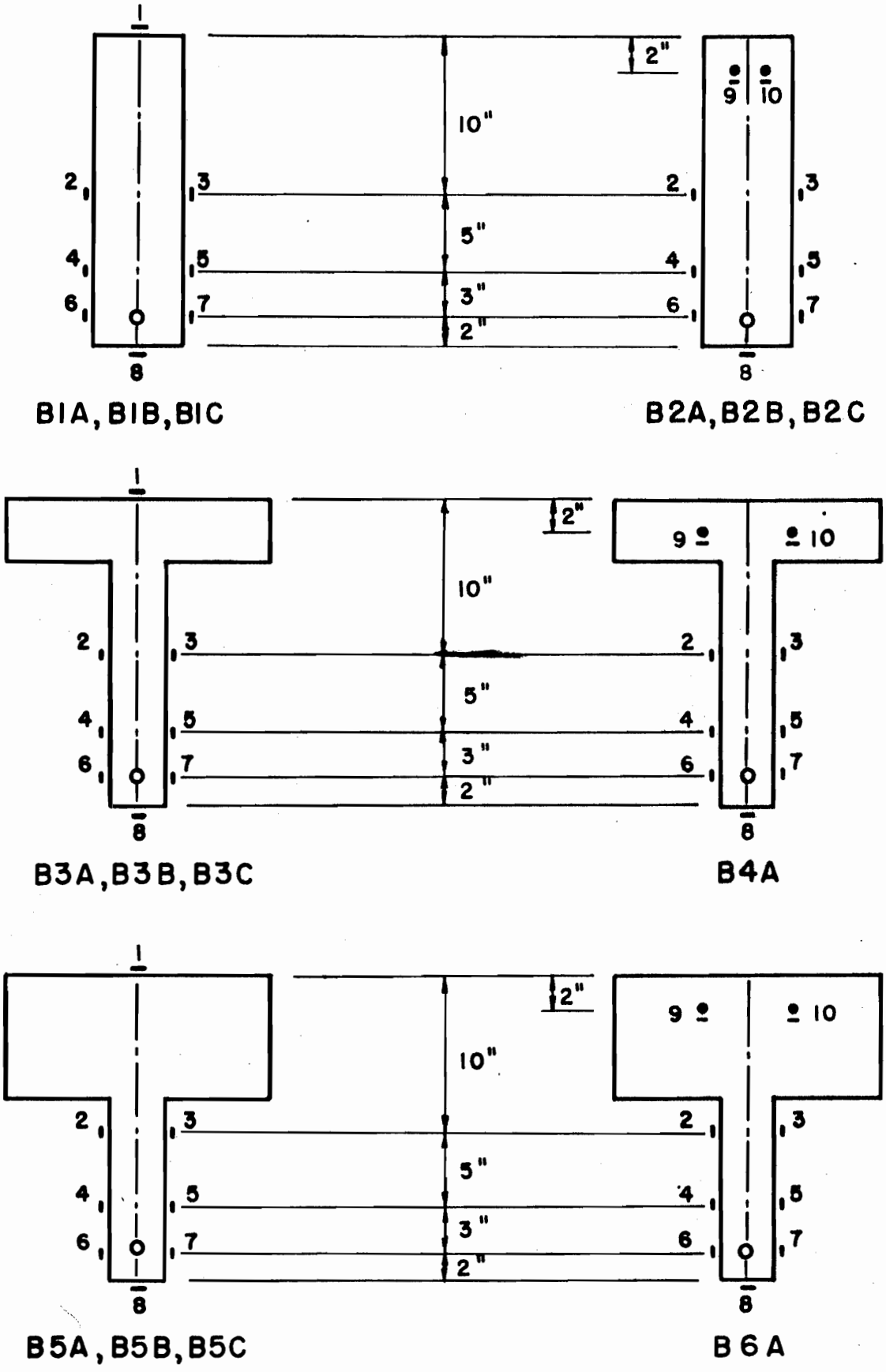

FIG. 9 LOCATION OF SR-4 GAGES AT MIDSPAN

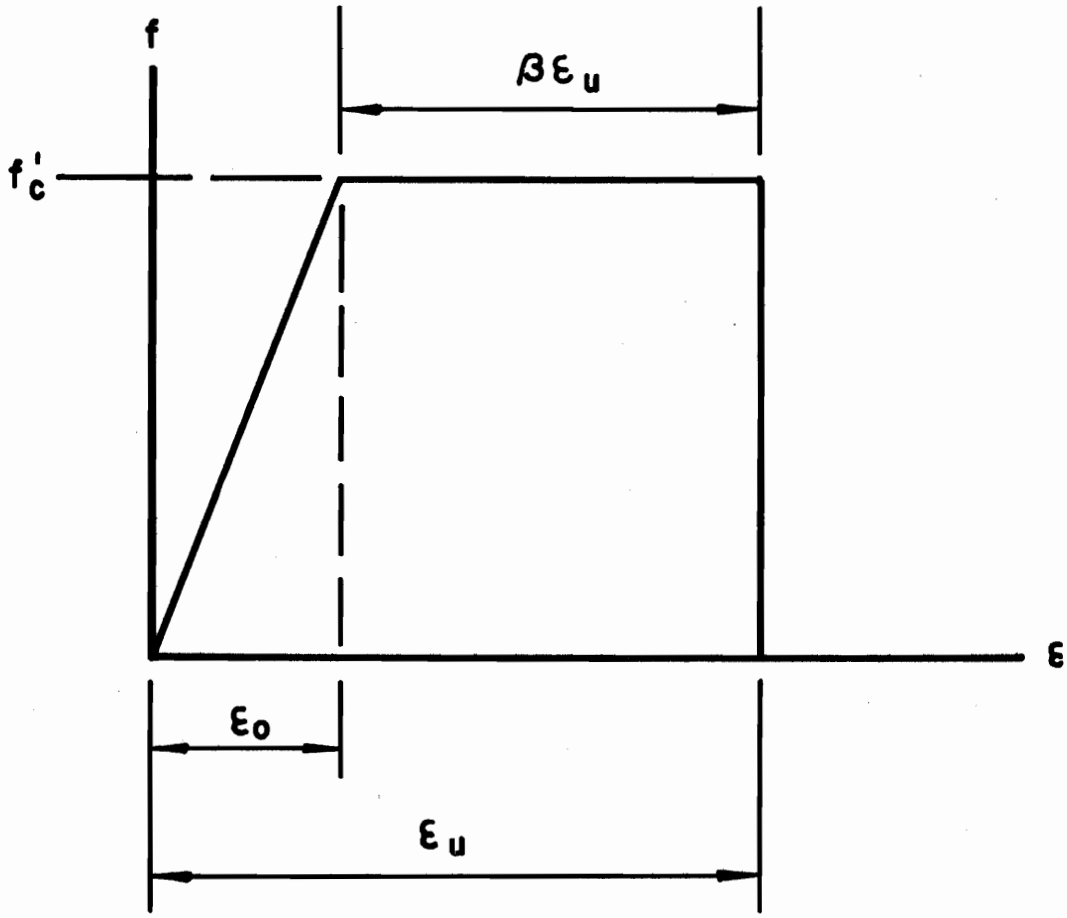

FIG. 10 ASSUMED COMPRESSIVE STRESS STRAIN CURVE BY JENSEN THEORY

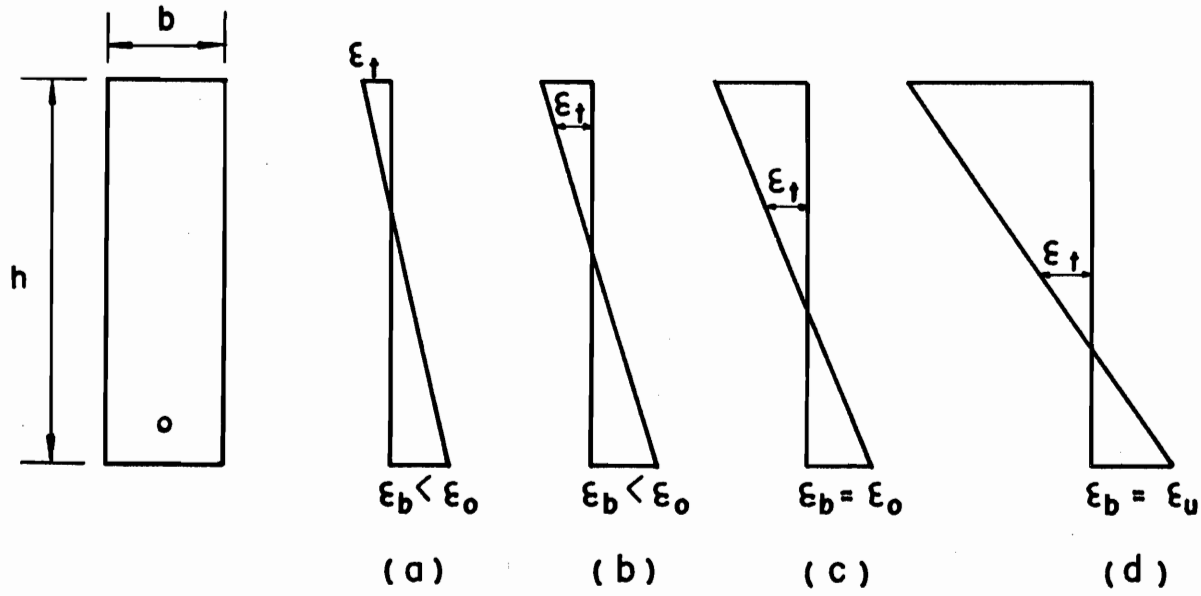

FIG. 11 STRAIN DISTRIBUTION UNDER INCREASING PRESTRESS FORCE OR EXTERNAL MOMENT (BEAM WITHOUT MILD STEEL IN TOP)

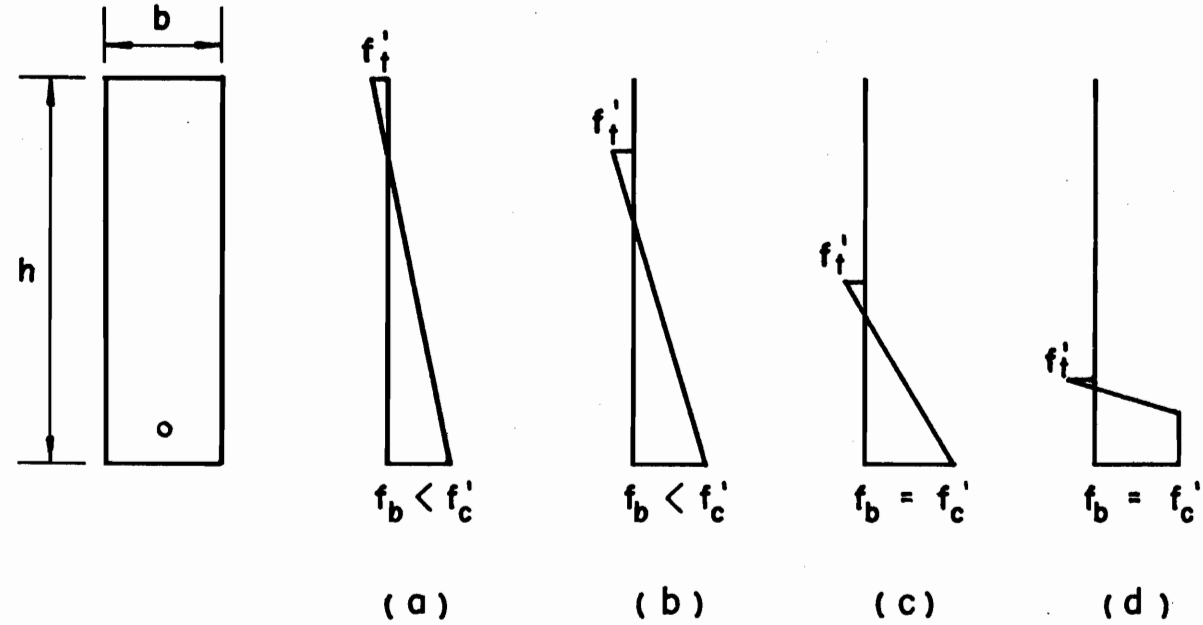

FIG. 12 STRESS DISTRIBUTION UNDER INCREASING PRESTRESS FORCE OR EXTERNAL MOMENT (BEAM WITHOUT MILD STEEL IN TOP)

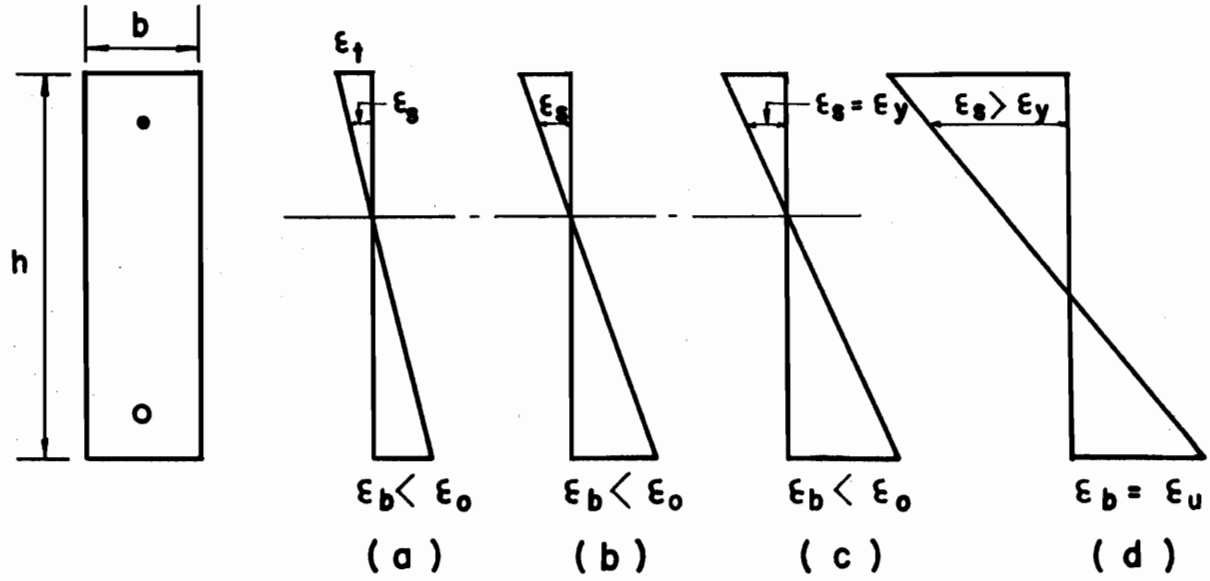

FIG. 13 STRAIN DISTRIBUTION UNDER INCREASING PRESTRESS FORCE OR EXTERNAL MOMENT (BEAM WITH MILD STEEL IN TOP)

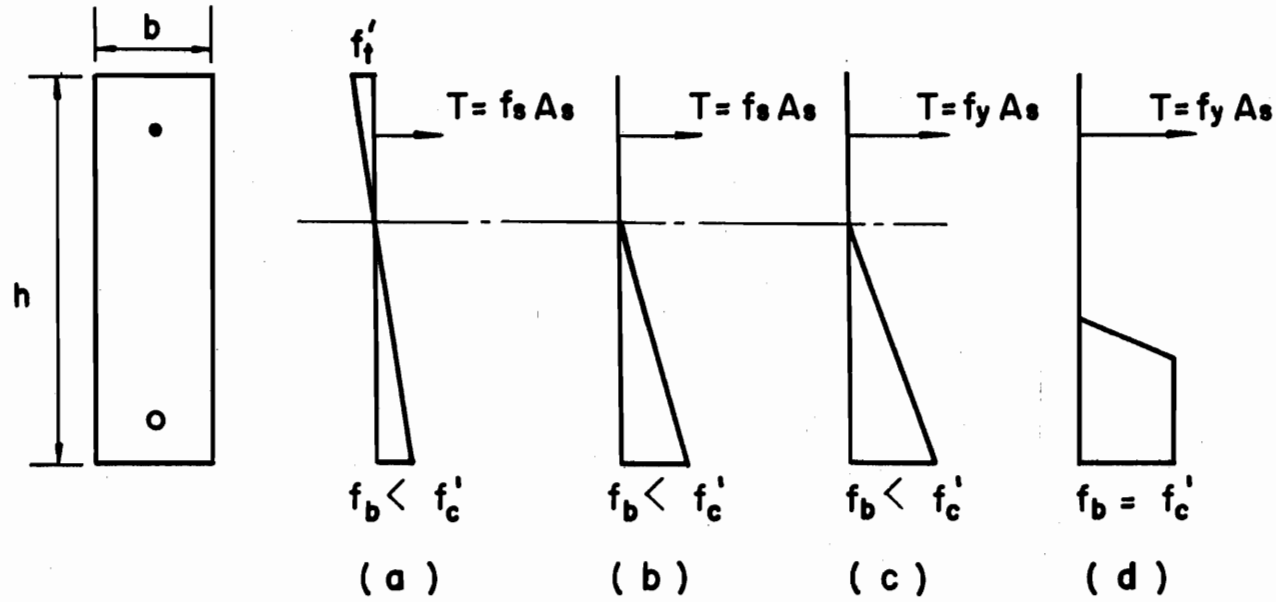

FIG. 14 STRESS DISTRIBUTION UNDER INCREASING PRESTRESS FORCE OR EXTERNAL MOMENT (BEAM WITH MILD STEEL IN TOP)

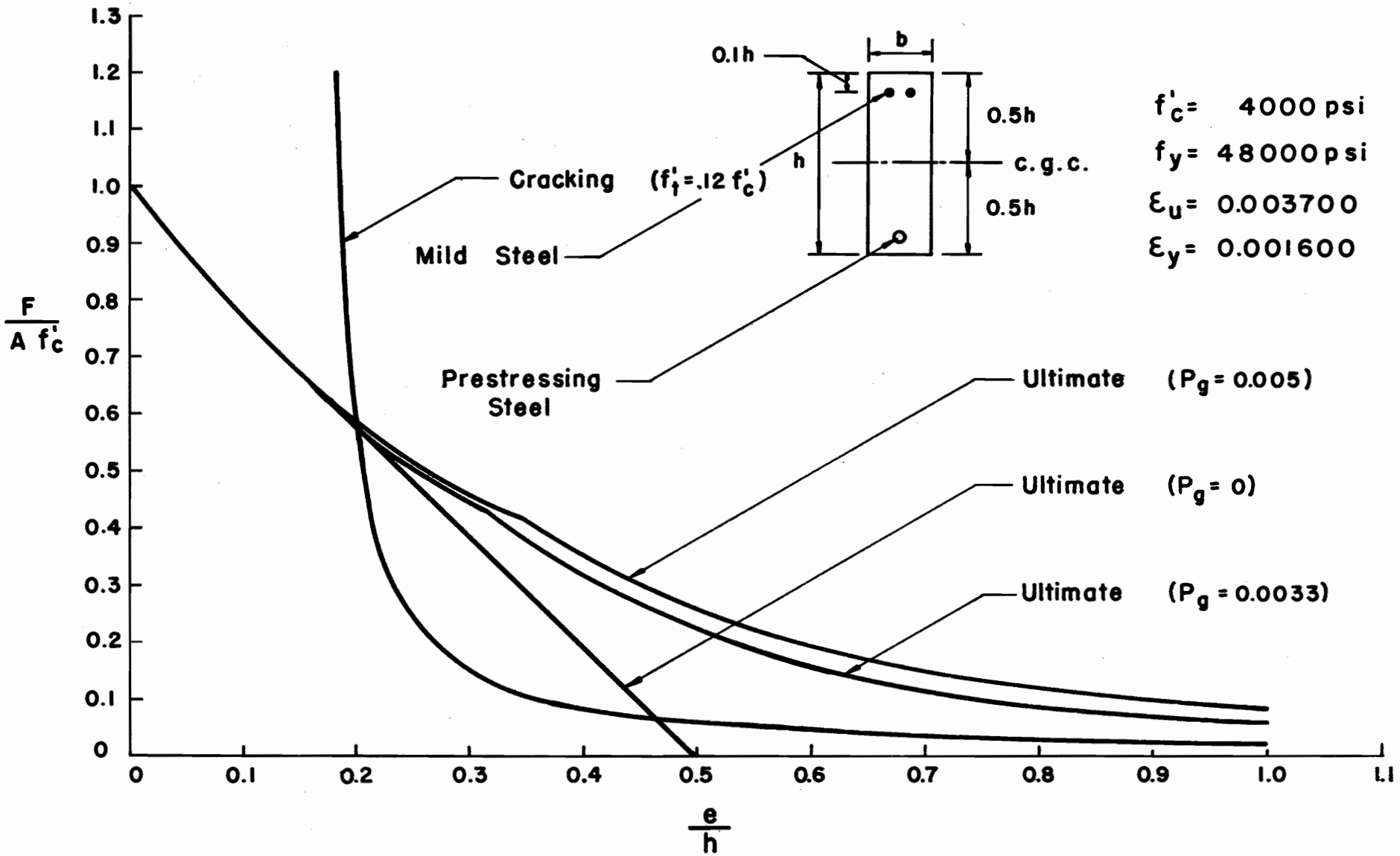

FIG. 15 THEORETICAL CRACKING AND ULTIMATE STRENGTH CURVES FOR A RECTANGULAR SECTION

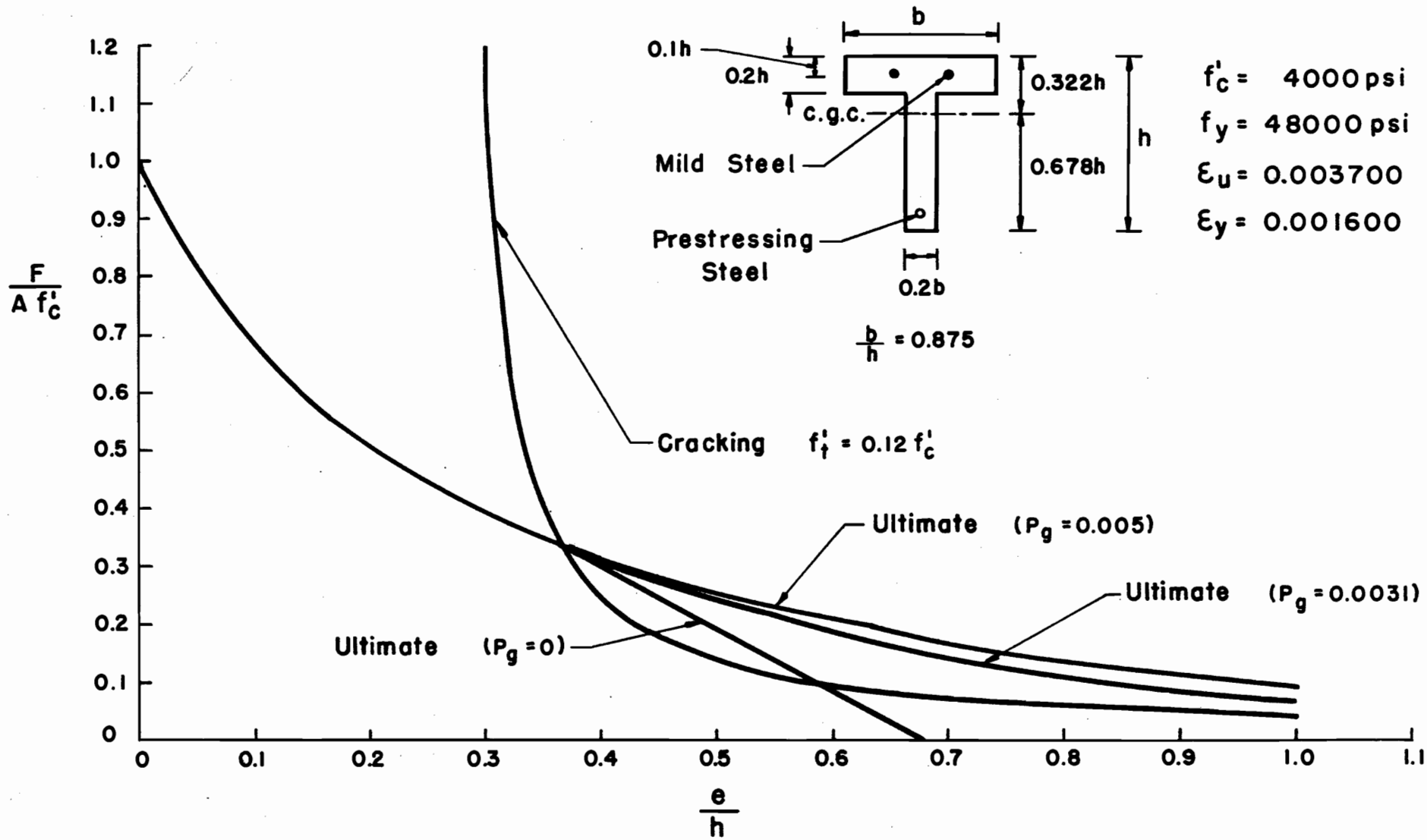

FIG. 16 THEORETICAL CRACKING AND ULTIMATE STRENGTH CURVES FOR A TEE SECTION

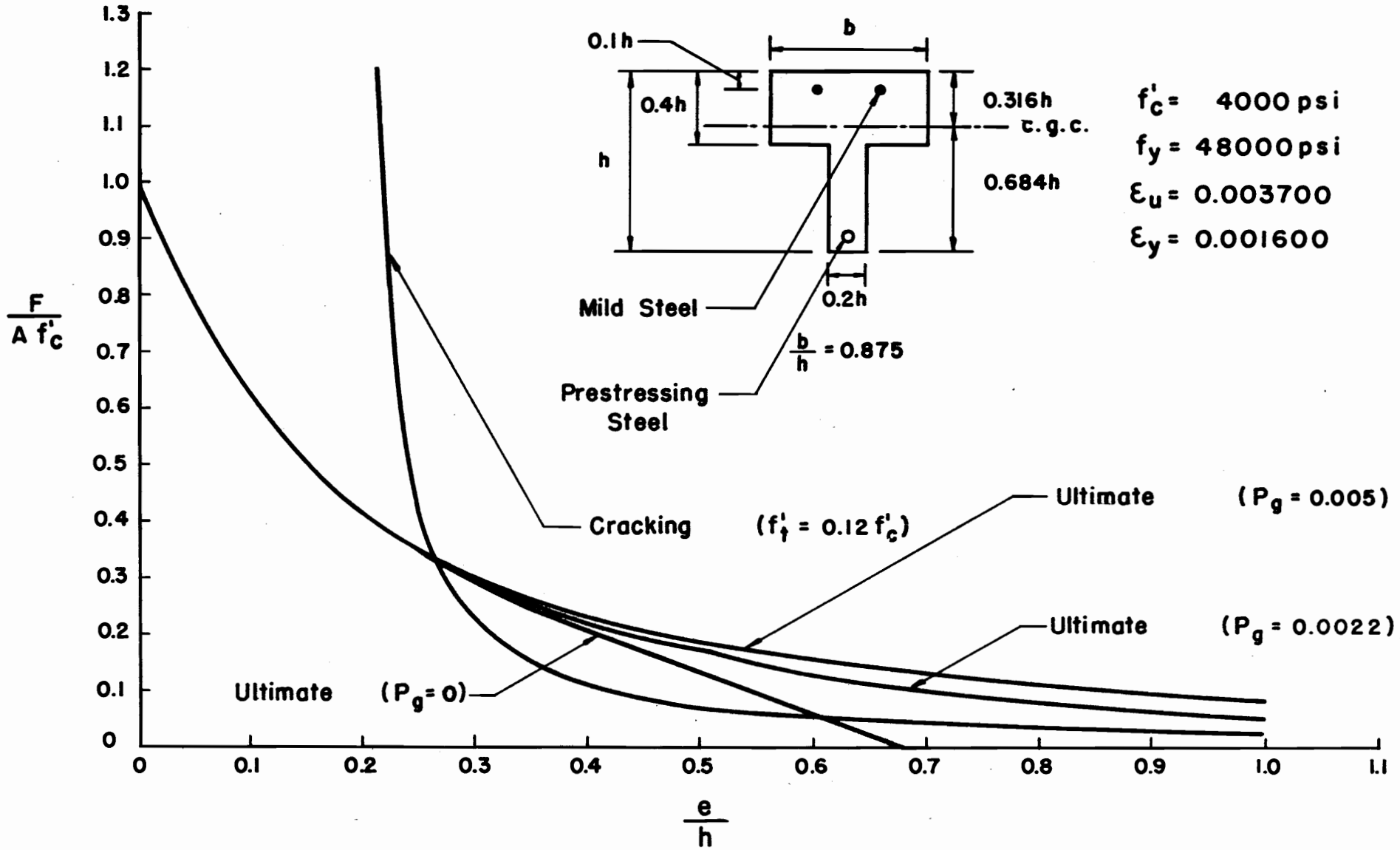

FIG. 17 THEORETICAL CRACKING AND ULTIMATE STRENGTH CURVES FOR A TEE SECTION

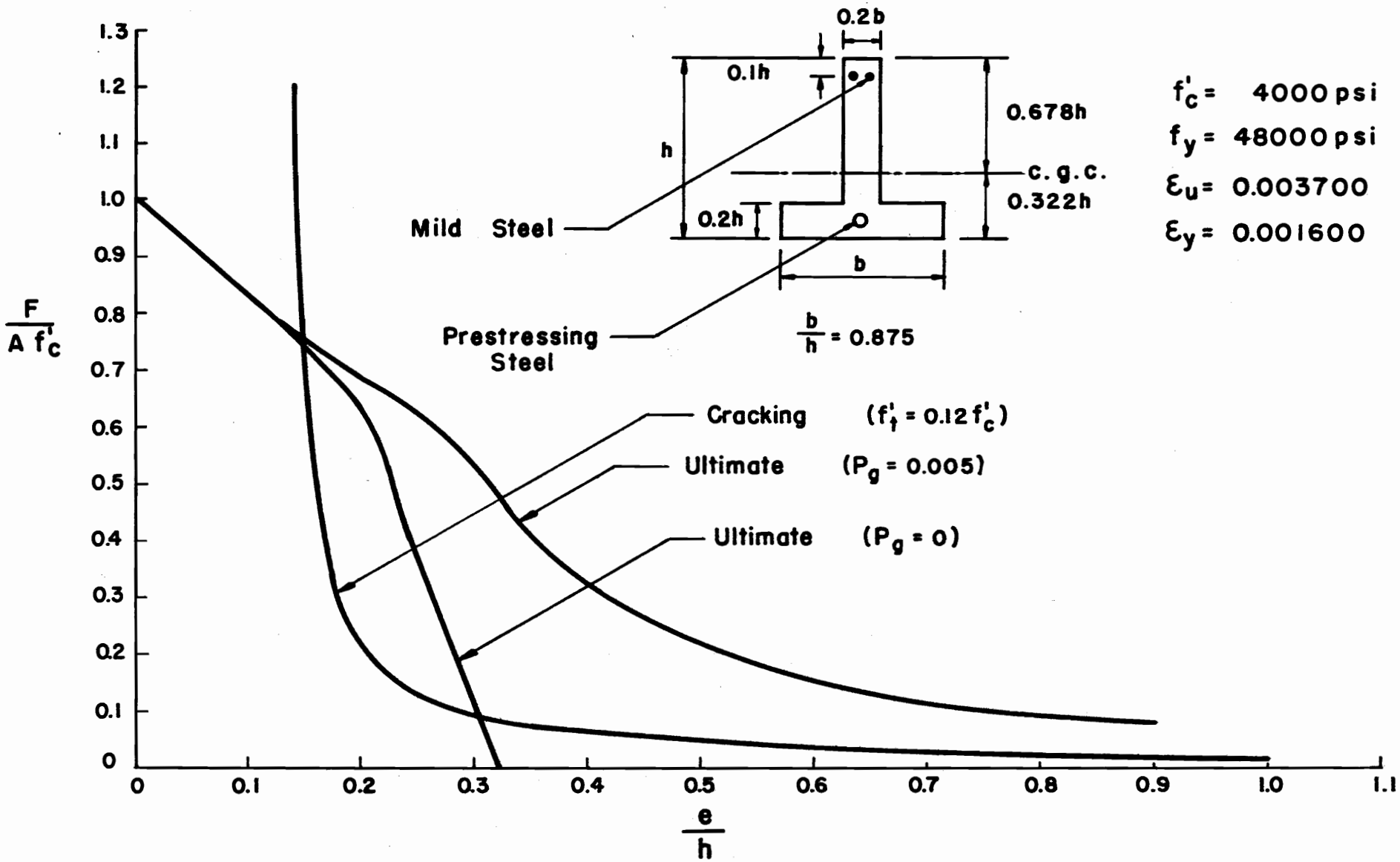

FIG. 18 THEORETICAL CRACKING AND ULTIMATE STRENGTH CURVES FOR AN INVERTED TEE SECTION

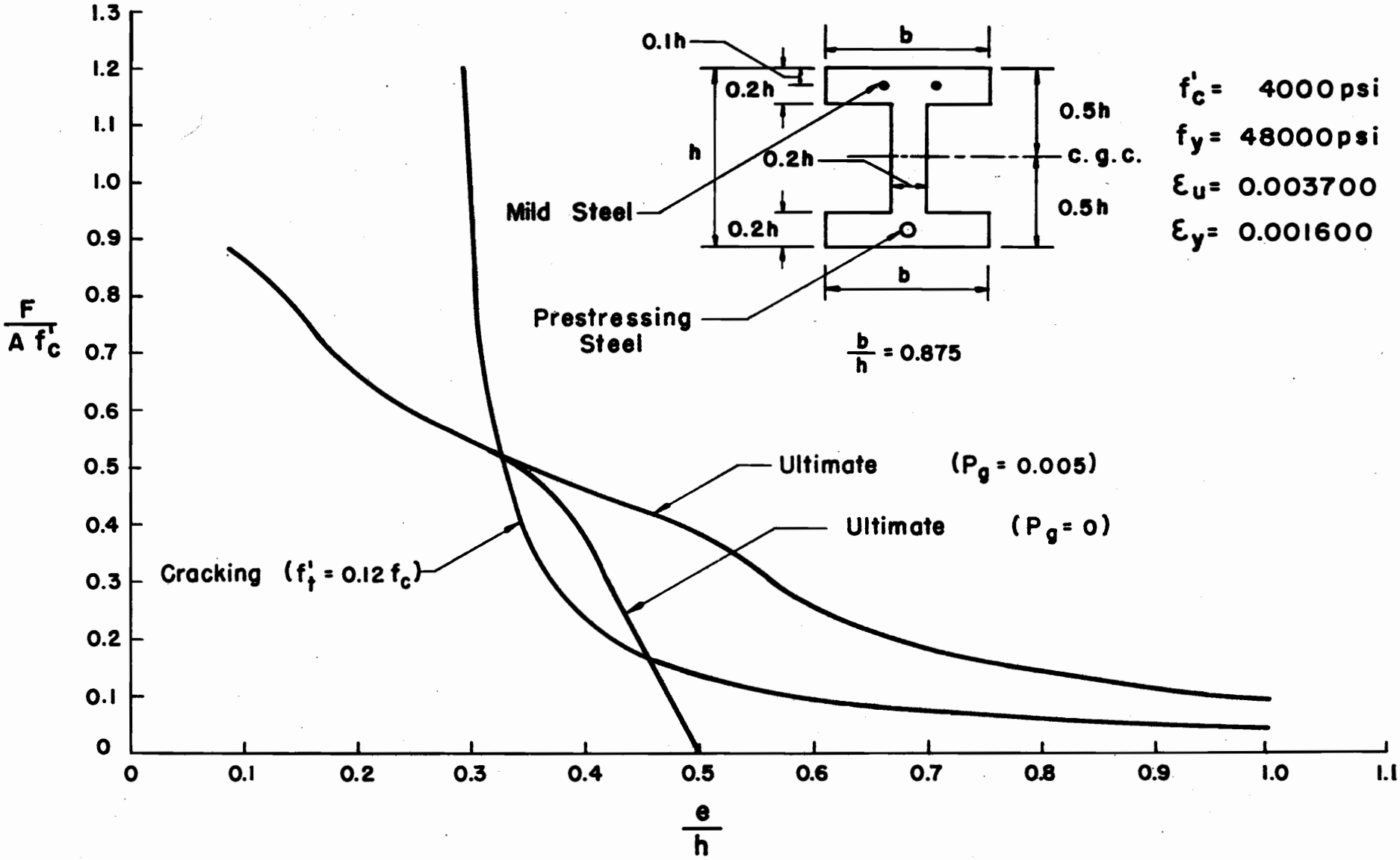

FIG. 19 THEORETICAL CRACKING AND ULTIMATE STRENGTH CURVES FOR AN I SECTION

BEAM B-1A

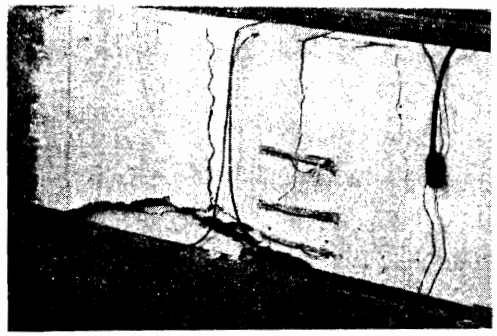

BEAM B-2A

BEAM B-1B

BEAM B-2B

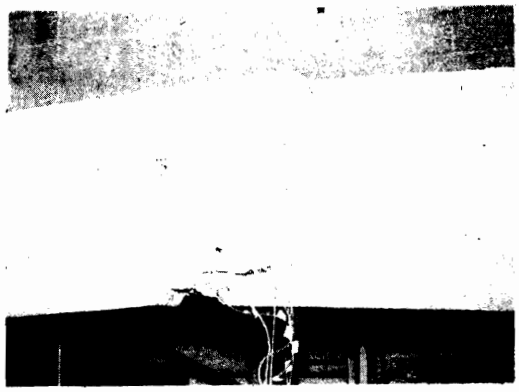

BEAM B-1C

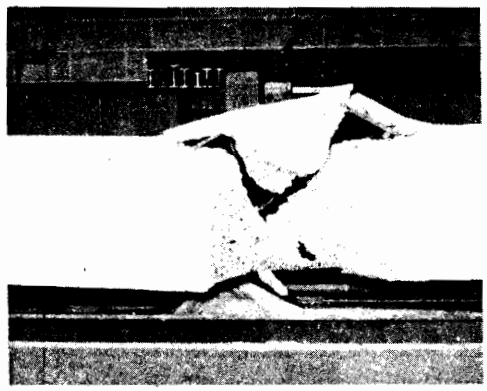

BEAM B-2C

FIG. 20 RECTANGULAR BEAM SPECIMENS AFTER FAILURE

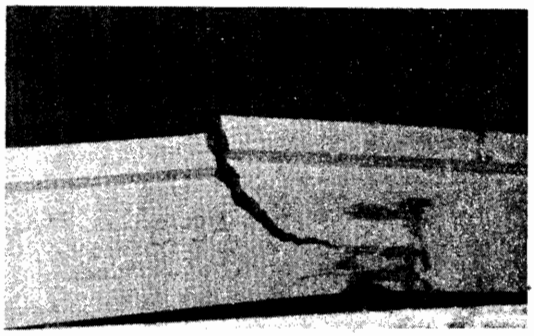

BEAM B-3A

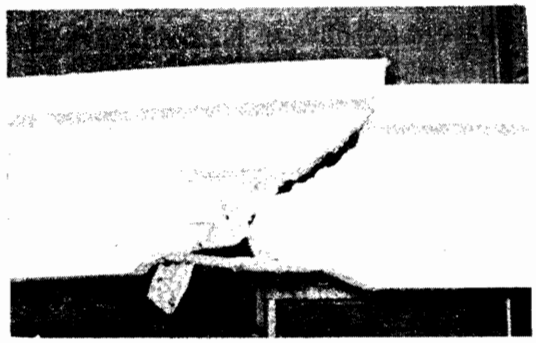

BEAM B-3C

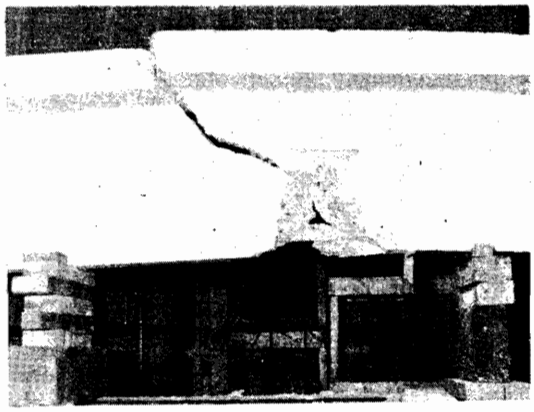

BEAM B-3B

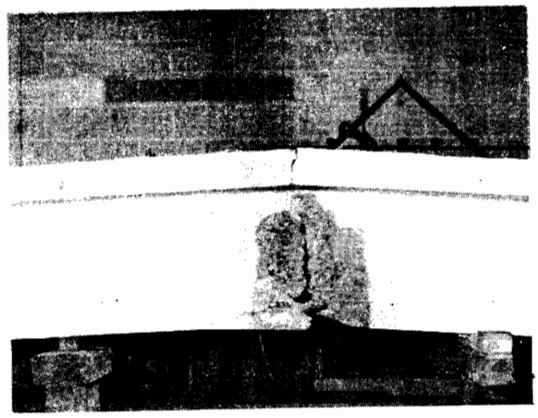

BEAM B-4A

FIG. 21 THIN-FLANGED TEE BEAM SPECIMENS AFTER FAILURE

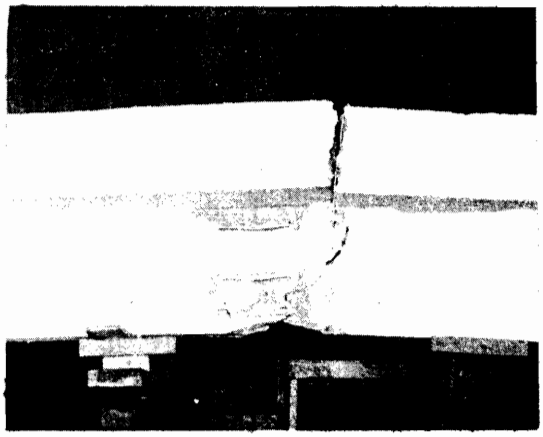

BEAM B-5A

BEAM B-5C

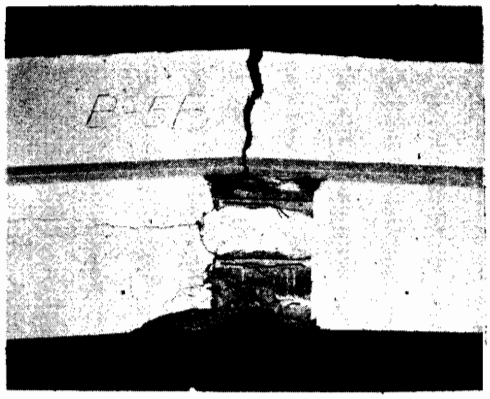

BEAM B-5B

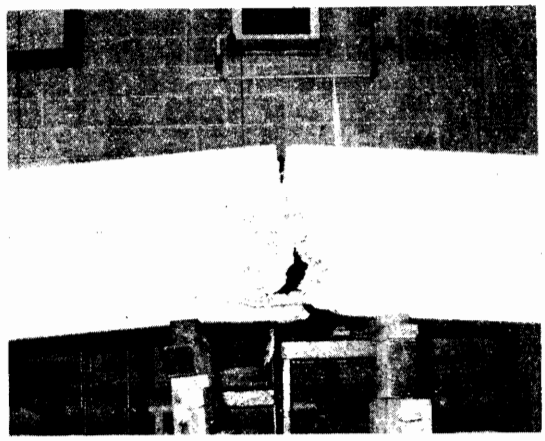

BEAM B-6A

FIG. 22 THICK - FLANGED TEE BEAM SPECIMENS AFTER FAILURE

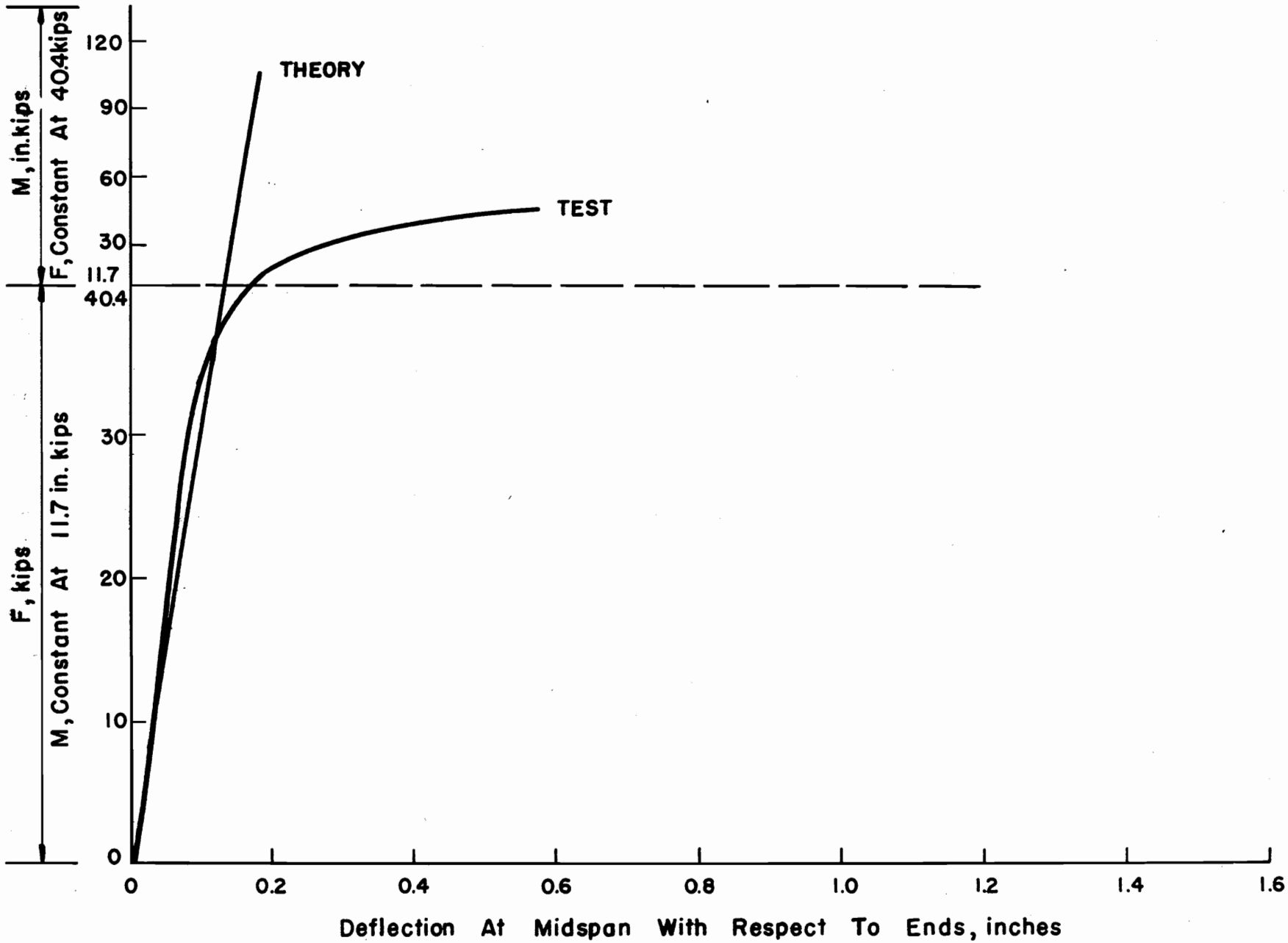

FIG. 23 Beam B-IA, PRESTRESS FORCE AND MOMENT vs CENTER DEFLECTION

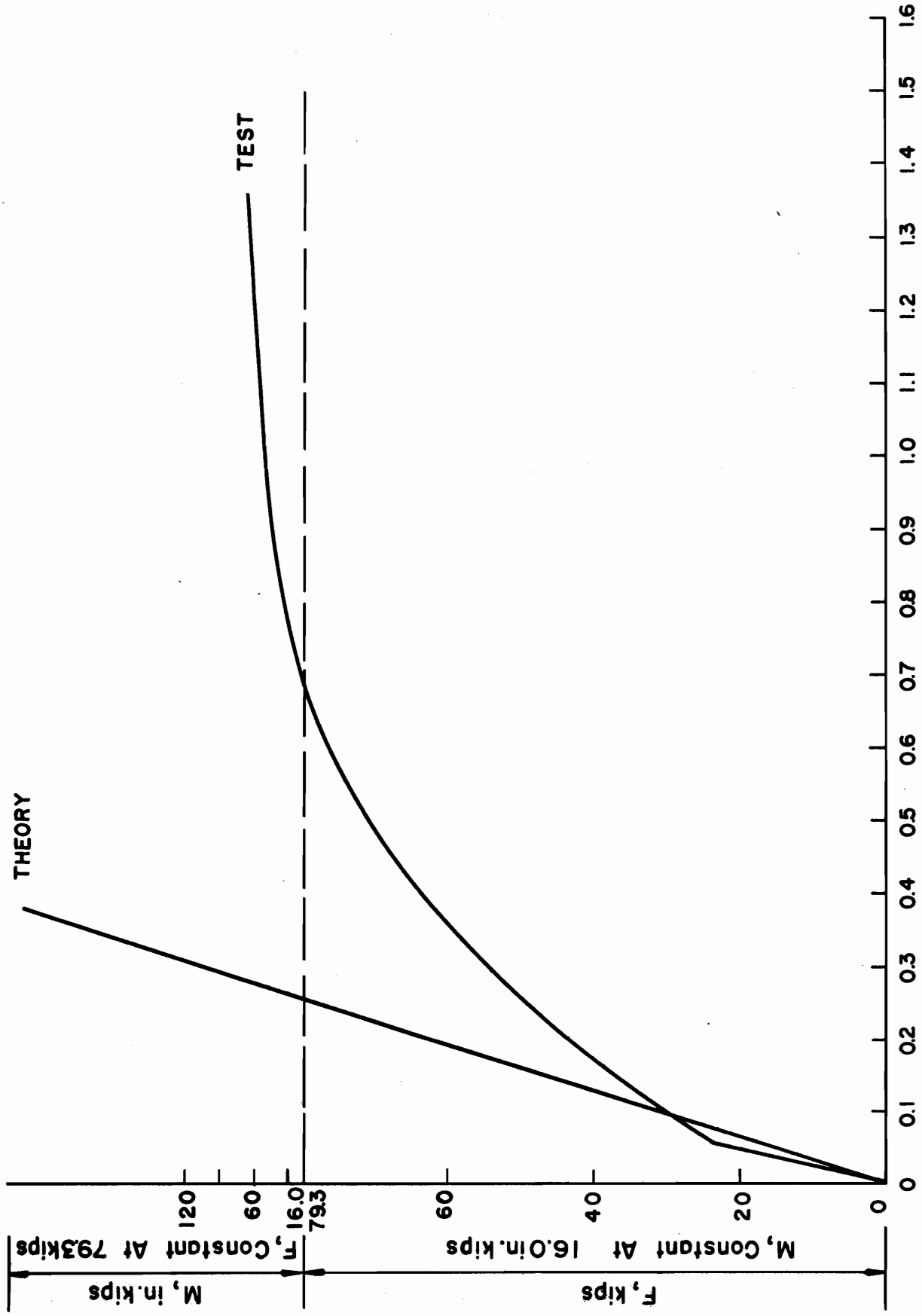

FIG. 24 Beam B-1B, PRESTRESS FORCE AND MOMENT vs CENTER DEFLECTION

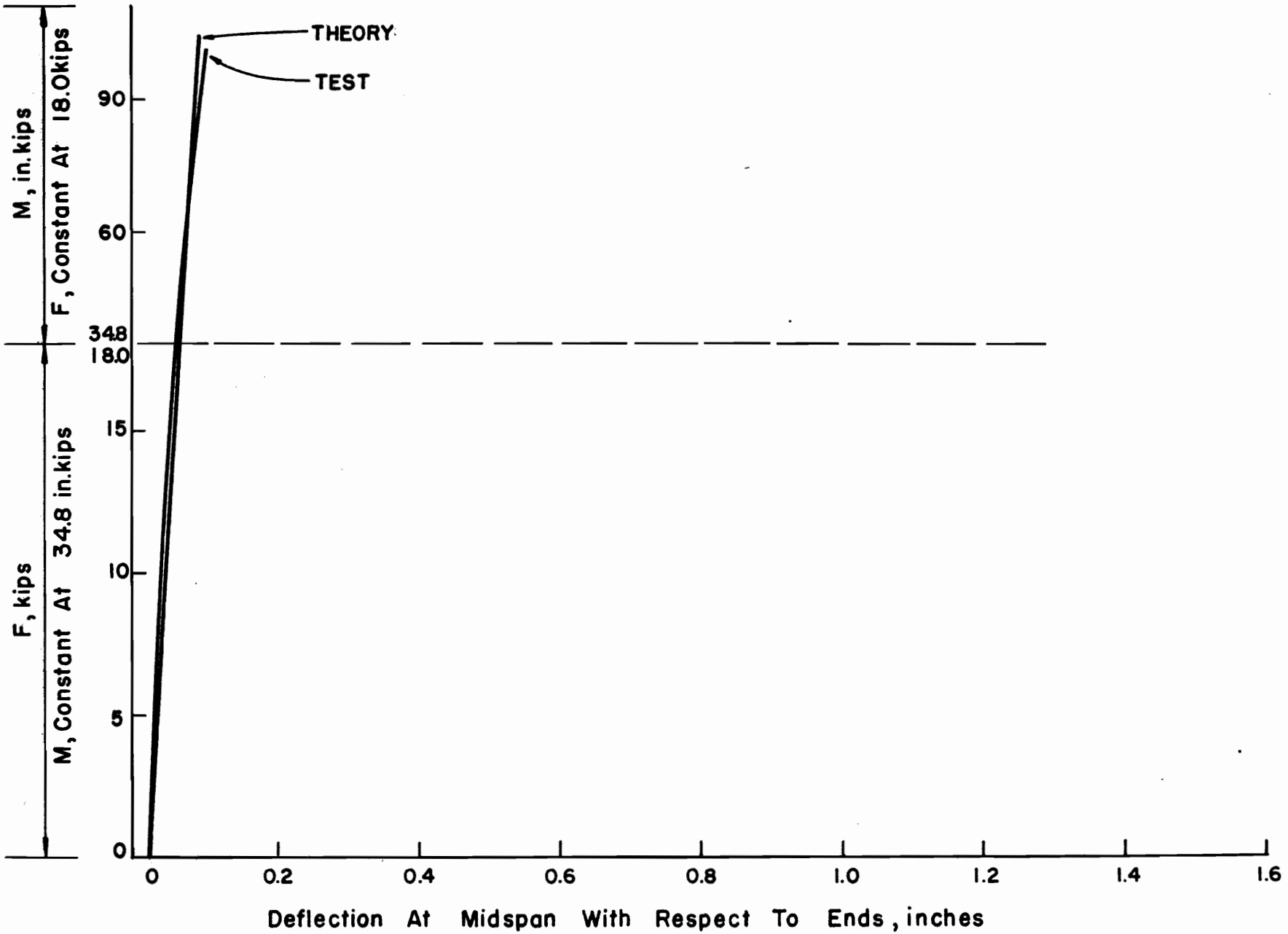

FIG. 25 Beam B-IC, PRESTRESS FORCE AND MOMENT vs CENTER DEFLECTION

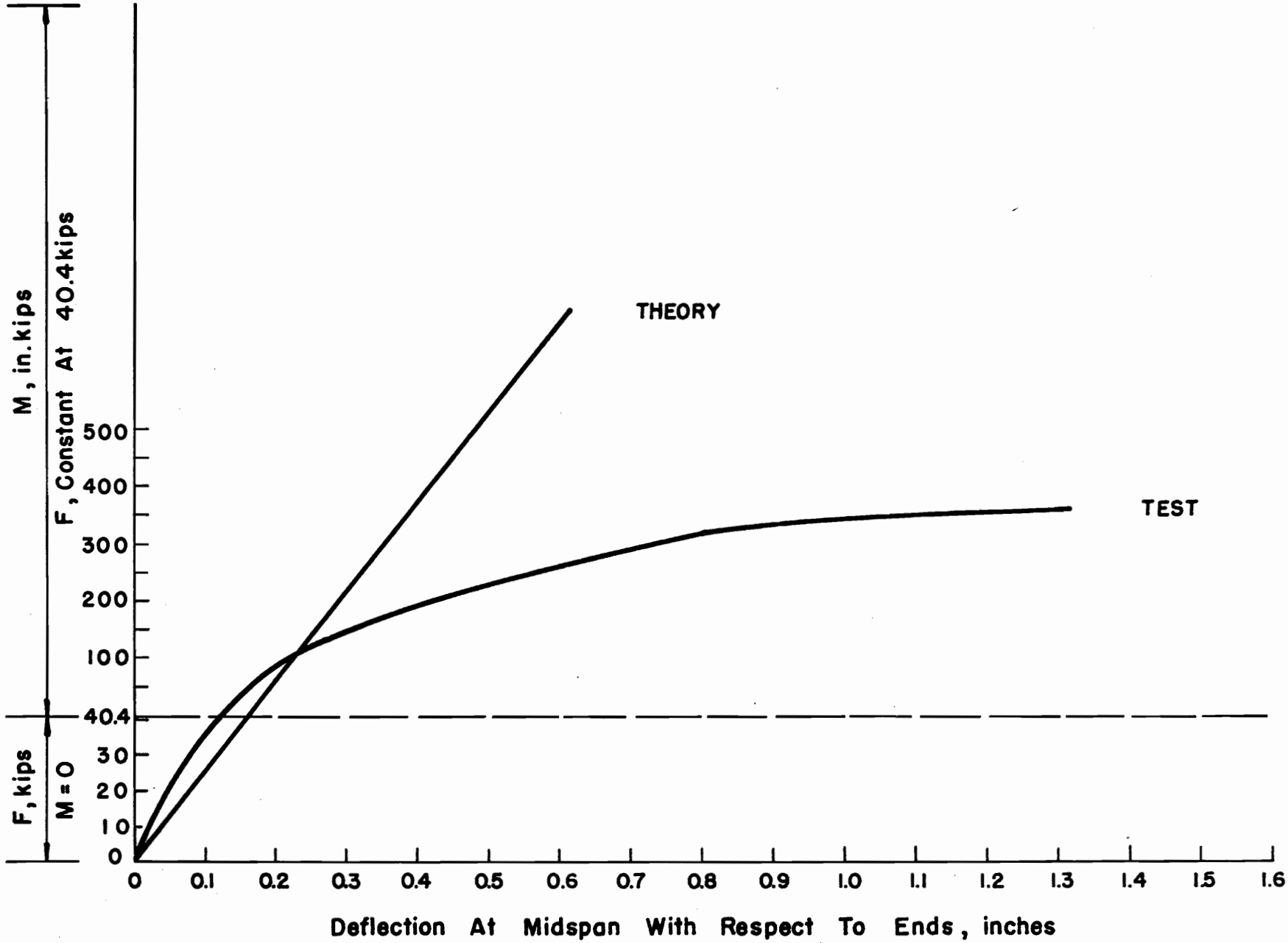

FIG. 26 Beam B-2A; PRESTRESS FORCE AND MOMENT vs CENTER DEFLECTION

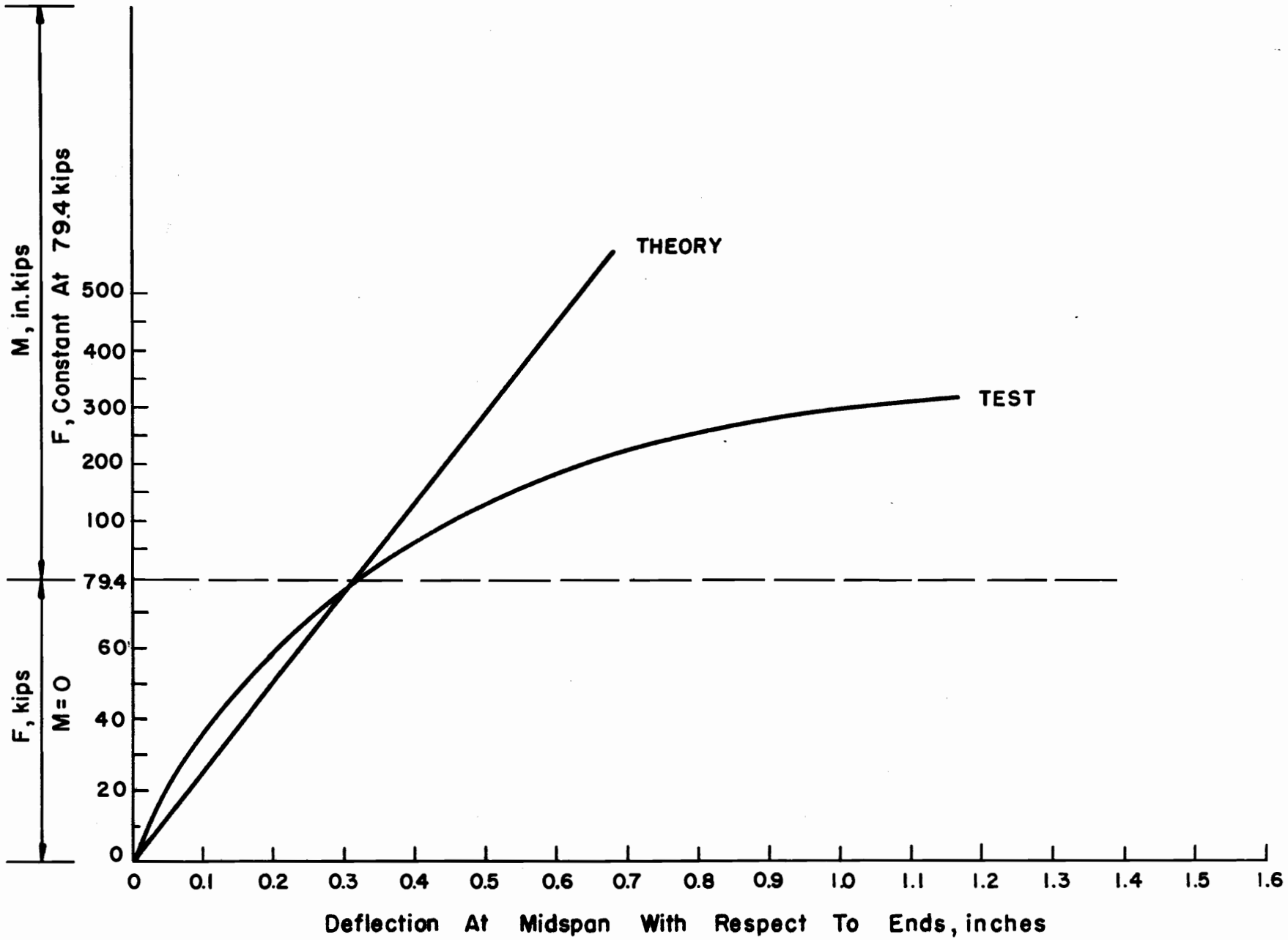

FIG. 27 Beam B-2B, PRESTRESS FORCE AND MOMENT vs CENTER DEFLECTION

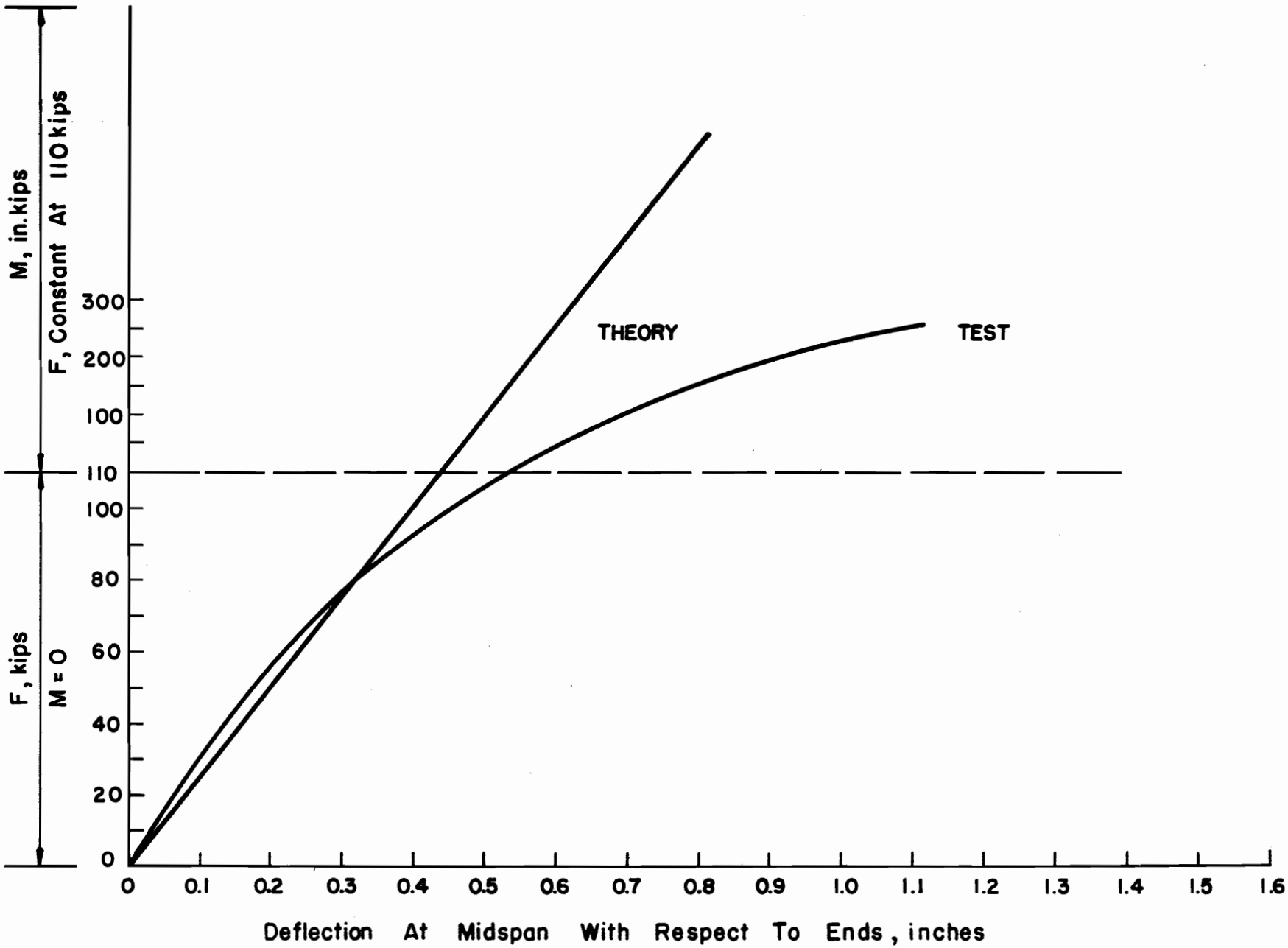

FIG. 28 Beam B-2C, PRESTRESS FORCE AND MOMENT vs CENTER DEFLECTION

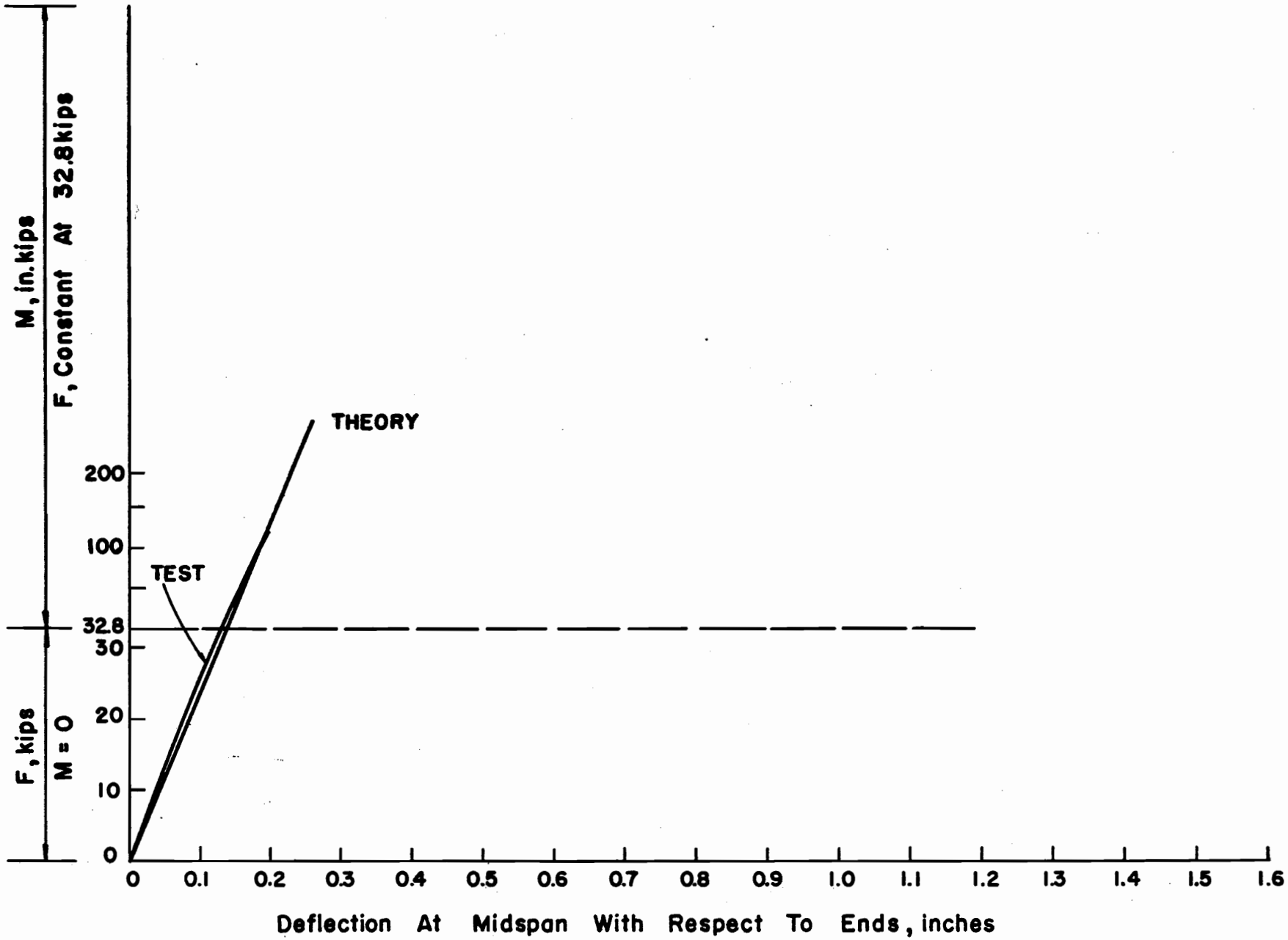

FIG. 29 Beam B-3A; PRESTRESS FORCE AND MOMENT vs CENTER DEFLECTION

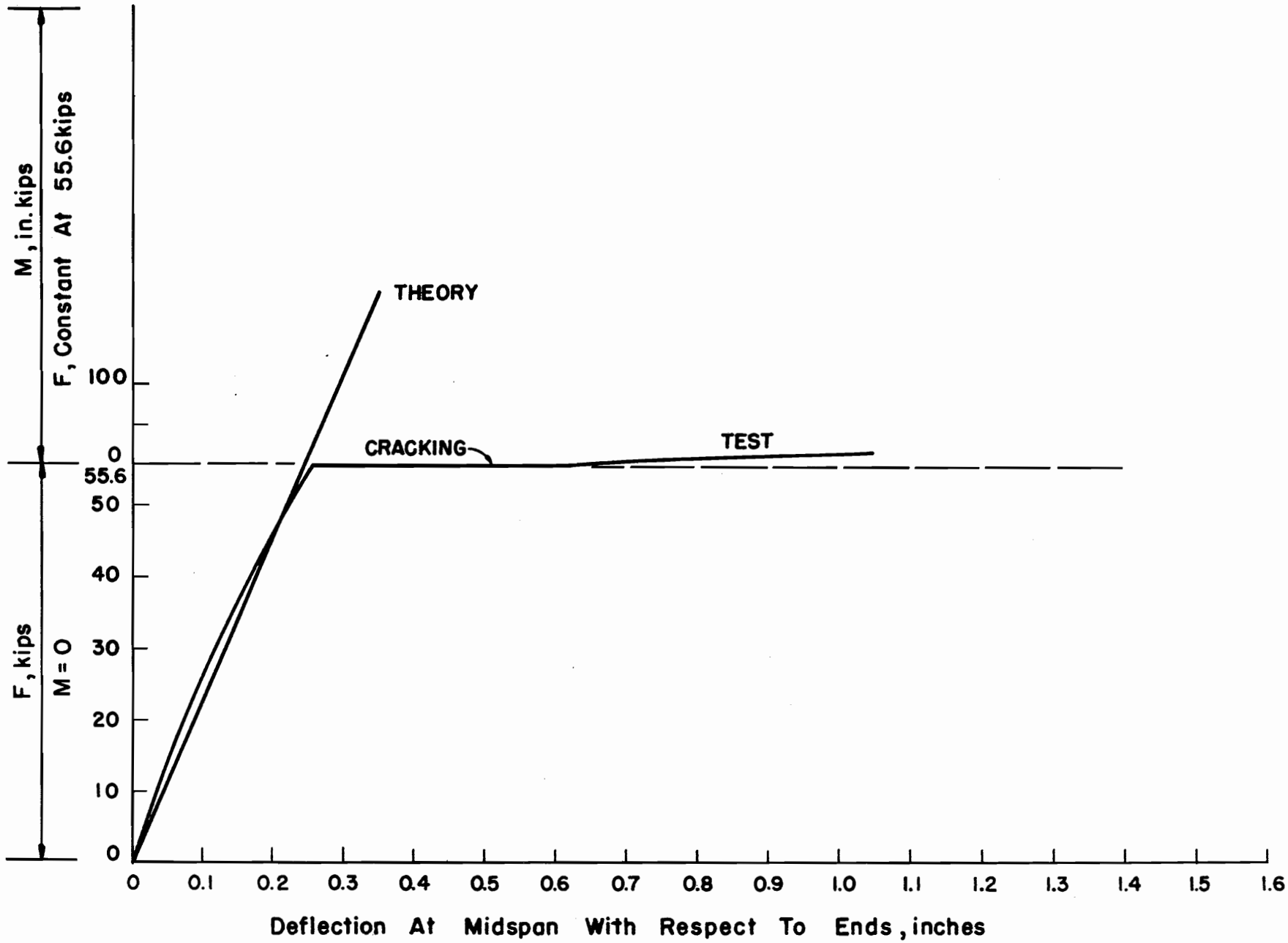

FIG. 30 Beam B-3B; PRESTRESS FORCE AND MOMENT vs CENTER DEFLECTION

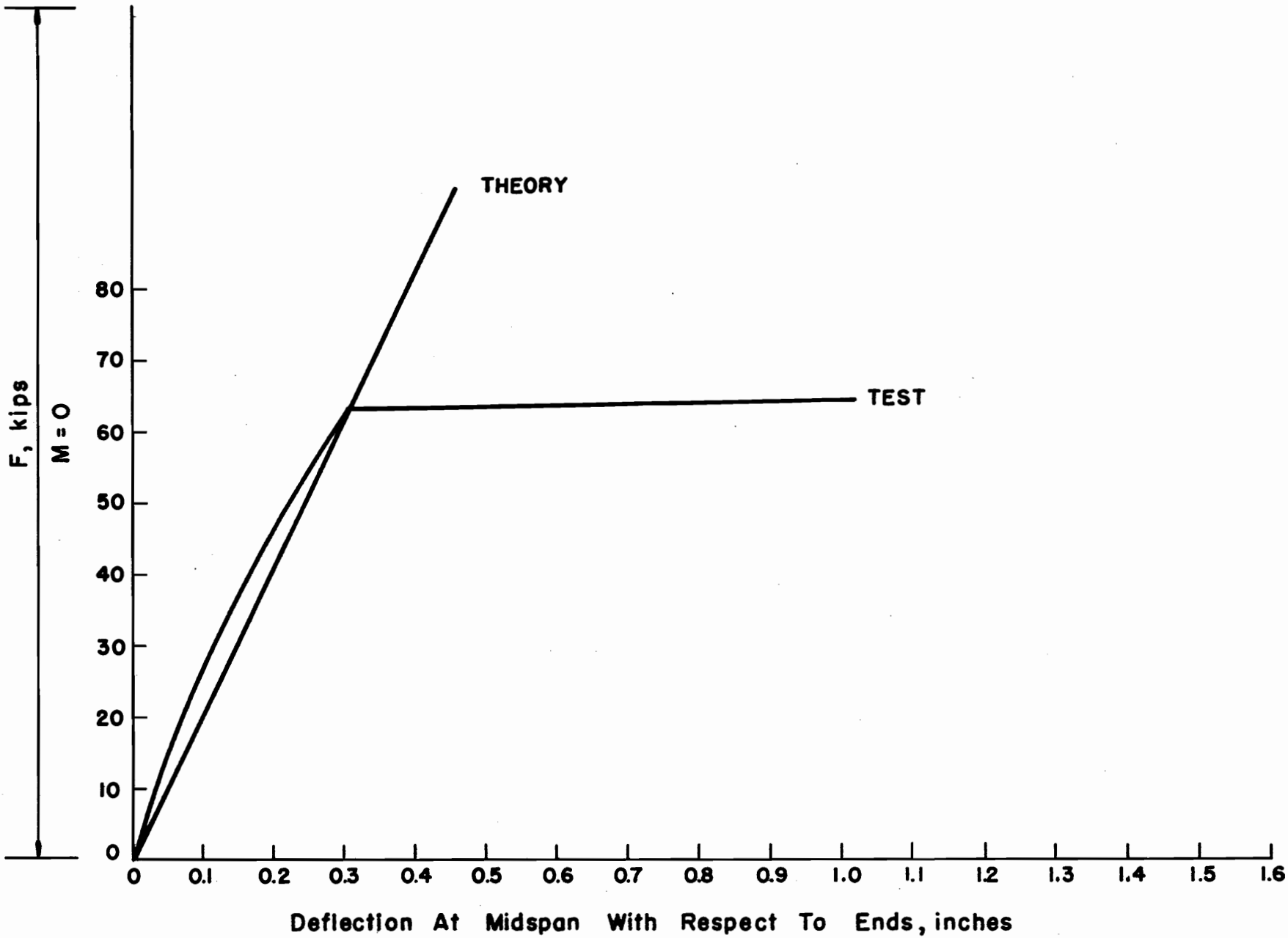

FIG. 31 Beam B-3C; PRESTRESS FORCE AND MOMENT vs CENTER DEFLECTION

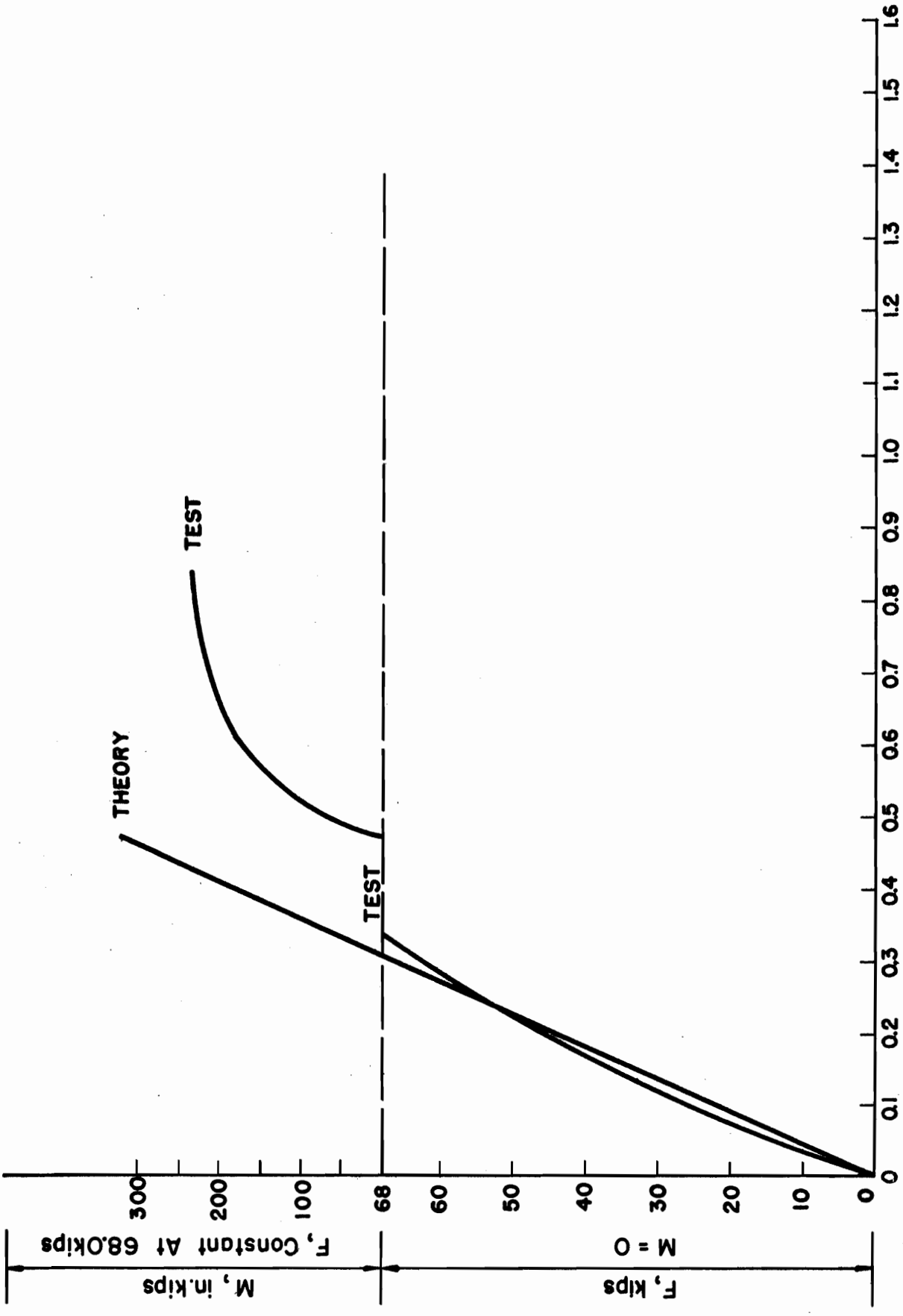

FIG. 32 Beam B-4A; PRESTRESS FORCE AND MOMENT vs CENTER DEFLECTION

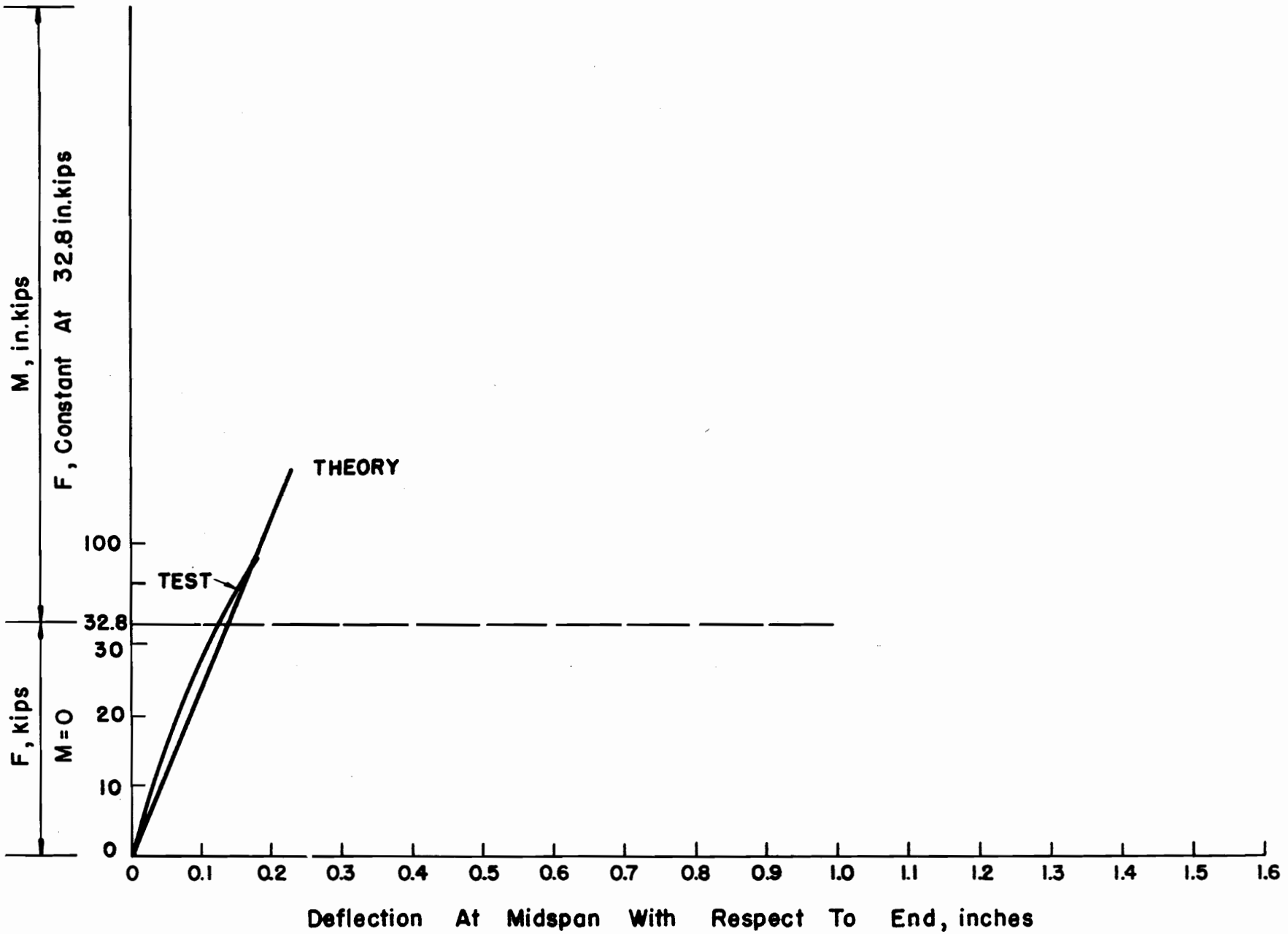

FIG. 33 Beam B-5A; PRESTRESS FORCE AND MOMENT vs CENTER DEFLECTION

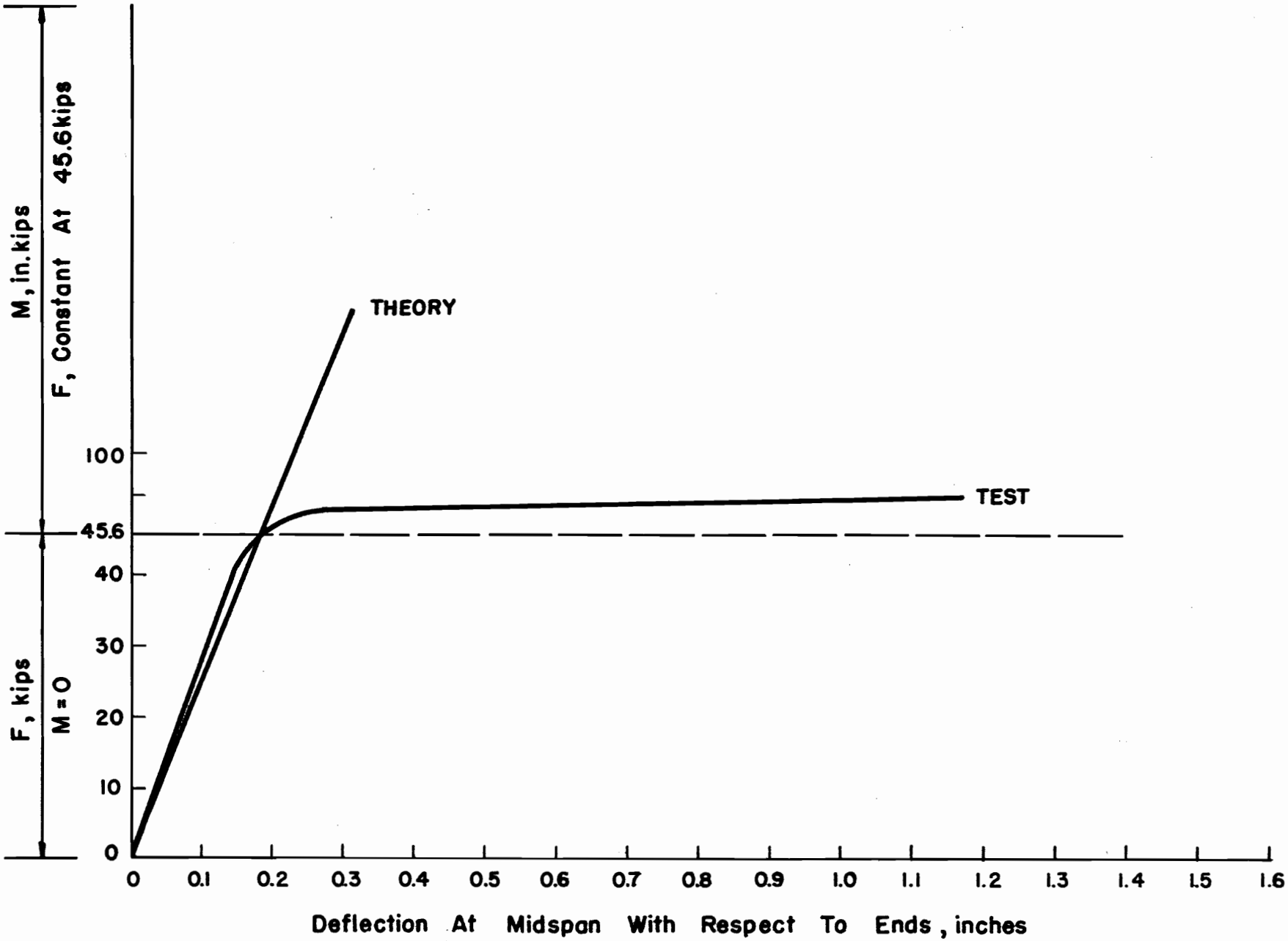

FIG. 34 Beam B-5B; PRESTRESS FORCE AND MOMENT vs CENTER DEFLECTION

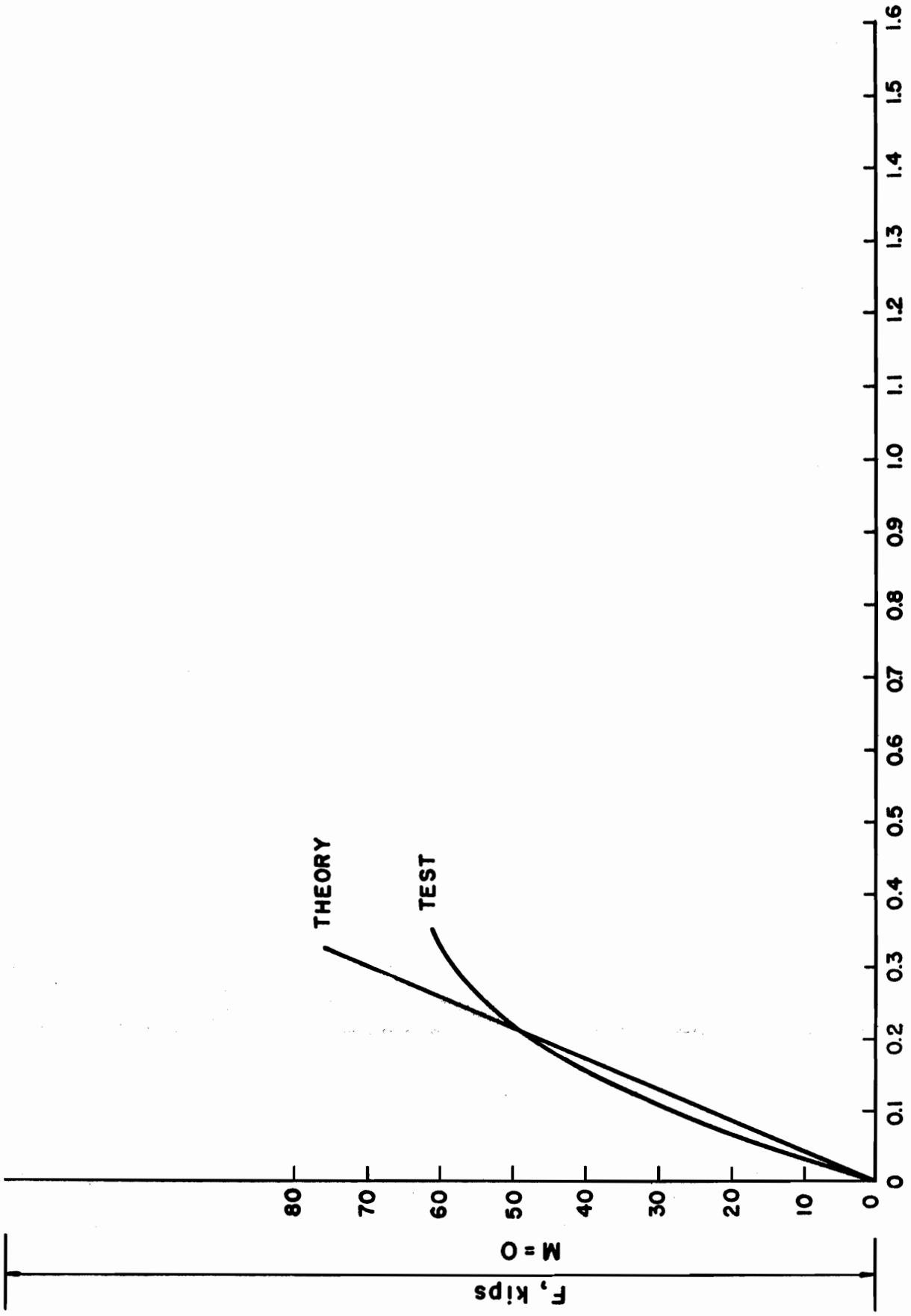

FIG. 35 Beam B-5C; PRESTRESS FORCE AND MOMENT vs CENTER DEFLECTION

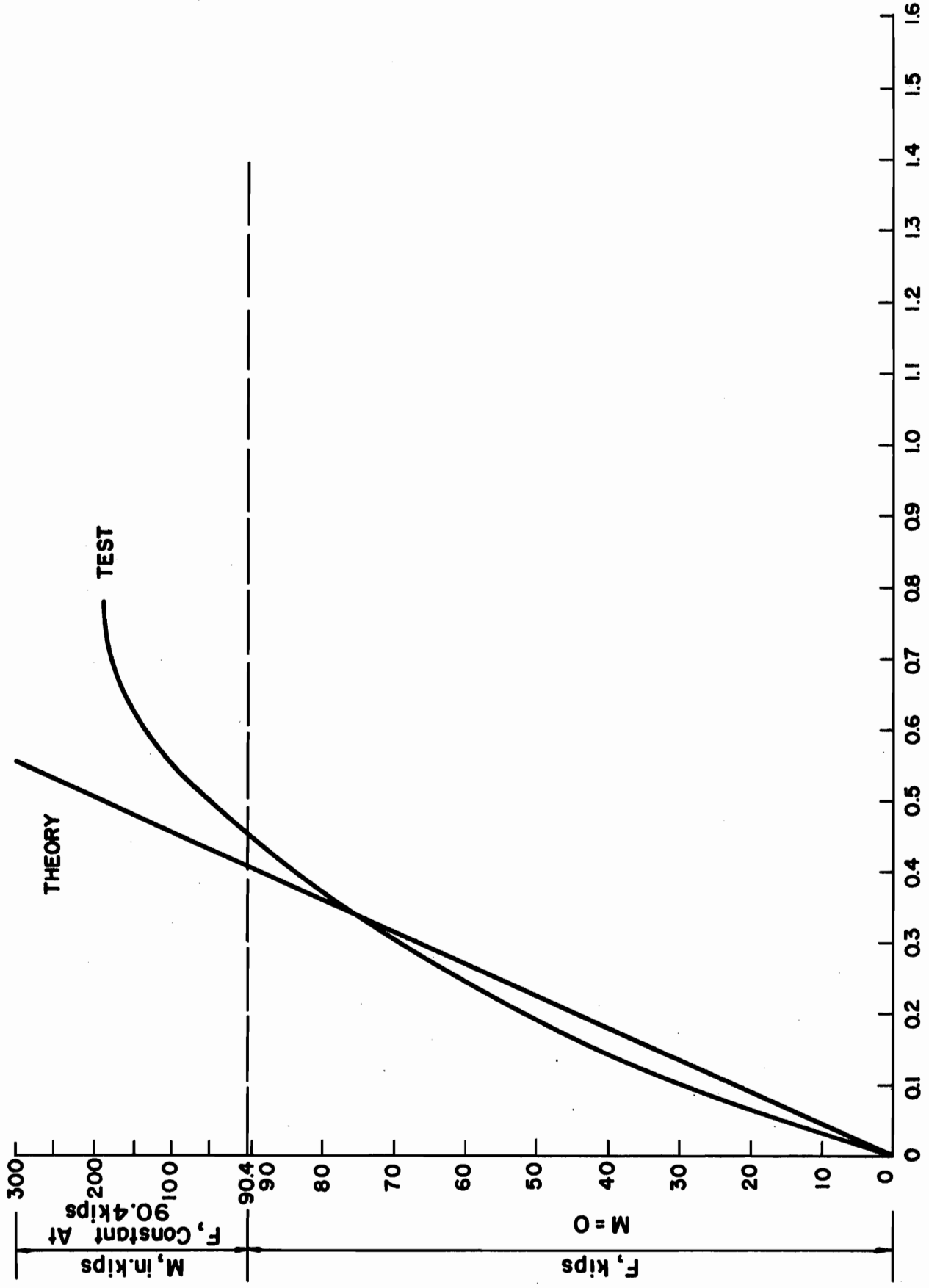

FIG. 36 Beam B-6A; PRESTRESS FORCE AND MOMENT vs CENTER DEFLECTION

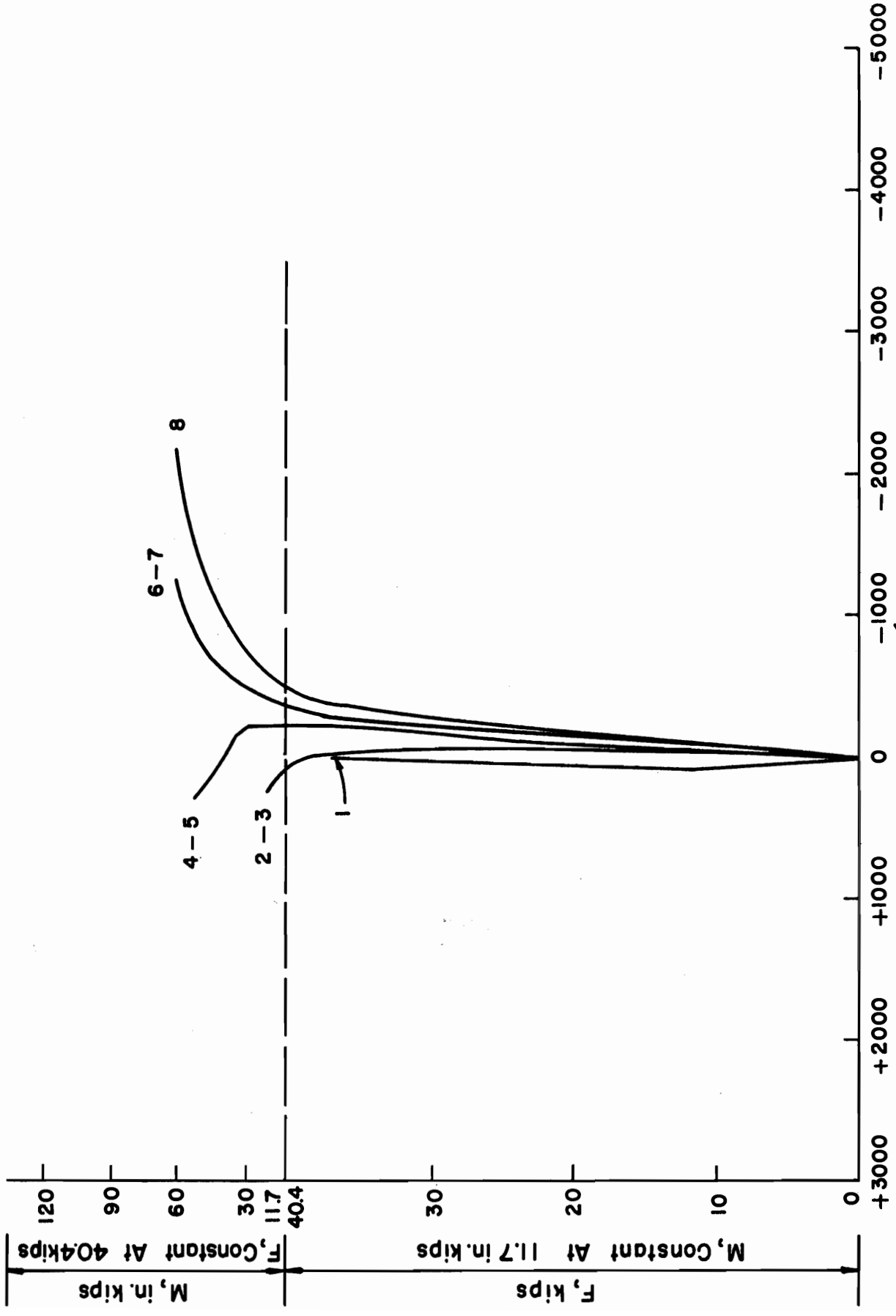

FIG. 37 Beam B-1A; PRESTRESS FORCE AND MOMENT vs UNIT STRAIN

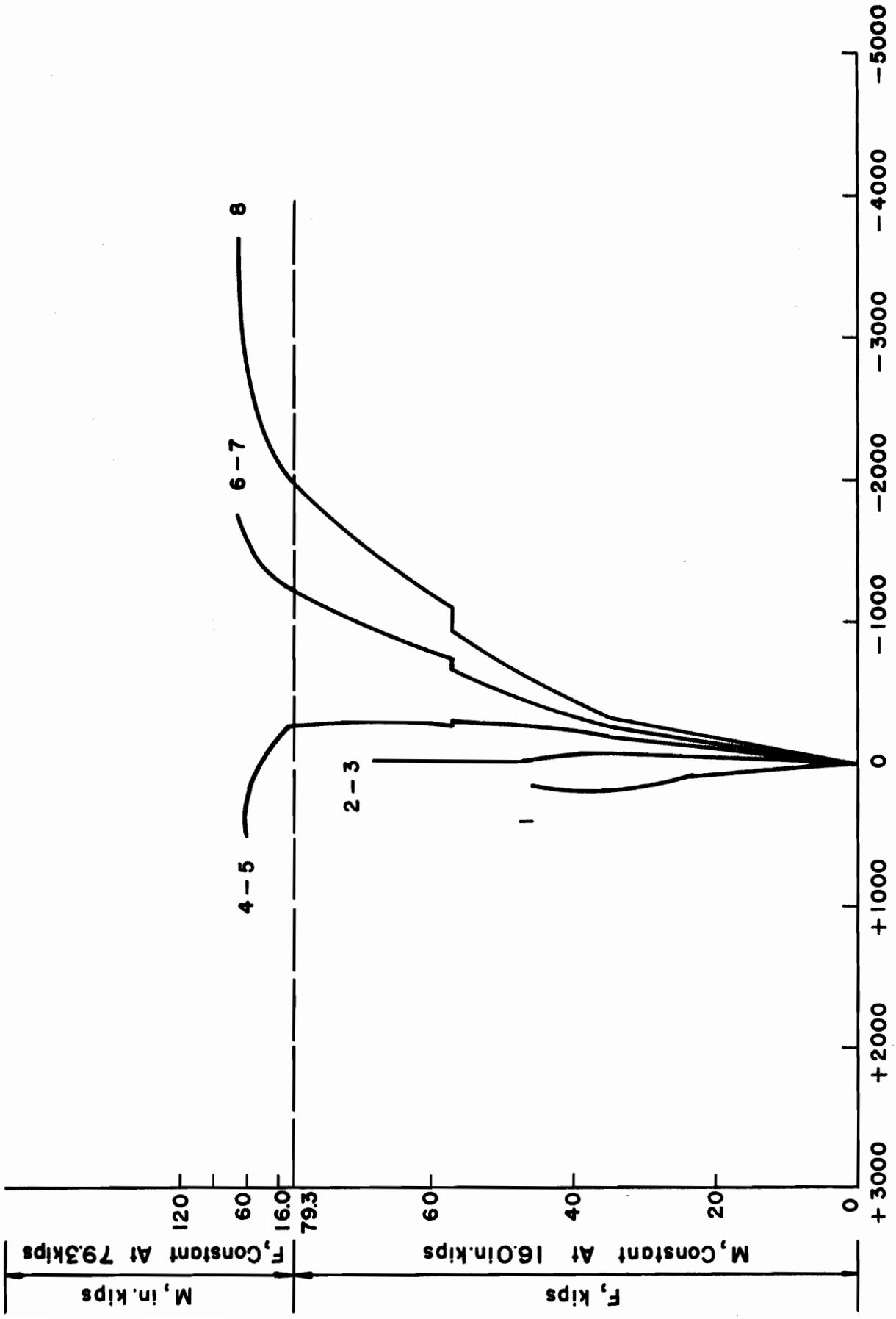

FIG. 38 Beam B-1B; PRESTRESS FORCE AND MOMENT vs UNIT STRAIN

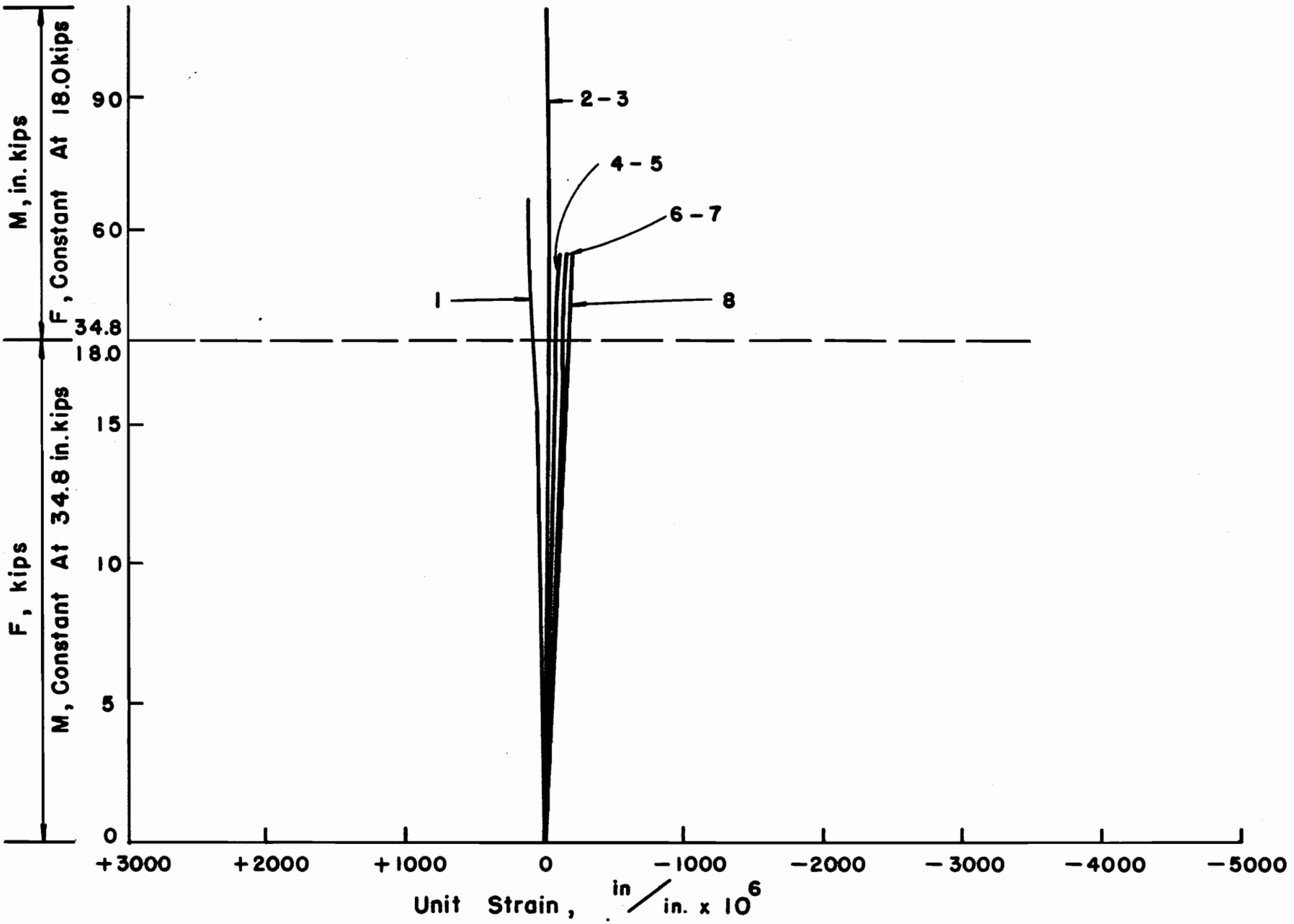

FIG. 39 Beam B-IC; PRESTRESS FORCE AND MOMENT vs UNIT STRAIN

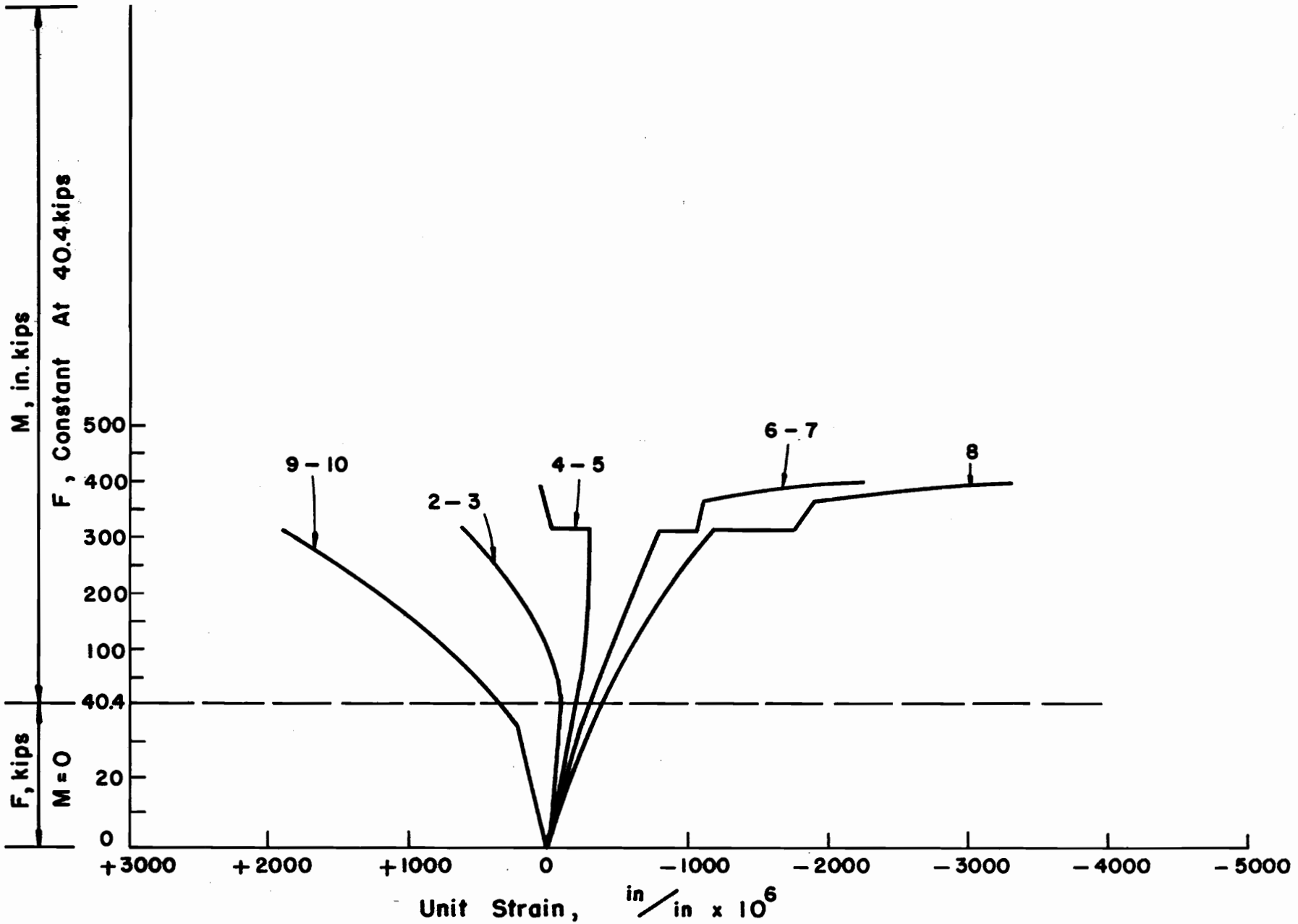

FIG. 40 Beam B-2A; PRESTRESS FORCE AND MOMENT vs UNIT STRAIN

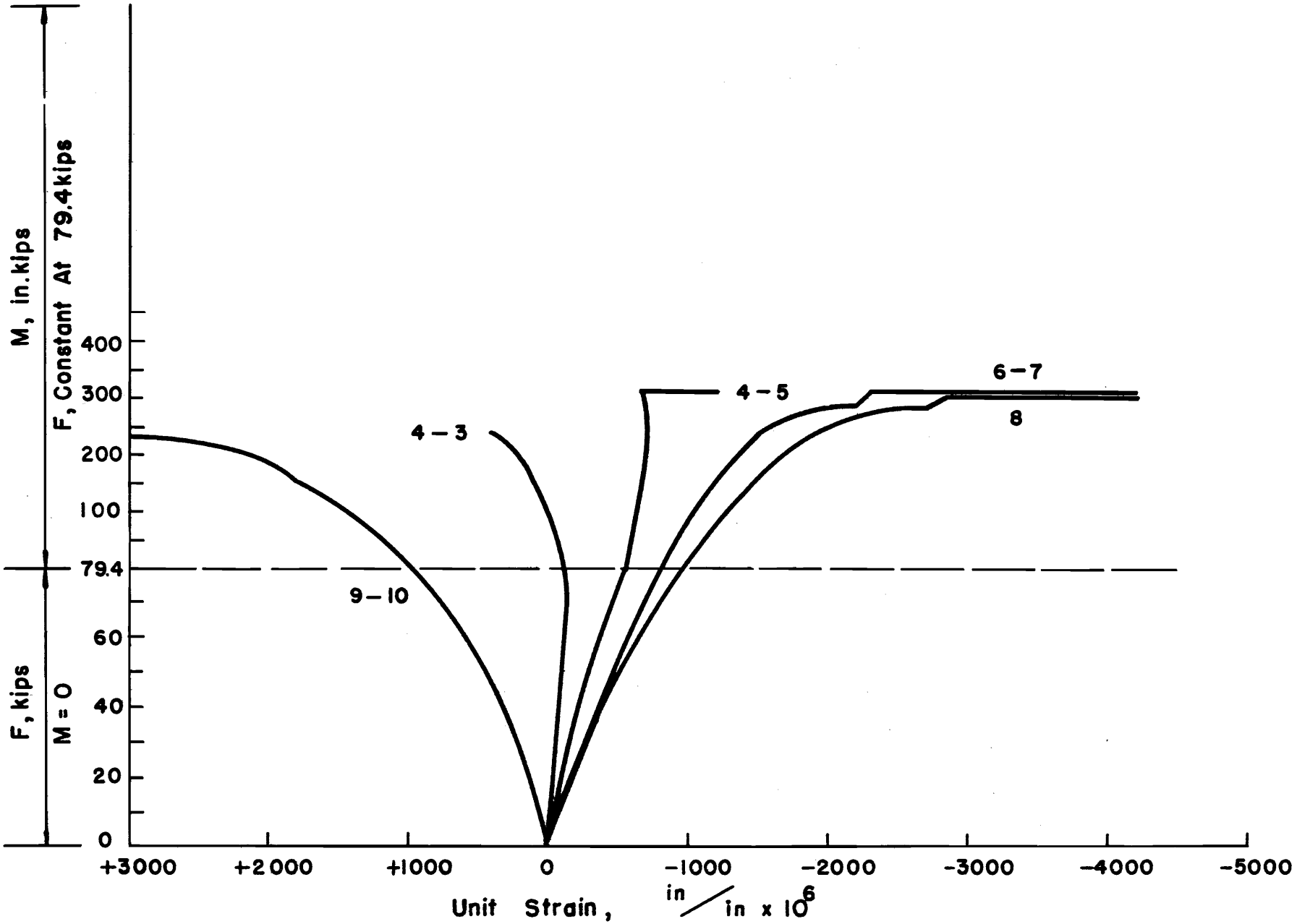

FIG. 41 Beam B-2B; PRESTRESS FORCE AND MOMENT vs UNIT STRAIN

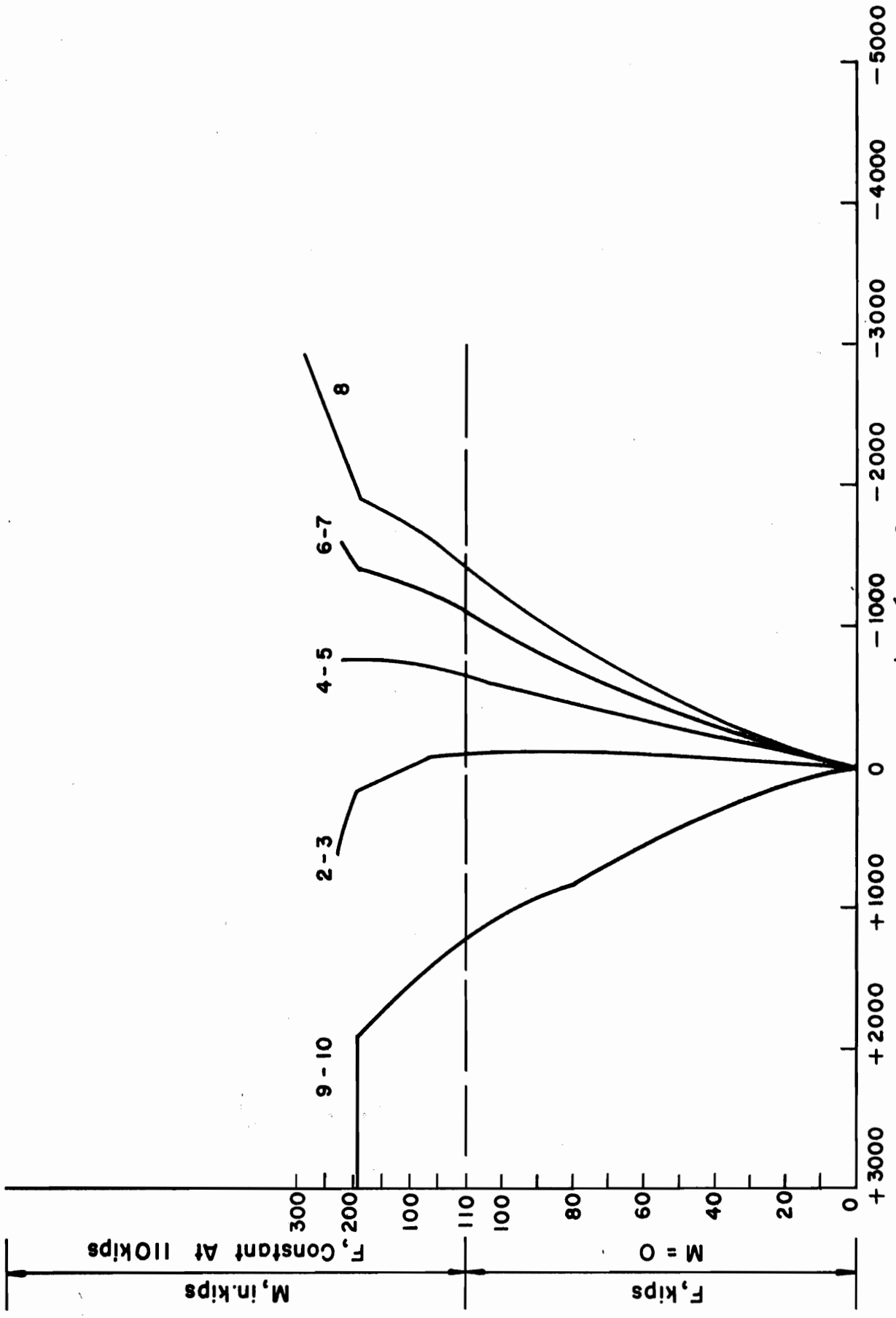

FIG. 42 Beam B-2C, PRESTRESS FORCE AND MOMENT vs UNIT STRAIN

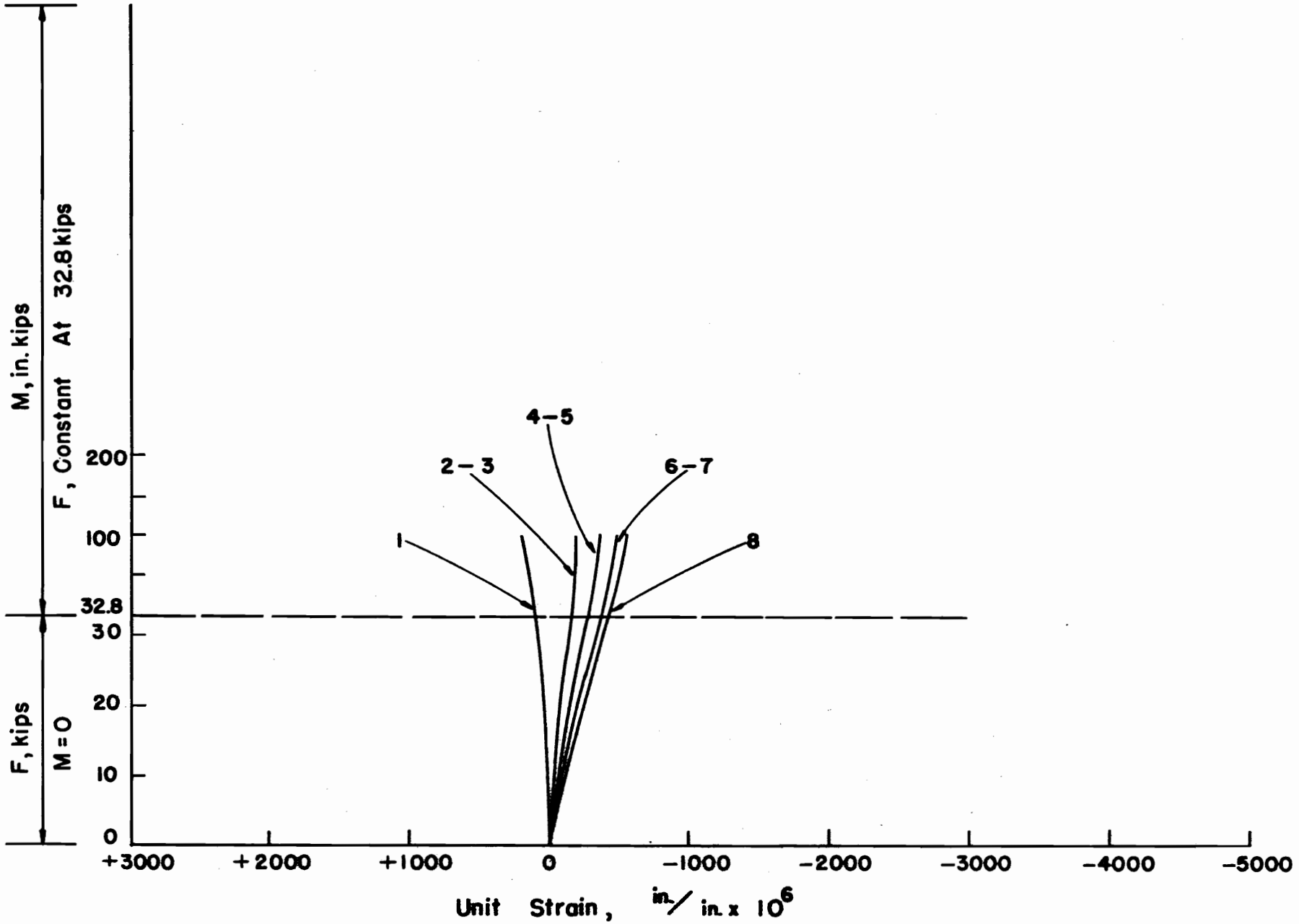

FIG. 43 Beam B-3A; PRESTRESS FORCE AND MOMENT vs UNIT STRAIN

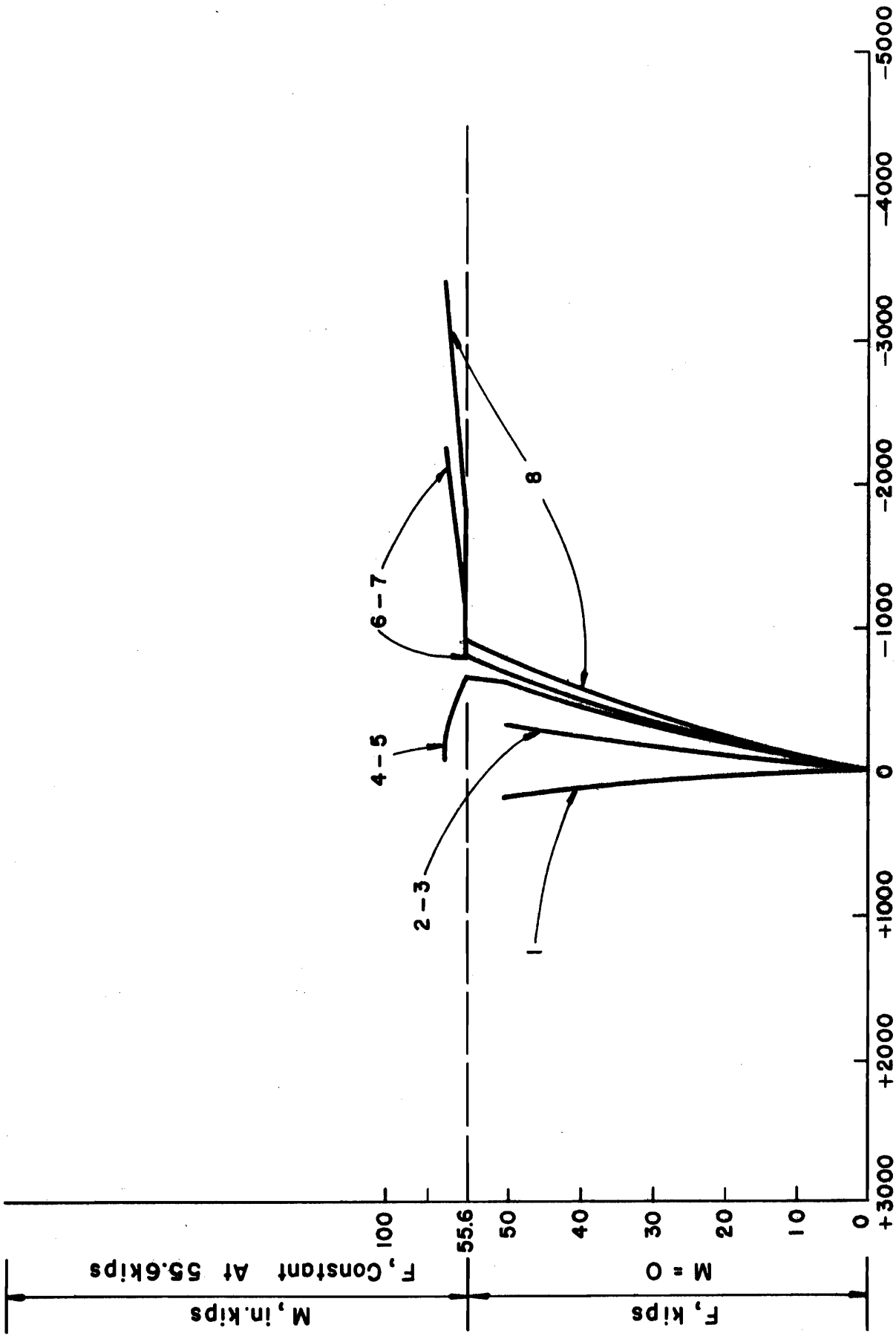

FIG. 44 Beam B-3B; PRESTRESS FORCE AND MOMENT vs UNIT STRAIN

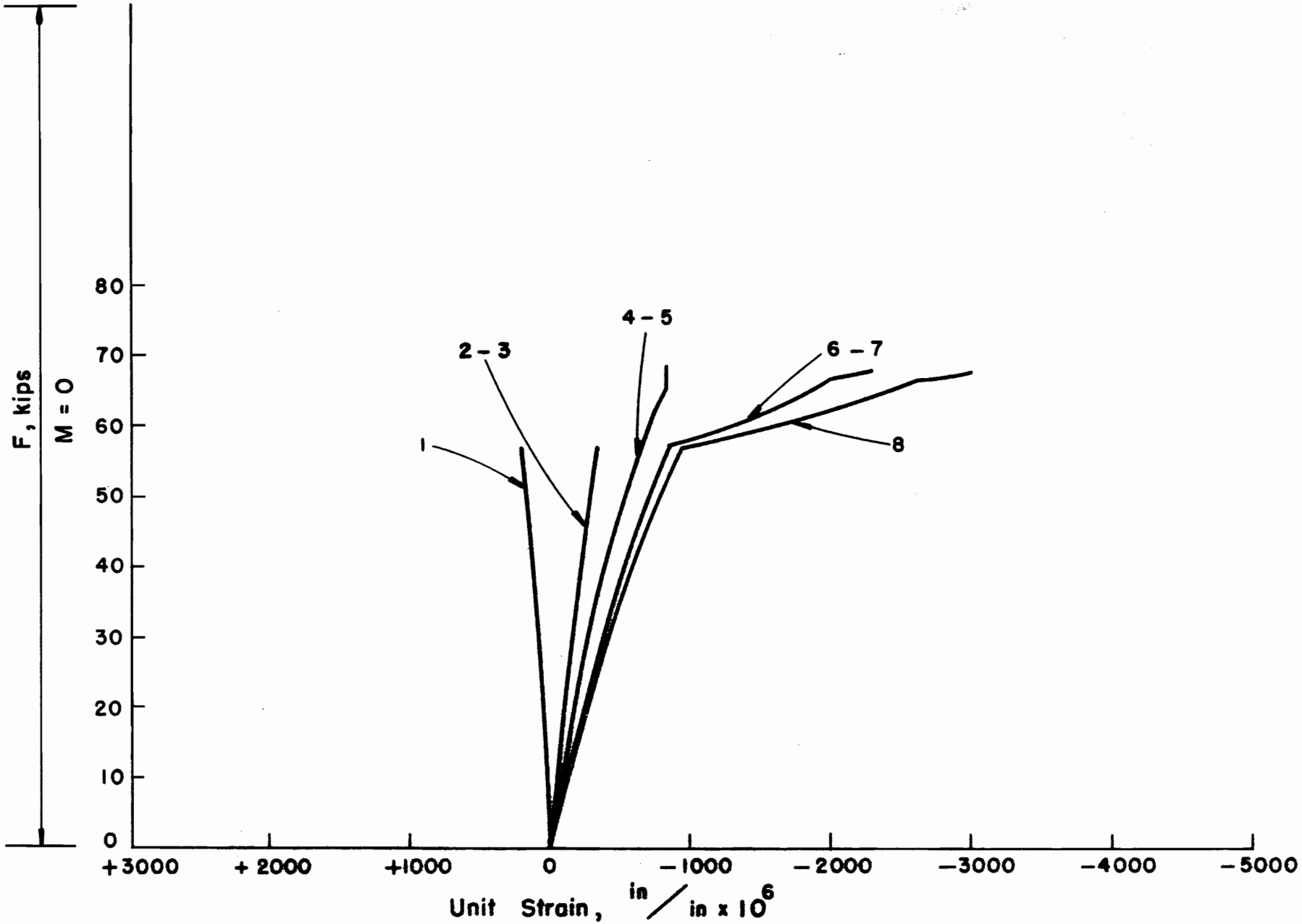

FIG. 45 Beam B-3C; PRESTRESS FORCE AND MOMENT vs UNIT STRAIN

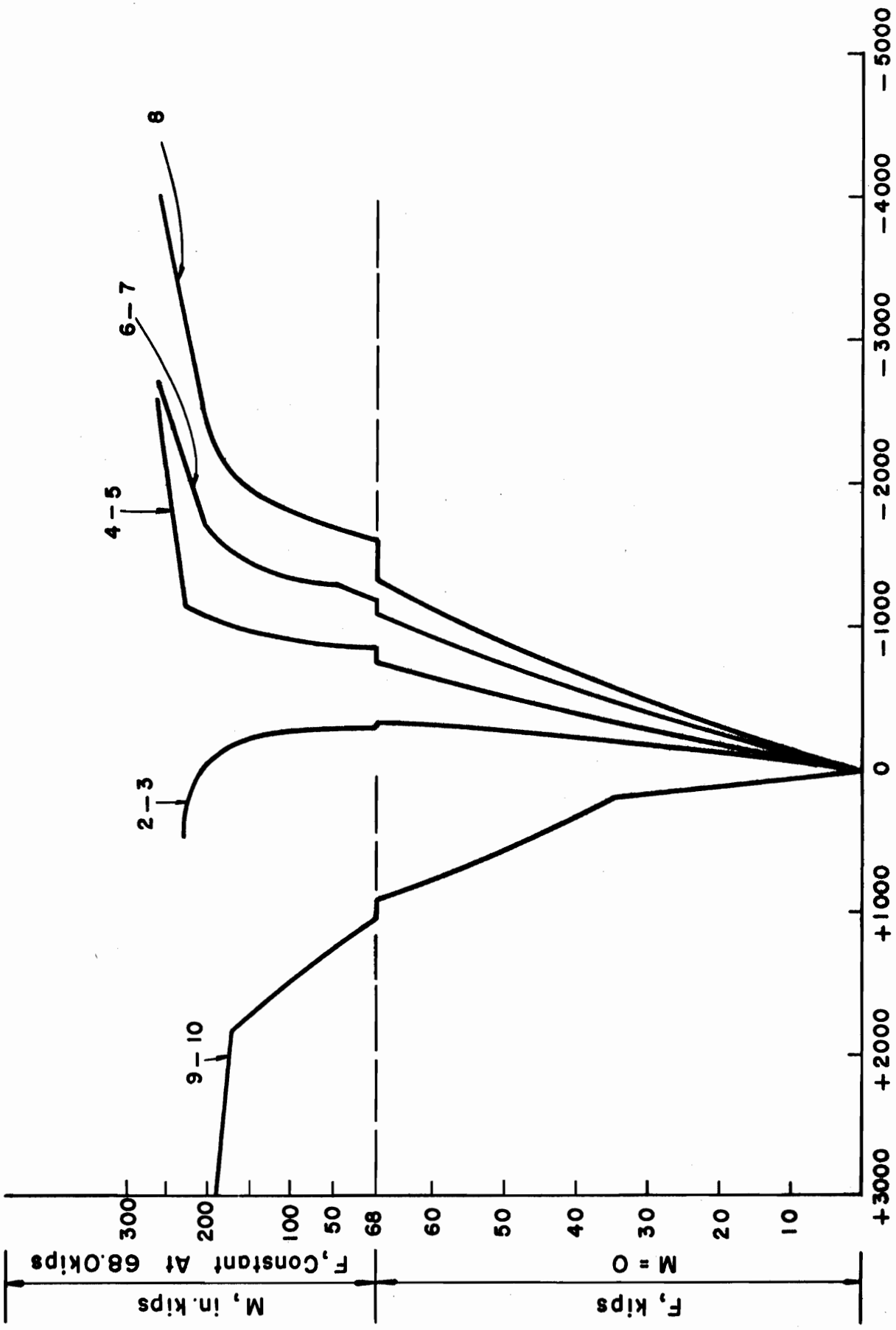

FIG. 46 Beam B-4A; PRESTRESS FORCE AND MOMENT vs UNIT STRAIN

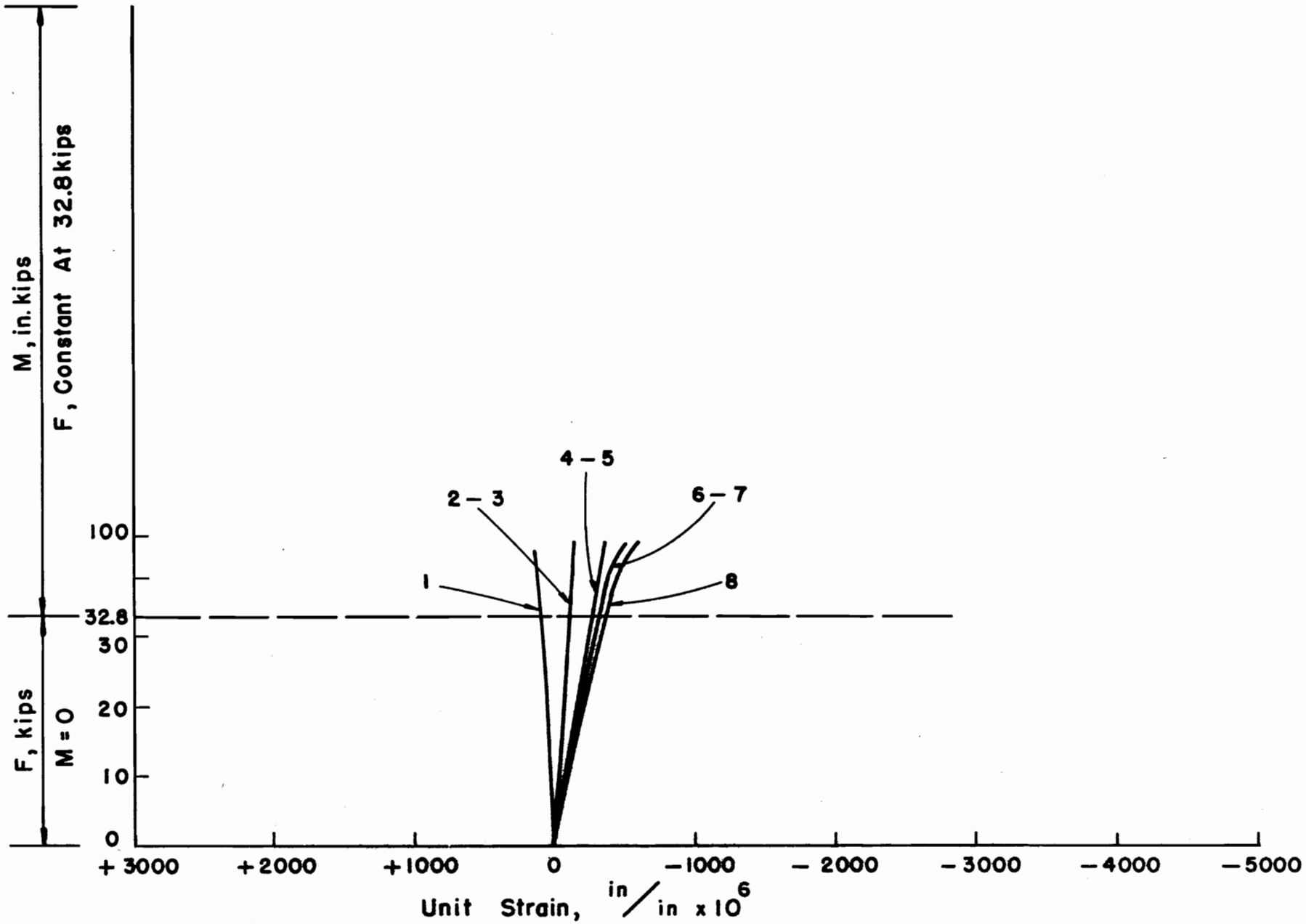

FIG. 47 Beam B-5A; PRESTRESS FORCE AND MOMENT vs UNIT STRAIN

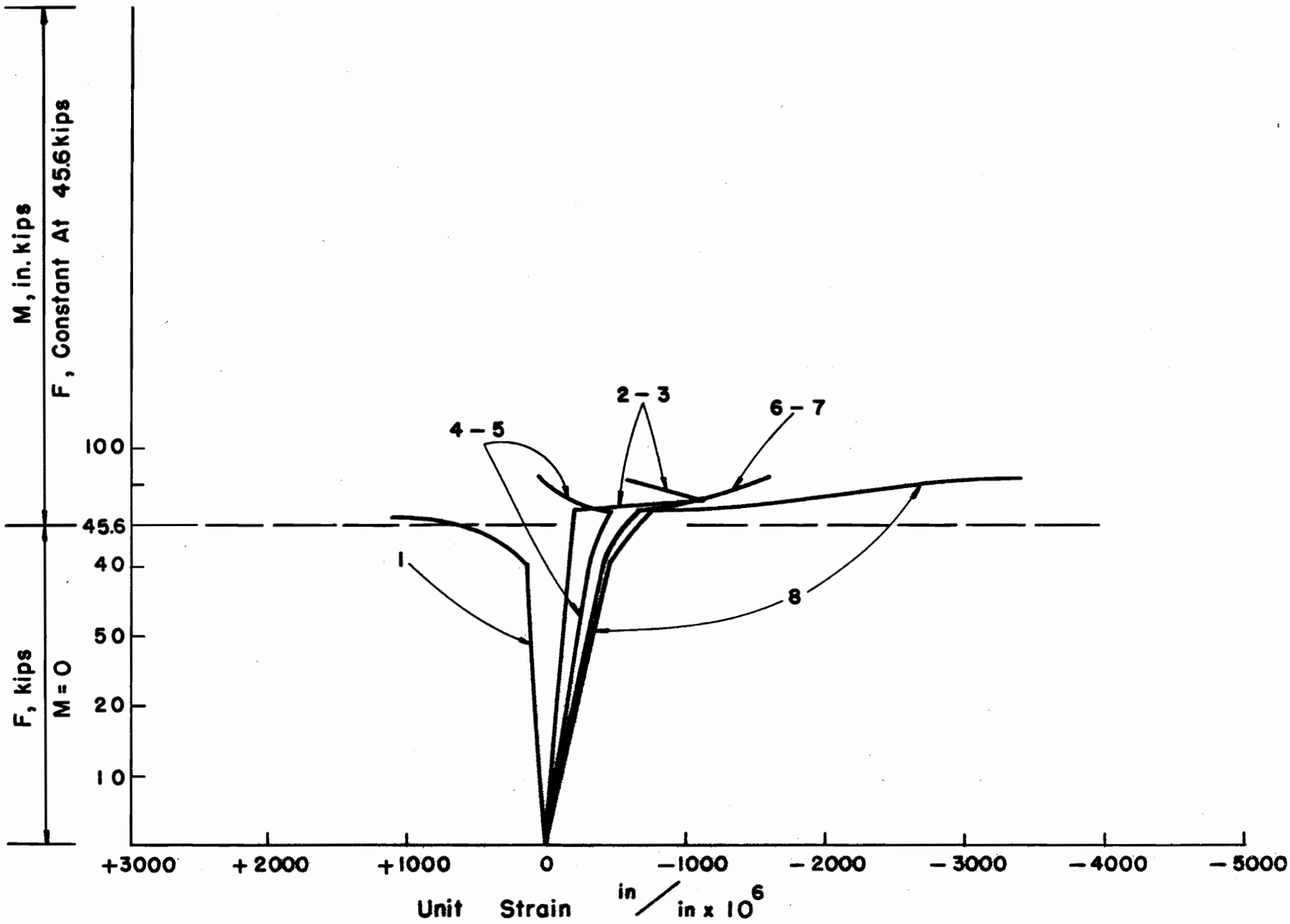

FIG. 48 Beam B-5B; PRESTRESS FORCE AND MOMENT vs UNIT STRAIN

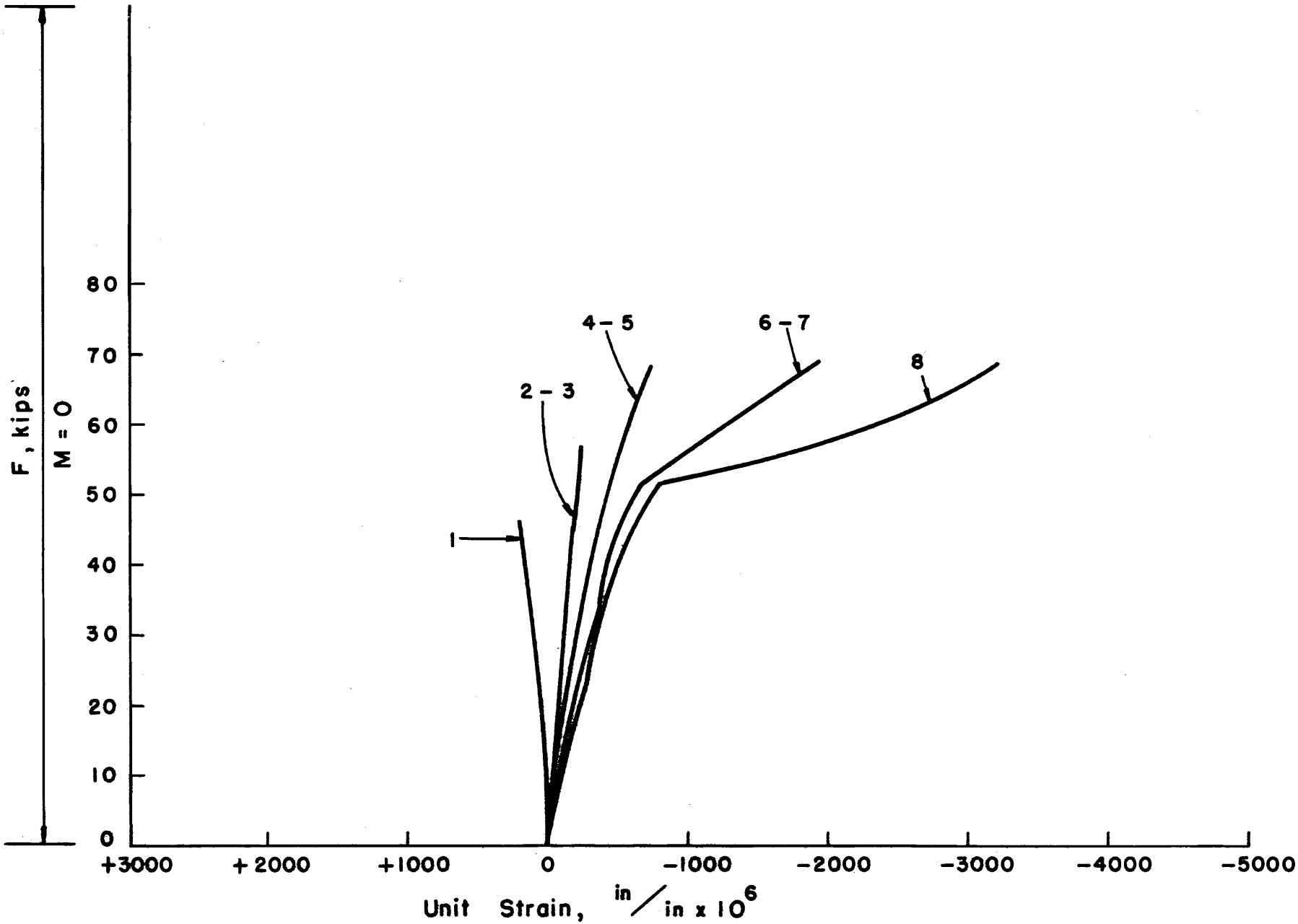

FIG. 49 Beam B-5C; PRESTRESS FORCE AND MOMENT vs UNIT STRAIN

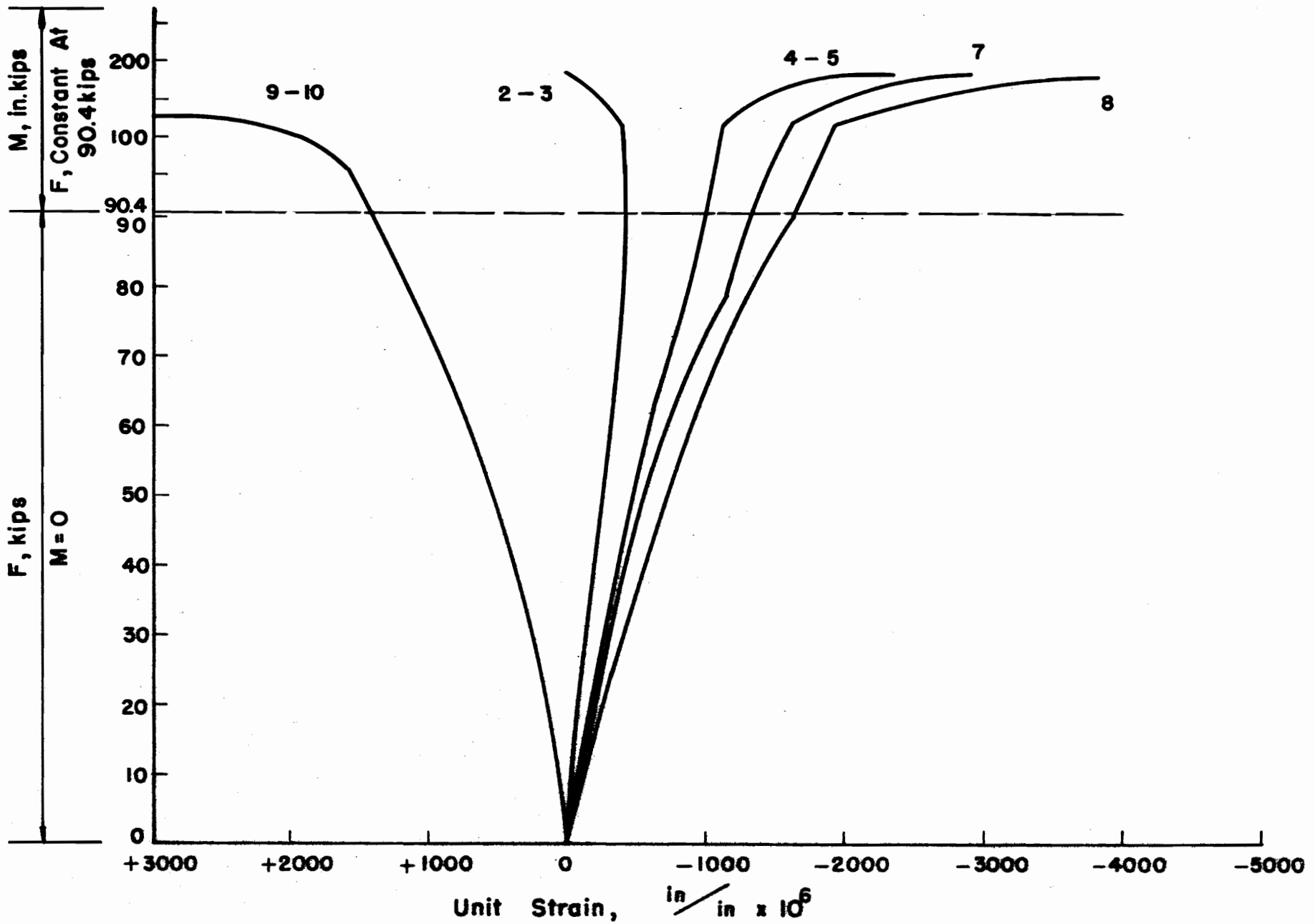

FIG. 50 Beam B-6A; PRESTRESS FORCE AND MOMENT vs UNIT STRAIN

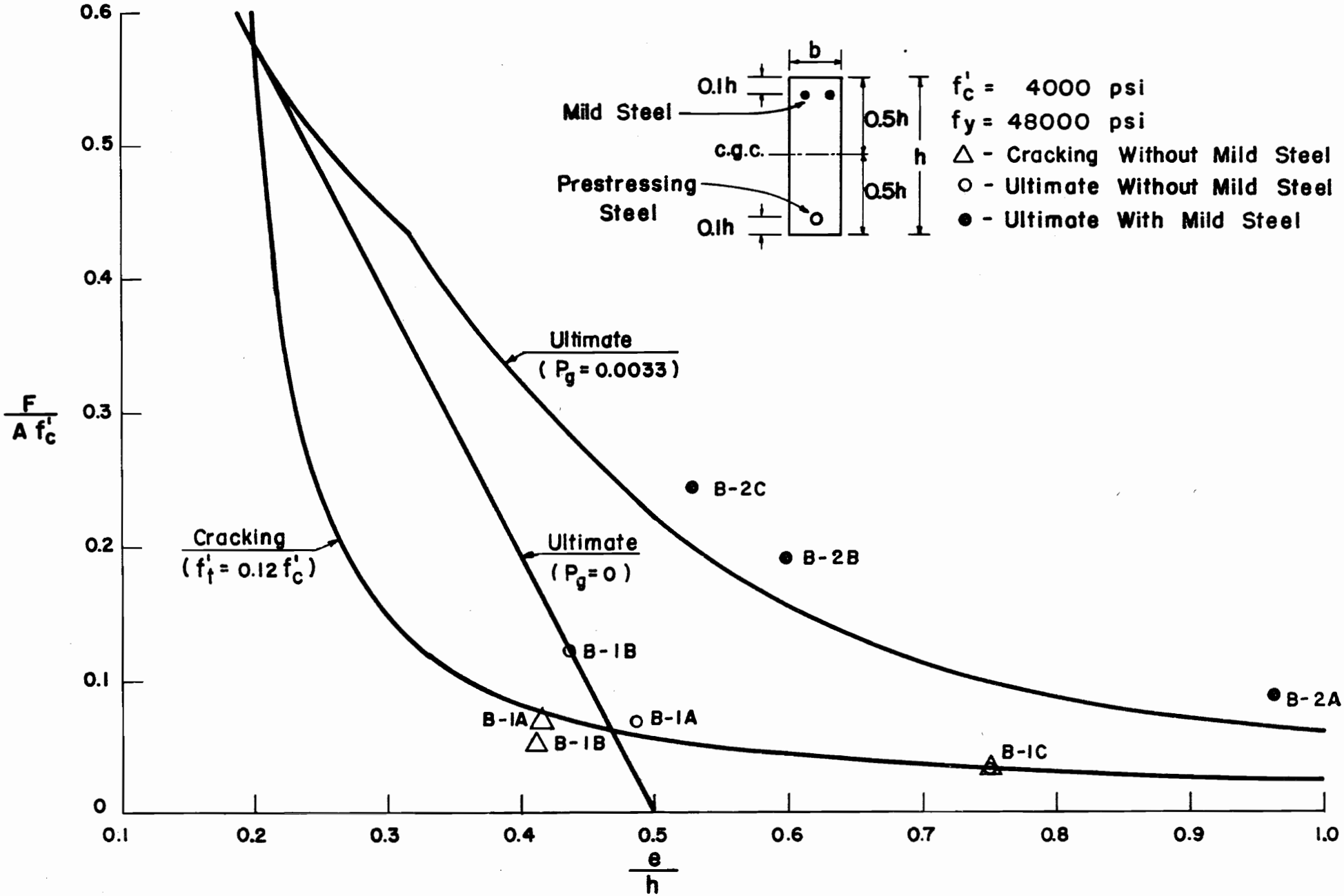

FIG. 51 CRACKING AND ULTIMATE STRENGTH CURVES FOR A RECTANGULAR SECTION

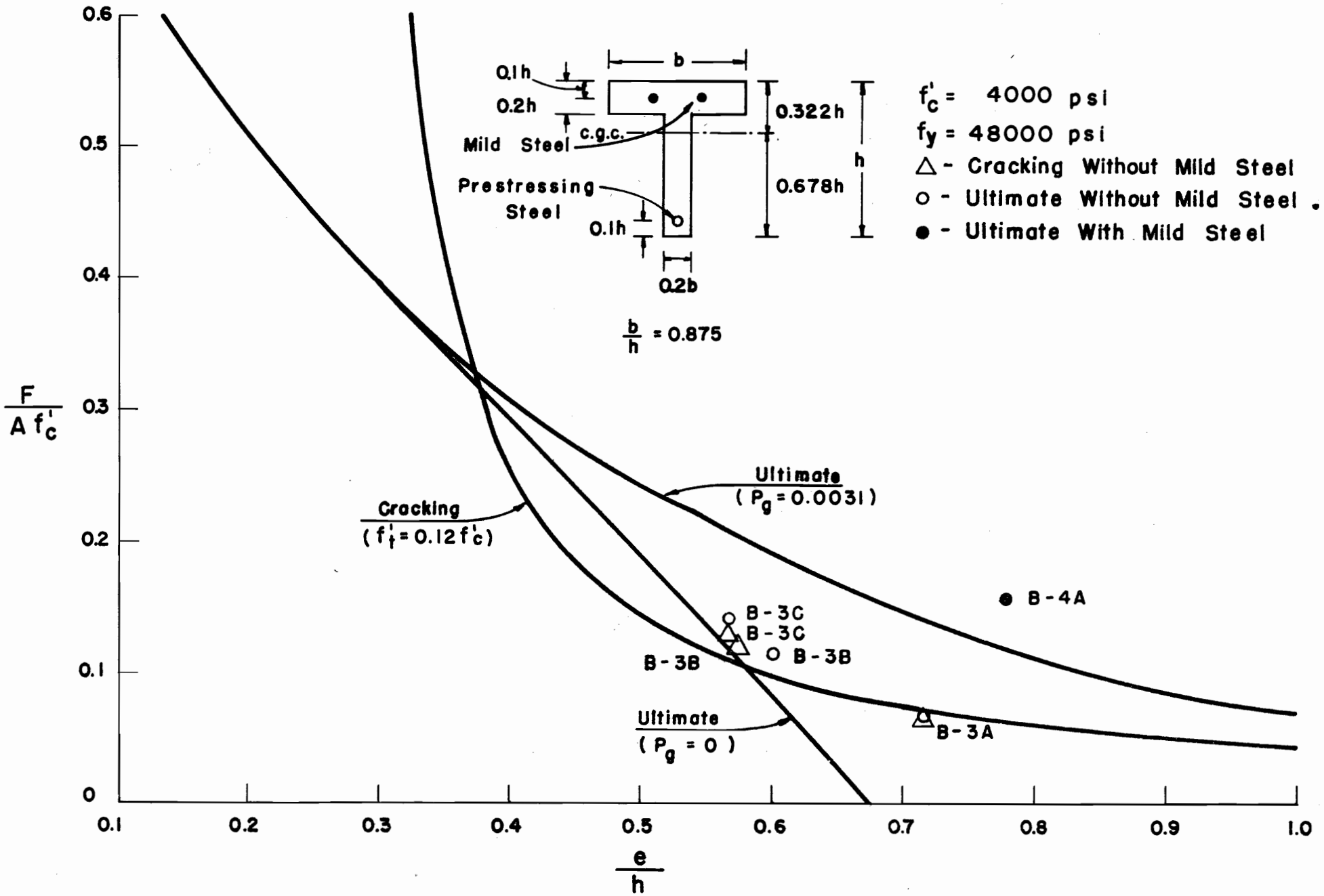

FIG. 52 CRACKING AND ULTIMATE STRENGTH CURVES FOR A TEE SECTION

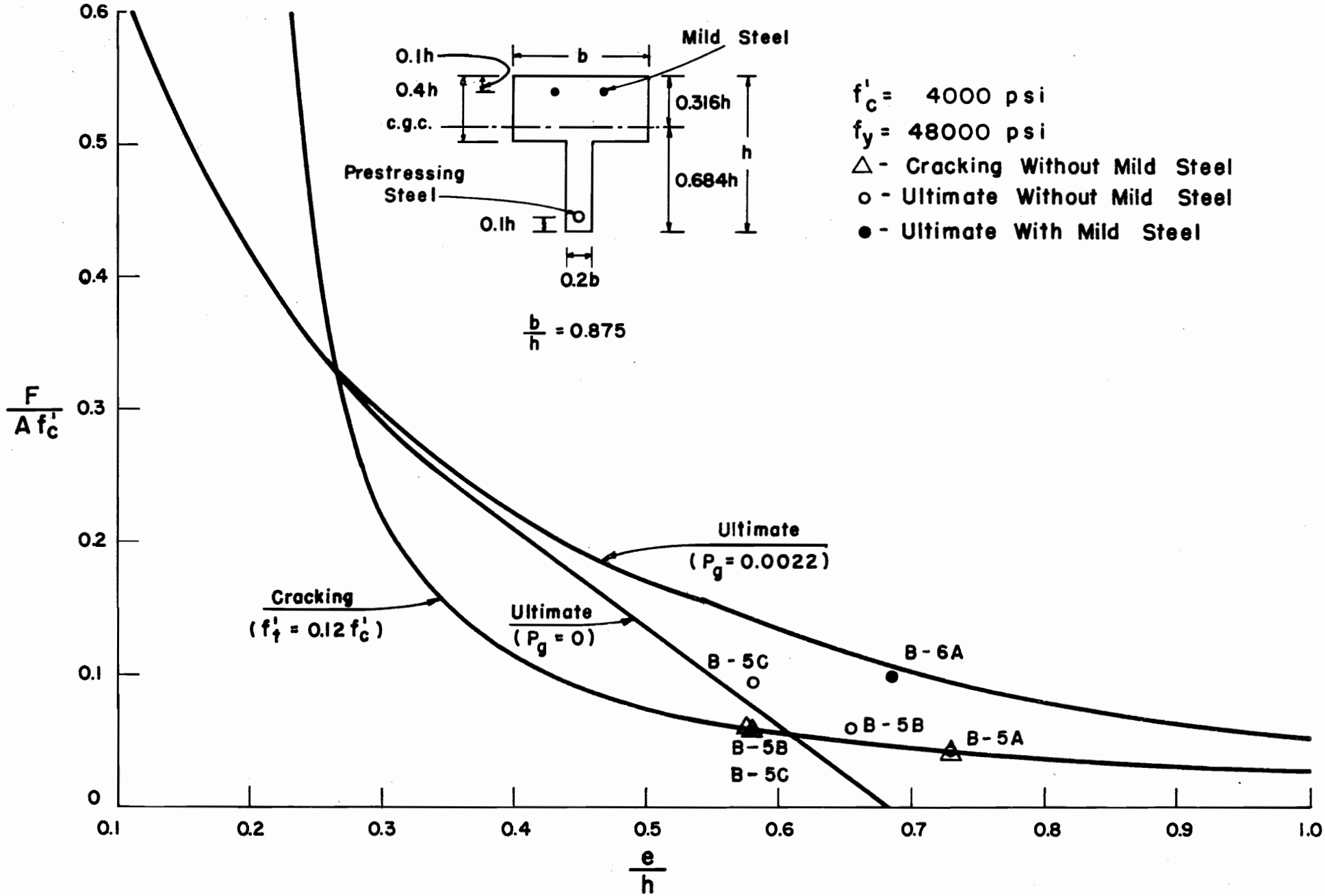

FIG. 53 CRACKING AND ULTIMATE STRENGTH CURVES FOR A TEE SECTION

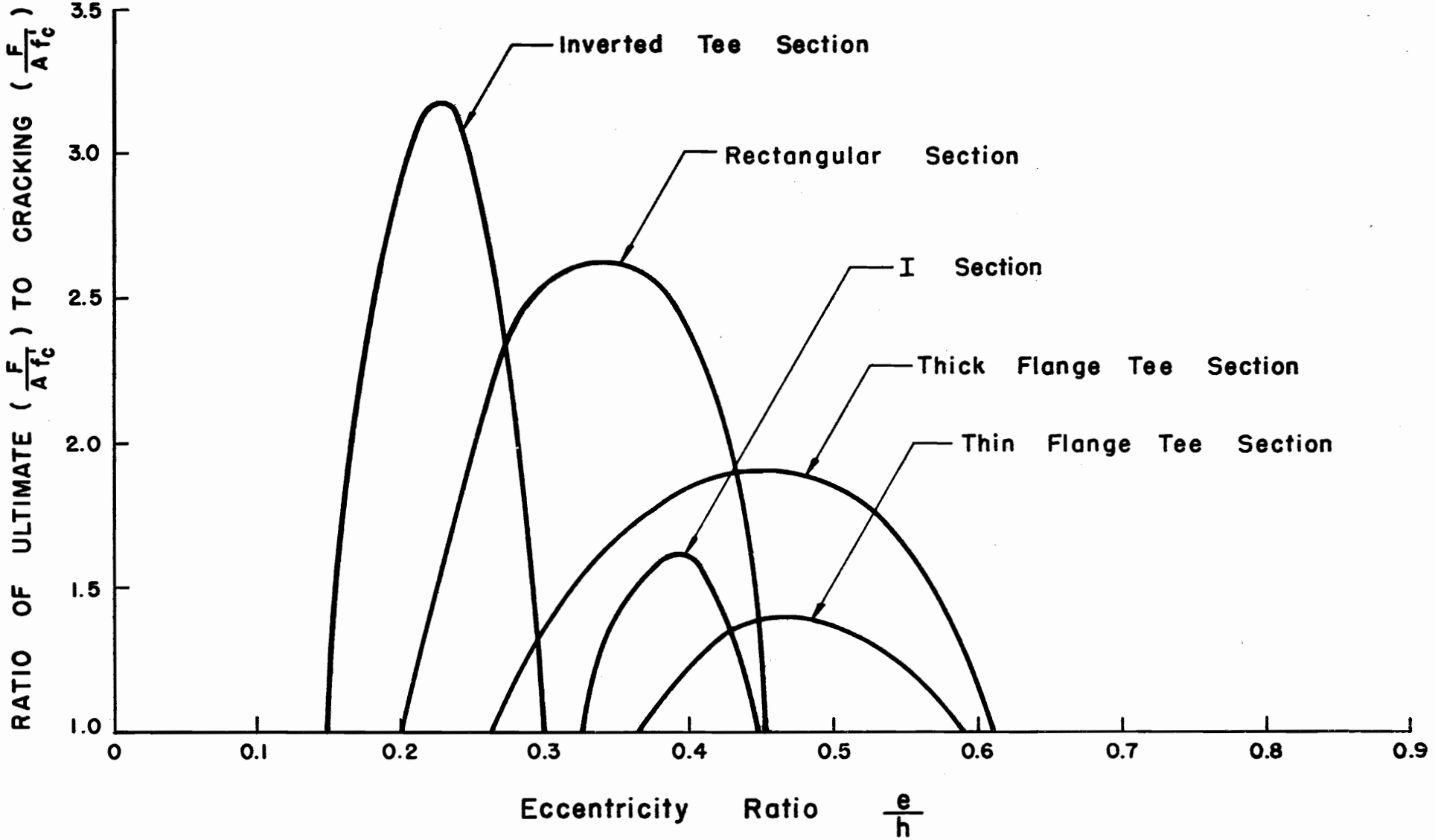

FIG. 54 RATIO OF ULTIMATE ($\frac{F}{A f'_c}$) TO CRACKING ($\frac{F}{A f'_c}$) FOR VARIOUS ECCENTRICITY RATIOS (BEAMS WITHOUT MILD STEEL)

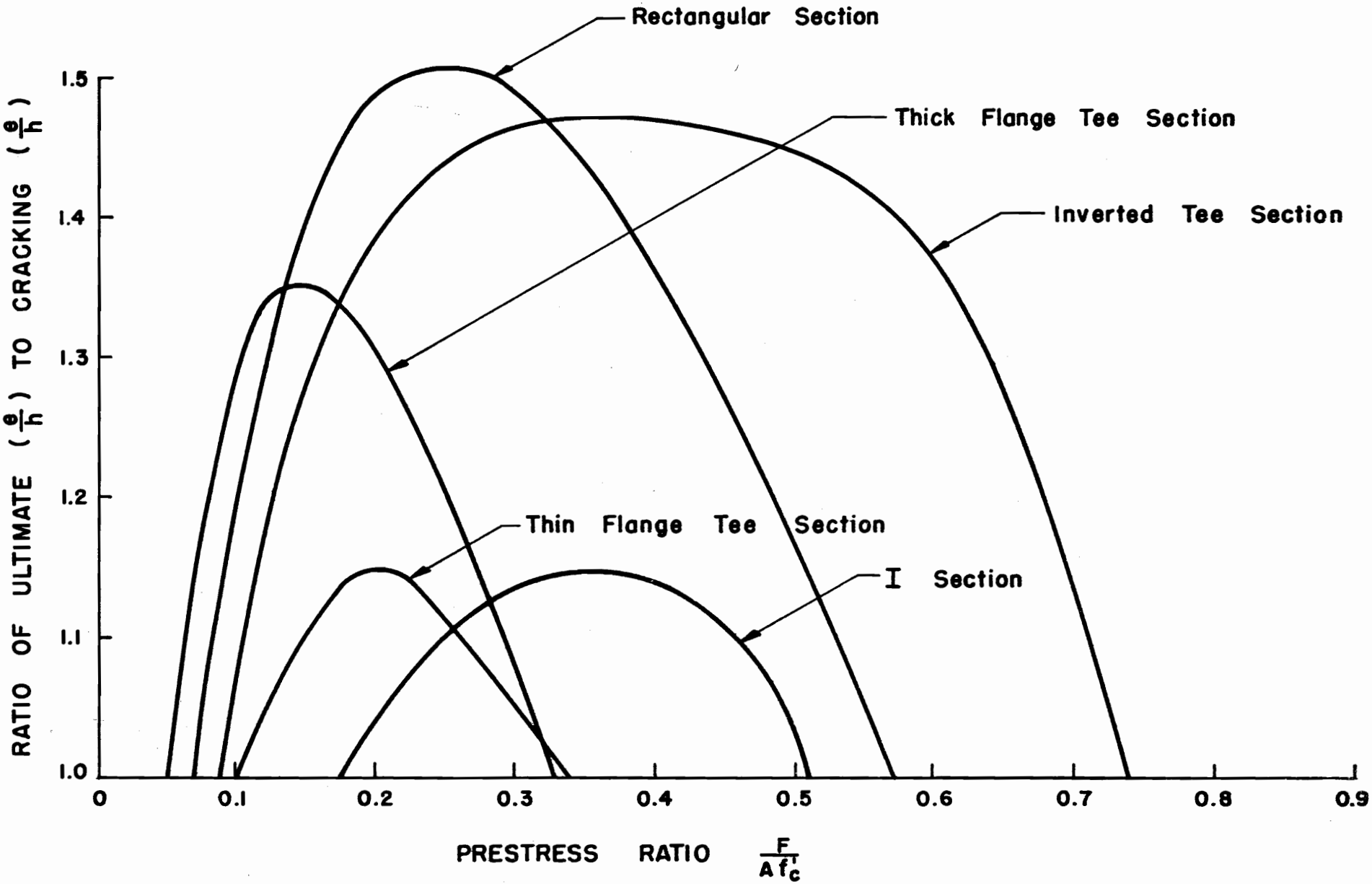

FIG. 55 RATIO OF ULTIMATE ($\frac{e}{h}$) TO CRACKING ($\frac{e}{h}$) FOR VARIOUS PRESTRESS RATIOS (BEAMS WITHOUT MILD STEEL)